Quantum fluctuations in mixtures and dipolar systems

Daniel Edler,
geboren am 8. Januar 1991 in Hannover, Germany

2022

Referent:
Prof. Dr. Luis Santos,
Institut für Theoretische Physik,
Leibniz Universität Hannover

Korreferent:
Prof. Dr. Rejish Nath Gopinathan Rejani,
Indian Institute of Science Education and Research, Pune, India

Korreferent:
Prof. Dr. Subhasis Sinha,
Indian Institute of Science Education and Research, Kolkata, India

Tag der Disputation:
8. Juli 2022

Abstract

Recent theoretical and experimental breakthrough results have revealed the importance of beyond-mean-field contributions in weakly-interacting systems when the mean-field energy is quasi-canceled due to the presence of competing interactions. This is in particular the case in Bose mixtures and in dipolar condensates. In this Thesis we have considered both cases, focusing on particular scenarios where quantum fluctuations result in a qualitatively new physics.

In the first part of the Thesis, we focus on binary mixtures. We consider in particular the case of a peculiar mixture in which one of the components present enhanced role of quantum fluctuations, whereas the second one is immiscible with the first. We show that this may be achieved in experiments using a three-component set up, in which two of the components are miscible and in the regime of mean-field quasi-cancellation, forming an effective scalar component, whereas a the third one is immiscible with the other two. We focus on how a quantum bubble formed by the effective scalar component, behaves in a bath formed by the third component. We show that the properties of the quantum bubble are very significantly affected by the modification introduced by quantum fluctuation in the equilibrium of pressures between bubble and bath. As a result, quantum fluctuations may significantly change the dependence of the bubble volume on the bath density. Furthermore, we show that quantum fluctuations modify the buoyancy criterion. Interestingly, once buoyancy sets in, it may be arrested by the effect of quantum fluctuations at an intermediate position between the center and the surface of the bath, in stark contrast with standard buoyancy in mean-field immiscible mixtures.

The second part of the Thesis is devoted to dipolar condensates, in which quantum fluctuations may play as well a surprisingly important role in the weakly-interacting regime. We focus in particular on the physics of dipolar condensates in quasi-one-dimensional geometries. By means of the so-called Hugenholz-Pines approach we analyze how the Lee-Huang-Yang correction resulting from quantum fluctuations experiences for growing density, a crossover from a one-dimensional dependence into a three-dimensional one. Such a crossover results from the role played by the transversal modes in the determination of the quantum correction, even if the condensate itself remains one-dimensional. We show that at low densities, quantum corrections differ very significantly from those in quasi-one-dimensional Bose-Bose mixtures due to the peculiar momentum dependence of the dipole-dipole interaction. As a result, quasi-one-dimensional dipolar condensates with a residual attractive mean-field term, may be stabilized against the forma-

tion of a bright soliton, forming rather a flat-top quantum droplet. Therefore, our results show that quantum fluctuations change radically the density profile and properties of a quasi-one-dimensional dipolar condensates.

Contents

IV Conclusion and Outlook   **103**

Part I

Introduction

Chapter **1**

From Ultra-cold gases to Bose-Einstein condensates

In 1924 a rejected paper draft by S. N. Bose about a clean derivation of Planck's distribution based on a fully-quantum statistical approach, raised A. Einstein's interest. Einstein translated Bose's work into German to get it published in "Zeitschrift für Physik" with the closing note that he was going to extend Bose's method to ideal gases of massive particles instead of photons.[Bos24] This announcement was followed shortly by a paper by him, which pointed out the incorrectness of a classical theory for a system of small temperature and volume, indicating a phase transition.[Ein25] In consequence, individually indistinguishable particles must collectively occupy the lowest energy state, now known as Bose-Einstein condensate (BEC).

Large-enough densities and sufficiently low temperatures are necessary to enter the quantum-degenerate regime. In experiments with cold helium, which were available at that time, for achievable temperatures one needs relatively large densities, which also imply strong interparticle interactions that make theoretical predictions difficult. Interactions result in a relatively small condensed fraction of typically 10 %[CW02], leaving the rest in excited states. Another disadvantage of large densities is posed by large three-body losses, which limit the lifetime of the system.

These problems may be avoided by working with much more dilute systems, such that the system remains in the weakly-interacting regime. However, this decreases
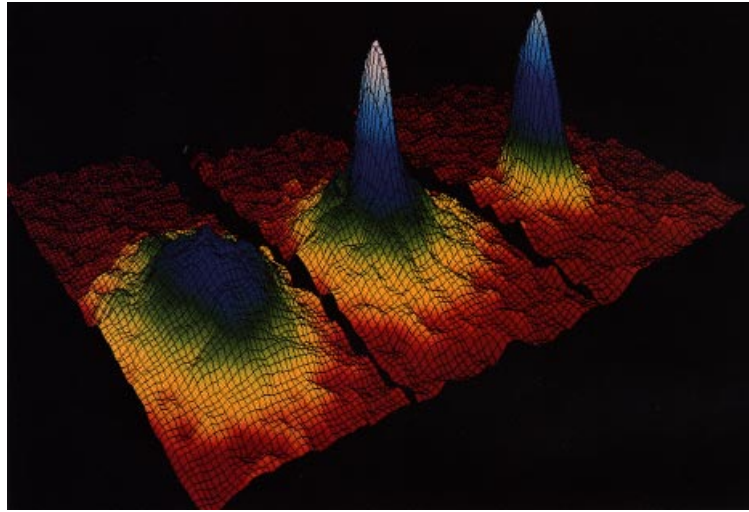
Figure 1.1: Three images of the momentum distributions of a gas of trapped rubid-
ium atoms at different temperatures. The left one shows the state at
the critical value for Bose-Einstein condensation. Hence only a thermal
Gaussian distribution is visible. Further evaporation reduces the tem-
perature and shows the emergence of a condensate peak in the center
plot. The right plot comes from a sample of a nearly pure condensate.
Picture reprinted from [Cor96].

the required temperature for quantum-degeneracy, which for typical ultra-cold
atom experiments goes down to the $100\,\mathrm{nK}$ to $1\,\mathrm{\mu K}$ regime for typical densities of
the order of $10^{-19}\,\mathrm{m}^{-3}$ to $10^{-21}\,\mathrm{m}^{-3}$. Such a low temperature cannot be reached
with standard cryogenic techniques, and demands sophisticated cooling techniques
like laser cooling and evaporative cooling.

The first BEC with a significant condensed fraction in the weakly-interacting
regime were created in 1995 in the groups of E. Cornell and C. Wieman with
rubidium[And+95], as well as with sodium in W. Ketterle's group[Dav+95]. In
Figure 1.1, one can see the iconic momentum distributions of the rubidum exper-
iment for different temperatures, and the emergence of the condensate. In 2001
both groups were rewarded with the Nobel prize in physics[01].

In this Chapter, we discuss the basics of Bose-Einstein condensation. In Sec. 1.1,
we provide a general discussion on ultra-cold ideal Bose gases. Section 1.2 focuses
on the phenomenon of Bose-Einstein condensation itself. Interactions are intro-
duced in Sec. 1.3. The chapter closes with the discussion of beyond-mean-field
corrections in Sec. 1.4 and of the validity of the local-density approximation in
Sec. 1.5.

1.1 Ultra-cold ideal gases

Cooling a system to a low-enough temperature brings it into the quantum-degenerate regime, where its properties are governed by quantum statistics. The half-integer spin *Fermions* follow *Fermi-Dirac statistics*, and Pauli's exclusion principle forbid them to occupy an state more than once. On the other hand there are the (full) integer spin *Bosons*, characterized by a many-body wave-function symmetric under exchange of any two particles. Bosons follow *Bose-Einstein statistics*, and in principle an arbitrary number of them may occupy a given state. For the rest of this Thesis we will restrict ourselves solely to the case of bosons.

To describe these systems one can use the grand canonical ensemble, characterized by the temperature T and the chemical potential μ. We consider first the case of an *ideal gas*—interparticle interactions are discussed later on in this chapter. The total Hamiltonian $\hat{H}$ is the sum over the individual one-body hamiltonians $\hat{h}_i$, i.e. $\hat{H} = \sum_i = \hat{h}_i$. Then we can get an explicit expression for the grand canonical partition function

$$Z(\mu, T, V) = \prod_{\mathbf{k}} \left(1 - e^{\beta(\mu - \varepsilon_{\mathbf{k}})} \right)^{-1} \tag{1.1.1}$$

where $1/\beta = k_B T$, k_B is the Boltzmann constant, and $\varepsilon_{\mathbf{k}}$ is the energy of the state $\mathbf{k}$. From thermodynamic principles we can infer the total number of particles by taking the negative partial derivative with respect to the chemical potential of the grand canonical potential $\Omega = \frac{-1}{\beta} \ln Z$ leading to

$$N = -\frac{\partial \Omega}{\partial \mu} = \sum_{\mathbf{k}} \frac{1}{e^{\beta(\varepsilon_{\mathbf{k}} - \mu)} - 1} = \sum_{\mathbf{k}} \langle N_{\mathbf{k}} \rangle \tag{1.1.2}$$

where $\langle N_{\mathbf{k}} \rangle$ is the mean occupation of the k-th energy level. It is important to note that the mean occupation $\langle N_{\mathbf{k}} \rangle$ diverges for $\beta(\varepsilon_{\mathbf{k}} - \mu) \to 0$. From this it should be clear that the chemical potential cannot take any value and must remain smaller than the minimal energy in the set $\{\varepsilon_{\mathbf{k}}\}$, i.e. $\mu < \min(\{\varepsilon_{\mathbf{k}}\})$. This prevents us from getting undefined or negative mean occupation numbers.

1.2 Ideal Bose-Einstein condensates

Let us consider an ideal Bose gas without any external trapping in a cubic box of volume V. In this case the single-particle Hamiltonians $\hat{h}_i$ have the simple

form $\hat{h}_i = \frac{\hat{p}_i^2}{2m}$. Its eigenenergies are those of a free particle $\varepsilon_{\mathbf{k}} = \frac{\hbar^2 k^2}{2m}$. The lowest energy is zero, and hence the chemical potential must always be negative, $\mu < 0$. When the chemical potential tends to zero, i.e. $\mu \to 0 = \varepsilon_0$, the term for $k = 0$ diverges in (1.1.2). Therefore, one should split this case from the rest. Let us call N_0 the *condensed component*, given by the number of particles in the lowest single-particle state of energy ε_0. We will denote as *thermal component* the sum of all other particles, $N' = \sum_{k>0} \langle N_k \rangle$. We can then rewrite the total number of particles as

$$N = N_0 + N'. \tag{1.2.3}$$

Moving into the thermodynamic limit where $N, V \to \infty$ but keeping the density $n = N/V$ constant, we can replace the sum by an integral, i.e.

$$\frac{N'}{V} \to \frac{1}{(2\pi)^3} \int_{k>0} \mathrm{d}^3 k \, \frac{1}{e^{\beta(\varepsilon_{\mathbf{k}} - \mu)} - 1}, \tag{1.2.4}$$

which can be integrated for $\mu = 0$, leading to the expression[Ued10]

$$n = n_0 + \frac{\zeta\left(\frac{3}{2}\right)}{\lambda_T^3} \tag{1.2.5}$$

where $\lambda_T = \sqrt{\frac{2\pi\hbar^2}{m k_B T}}$ is the *thermal de Broglie wavelength* and $\zeta(3/2) \approx 2.612$ is the Riemann zeta function evaluated at 3/2 [Ued10]. From Eq. (1.2.5) we can see that as soon as the *phase space density* $n\lambda_T^3$ is larger than $\zeta(3/2)$ any additional particle must be in the lowest state of $k = 0$. This is the *Bose-Einstein Condensate*.

Quantum degeneracy, given by the condition $n\lambda_T^3 > \zeta(3/2)$, may be interpreted as the regime in which the wave-functions of individual particles, which are delocalized in a length scale given by λ_T, overlap significantly, resulting in a dominant role of quantum statistics. From the critical phase space density, i.e. $n\lambda_T^3 = \zeta(3/2)$, we can define the *critical temperature* T_0 for condensation as the temperature for which the macroscopical population of the ground state sets in:

$$k_B T_0 = \frac{2\pi\hbar^2}{m} \left(\frac{n}{\zeta(3/2)}\right)^{2/3}. \tag{1.2.6}$$

Note that a very low density, as that of typical experiments, result in a very low critical temperature for condensation.

1.3 Weakly-interacting Bose gases

Up to now we have assumed an ideal gas, and indeed the BEC transition is in principle a purely quantum-statistical effect. However, inter-particle interactions do play a crucial role in the properties of ultra-cold gases, despite their extreme diluteness. In this section, we first briefly review some ideas of scattering theory, and then discuss the mean-field treatment of interacting BECs.

1.3.1 Scattering theory

We consider dilute gases, with a mean interatomic distance much larger than the typical range of the interatomic potential $\mathbf{r}_0$, i.e. $n^{-1/3} \ll |\mathbf{r}_0|$. Therefore we can restrict our model to interactions involving only two particles simultaneously.

Let us consider two particles, labeled as 1 and 2. They are located at $\mathbf{r}_1$, $\mathbf{r}_2$ and have masses m_1, m_2. The particles interact via a central potential $V(\mathbf{r})$, with $\mathbf{r} = \mathbf{r}_1 - \mathbf{r}_2$. The two-particle Hamiltonian can then be written in the form:

$$\hat{H} = \hat{H}_R + \hat{H}_r = -\frac{\hbar^2 \nabla_R^2}{2(m_1 + m_2)} - \frac{\hbar^2 \nabla^2}{2m_{12}} + V(\mathbf{r}) \tag{1.3.7}$$

where $\mathbf{R} = \frac{m_1 \mathbf{r}_1 + m_2 \mathbf{r}_2}{m_1 + m_2}$ is the center of mass position, ∇_R^2 is the Laplacian operator with respect to $\mathbf{R}$, ∇^2 is the Laplacian with respect to $\mathbf{r}$, and m_{12} is the reduced mass. Hence the Hamiltonian splits into the center-of-mass movement, which will not be of interest in the following discussion, and the relative motion.

For a sufficiently dilute gas the mean interatomic distance is much larger than the radius of the interparticle potential r_0, i.e. $n^{1/3} \ll r_0$ where $V(r > r_0) \cong 0$. The asymptotic form for $|\mathbf{r}| \to \infty$ of the wave-function $\psi_k(\mathbf{r})$ can be written in the form [Ing+99]

$$\psi_k(\mathbf{r})|_{r \to \infty} = e^{i\mathbf{r} \cdot \mathbf{k}} + f_k(\theta) \frac{e^{irk}}{r}. \tag{1.3.8}$$

Equation (1.3.8) describes an incoming wave and a scattered spherical wave with the angle $\theta = \arccos(\mathbf{r} \cdot \mathbf{k})$ dependent factor $f_k(\theta)$, the *scattering amplitude*. This factor includes all information of the scattered potential.

The general solution is found by expressing the wave-function in the basis of eigenfunctions of the angular momentum operators $\hat{L}^2$ and $\hat{L}_z$, splitting the wave function into an angular-dependent part and a radial one. For a given value of k the

radial part then needs to be solved for all possible values of l. Since we are dealing with spin-less bosons, odd angular momentum numbers l do not contribute to the scattering due to symmetry.

The time-independent Schrödinger equation described by the Hamiltonian in (1.3.7) can be solved in the relevant asymptotic case. In the low-energy limit, $kr_0 \ll 1$, only the $l = 0$ component is relevant, and the scattering amplitude simplifies to

$$f_{k \to 0} = -a_{12} \tag{1.3.9}$$

where a_{12} is called the *scattering length* between the particles 1 and 2. A more detailed derivation can be found in various textbooks [Nol15; Ing+99].

As it is clear from Eq. (1.3.9), the low-energy scattering is characterized by a_{12}. As a result, we may replace the actual potential $V(\mathbf{r})$ by a pseudopotential that leads to the same scattering length:

$$V(\mathbf{r} - \mathbf{r}') = g_{12}\delta^{(3)}(\mathbf{r} - \mathbf{r}') \tag{1.3.10}$$

where $g_{12} = \frac{2\pi\hbar^2 a_{12}}{m_{12}}$ is the coupling constant, and $\delta^{(3)}(\mathbf{r})$ is the three-dimensional delta function. In the following, we restrict ourselves to systems consisting of only one kind of particles and hence drop the subindices. Later in Chapter 2 and 4, we will consider systems built by two and three different species, respectively.

Feshbach resonances

Interestingly, the value of the scattering length can be controlled to a large extent basically at will. Because of its great importance, we outline in the following the concept of *Feshbach resonances*. It was first independently formulated by H. Feshbach in 1958 in the context of nuclear physics [Fes58] and U. Fano in 1961 in the context of atomic physics [Fan61]. This section gives a short overview. More detailed discussions on this topic can be found in [Tim+99; BDZ08; Chi+10].

The molecular potential curve $V_{\mathrm{bg}}(r)$, as shown in black in the left panel of Fig. 1.2, represents the energetically *open channel* or *entrance channel*. Let us consider a collision process of small energy E. For large distances r it asymptotically connects to two free atoms. A second molecular potential curve $V_c(r)$ will be denoted as the *closed channel*. The Feshbach resonance occurs when one of the bound diatomic states of the closed channel couple resonantly to the open channel. The
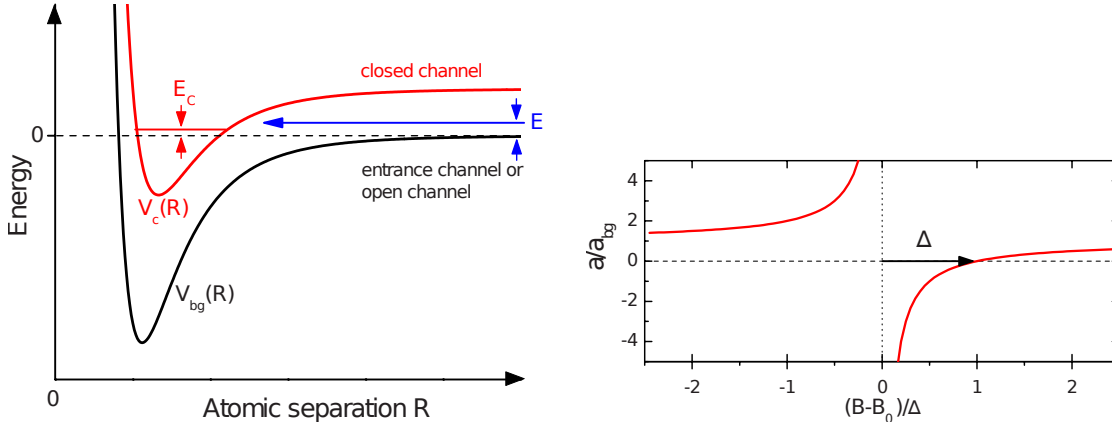
Figure 1.2: (Left) Two-channel model for a Feshbach resonance. Two particles collide with small energy E which can couple to an energy level in the closed channel. (Right) Such a coupling, which may be controlled with an external magnetic field, results in a modified scattering length, which presents a typical divergent curve at the resonance. Reprinted from [Chi+10].

two scattered particles are then temporarily in a quasi-bound state. An external-applied magnetic field can tune the energy difference between the channels, and hence influence the coupling.

The scattering length at a magnetically tuned Feshbach resonance can be well described by the expression

$$a(B) = a_{\mathrm{bg}} \left(1 - \frac{\Delta B}{B - B_0} \right) \qquad (1.3.11)$$

where B_0 is the magnetic field of position of the resonance, a_{bg} is the *background scattering length* incorporating the direct scattering effects without the bound state and ΔB is the resonance width. The right panel of Fig. 1.2 shows the behavior of $a(B)$. Note that Feshbach resonances allow for controlling not only the absolute value of the scattering length, but also its sign. As a result, with the use of these resonances and irrespective of its natural value, experiments can create repulsive ($a > 0$) and attractive ($a < 0$) interactions, and all the way from ideal gases ($a = 0$) to unitary gases ($a = \pm\infty$).

9

1.3.2 Mean-field description

A system of N identical spin-less bosons in an external potential V_ext with inter-particle interactions given by the interaction potential V_int is described by the Hamiltonian

$$
\hat{H} = \int \mathrm{d}^3 r\, \hat{\Psi}^\dagger \left(\frac{-\hbar^2}{2m} \nabla^2 + V_\text{ext}(\mathbf{r}) \right) \hat{\Psi}
$$
$$
+ \frac{1}{2} \int \mathrm{d}^3 r\, \mathrm{d}^3 r'\, \hat{\Psi}^\dagger(\mathbf{r}) \hat{\Psi}^\dagger(\mathbf{r}') V_\text{int}(\mathbf{r} - \mathbf{r}') \hat{\Psi}(\mathbf{r}') \hat{\Psi}(\mathbf{r}), \qquad (1.3.12)
$$

where $\hat{\Psi}^\dagger(\mathbf{r})$ is the creation field operator, and $\hat{\Psi}$ is its adjoint annihilation field operator, which satisfy the usual bosonic commutation relations $\left[\hat{\Psi}^\dagger(\mathbf{r}), \hat{\Psi}^\dagger(\mathbf{r}') \right] = \left[\hat{\Psi}(\mathbf{r}), \hat{\Psi}(\mathbf{r}') \right] = 0$ and $\left[\hat{\Psi}(\mathbf{r}), \hat{\Psi}^\dagger(\mathbf{r}') \right] = \delta^{(3)}(\mathbf{r} - \mathbf{r}')$. The first line in Eq. (1.3.12) represents the kinetic and external trapping contribution, whereas the second one is given by the two-body interactions. Because of the previously demanded diluteness $na^3 \ll 1$, we neglect all terms involving more than two particles.

The Hamiltonian in Eq. (1.3.12) describes the many-body system, but it is very difficult to obtain both analytical and numerical results from it once the number of particles N grows beyond a small number. By using the *mean-field description* one can simplify the analysis, which typically achieves excellent agreement with BEC experiments in the weakly-interacting regime (although not under all circumstances as we will discuss at several points in this Thesis).

N. N. Bogoliubov tackled this problem in 1946 [Bog47]. He considered a system where the number of particles in the condensate N_0 is large and of the same order as the total number of particles, i.e. $N_0 \sim N \gg 1$. Bogoliubov's idea was to replace the creation and annihilation operators related to $k = 0$ with the real numbers $\sqrt{N_0}$, i.e.

$$
\hat{a}_0 \,, \hat{a}_0^\dagger \cong \sqrt{N_0}. \qquad (1.3.13)
$$

This is known as the *Bogoliubov approximation.*

Further, he proposed to separate the condensate part from the bosonic field operator by rewriting it in the form:

$$
\hat{\Psi}^\dagger(\mathbf{r}) = \Psi(\mathbf{r}) + \hat{\delta\psi}^\dagger(\mathbf{r}), \qquad \hat{\Psi}(\mathbf{r}) = \Psi(\mathbf{r}) + \hat{\delta\psi}(\mathbf{r}), \qquad (1.3.14)
$$

where $\Psi(\mathbf{r}) = \langle \hat{\Psi} \rangle$ is the mean-field, and the non-condensed part (which at zero temperature describes quantum fluctuations) is characterized by the operators $\hat{\delta\psi}^\dagger$

and $\hat{\delta\psi}$. These operators can be neglected at zeroth order, and their effect may be considered in perturbation theory. $\Psi(\mathbf{r}) = \psi_0(\mathbf{r})\sqrt{N_0}$ acts as the condensate wave function.

Gross-Pitaevskii equation

Let us at this point establish the equation that characterizes the condensate wave function. We start with the time evolution of the field operator. By using Heisenberg equations of motion $i\hbar\partial_t\hat{\Psi}(\mathbf{r},t) = [\hat{\Psi}(\mathbf{r},t), \hat{H}]$ and the bosonic commutation rules we get

$$i\hbar\hat{\Psi}(\mathbf{r},t) = \left\{-\frac{\hbar^2\nabla^2}{2m} + V_{\text{ext}}(\mathbf{r}) + \int \mathrm{d}^3r'\,\hat{\Psi}^\dagger(\mathbf{r}',t)V_{\text{int}}(\mathbf{r}-\mathbf{r}')\hat{\Psi}(\mathbf{r},t)\right\}\hat{\Psi}(\mathbf{r},t). \tag{1.3.15}$$

We can then apply the Bogoliubov approximation, and replace the field operators with the condensate wave-function $\Psi(\mathbf{r},t) = \sqrt{N}\psi(\mathbf{r},t)$, neglecting all the other terms. When the interaction potential is governed by short-range contact processes we can use the pseudopotential from Eq. (1.3.10), arriving at the so-called *Gross-Pitaevskii equation* (GPE):

$$i\hbar\frac{\partial\psi(\mathbf{r},t)}{\partial t} = \left(-\frac{\hbar^2\nabla^2}{2m} + V_{\text{ext}}(\mathbf{r}) + gN|\psi(\mathbf{r},t)|^2\right)\psi(\mathbf{r},t). \tag{1.3.16}$$

This non-linear Schrödinger equation, which describes the dynamics of the condensate wave-function, was first derived independently by E. P. Gross and L. P. Pitaevskii in 1961 [Gro61; Pit61].

From the time-dependent equation, we may derive the time-independent GPE that will provide the ground-state of the system. Note that from the definition of mean-field, $\Psi(\mathbf{r},t) = \langle\hat{\Psi}\rangle$. Let us consider the stationary state.

Since in zeroth order we may write $\hat{\Psi} = \psi_0(\mathbf{r})\hat{a}_0$, we should interpret the mean-field as $\Psi(\mathbf{r},t) = \langle(N-1)(t)|\psi_0(\mathbf{r})\hat{a}_0|N(t)\rangle$, where $|N(t)\rangle = e^{-iE(N)t/\hbar}|N(0)\rangle$ is the stationary state for N particles, with energy $E(N)$. Then:

$$\begin{aligned}\Psi(\mathbf{r},t) &= e^{-i[E(N)-E(N-1)]t/\hbar}\langle(N-1)(t=0)|\psi_0(\mathbf{r})\hat{a}_0|N(0)\rangle \\ &= e^{-i\mu t/\hbar}\Psi(\mathbf{r},0),\end{aligned} \tag{1.3.17}$$

where μ is the chemical potential. Hence for the stationary condensate wave function, the phase evolves with the chemical potential, rather than with the energy itself. Plugging $\psi(\mathbf{r}, t) = e^{-i\mu t/\hbar}\psi(\mathbf{r}, 0)$ into Eq. (1.3.18), we obtain the time-independent GPE:

$$\mu\psi(\mathbf{r}) = \left(-\frac{\hbar^2\nabla^2}{2m} + V_{\text{ext}}(\mathbf{r}) + gN|\psi(\mathbf{r})|^2\right)\psi(\mathbf{r}), \qquad (1.3.18)$$

which we will employ to determine the ground-state of the condensate.

1.3.3 Thomas-Fermi regime

When the condensate density, $n(\mathbf{r}) = |\Psi(\mathbf{r})|^2$, varies slowly in space, we may neglect the kinetic energy, since it depends on the Laplacian ∇^2. This is the so-called *Thomas-Fermi regime* (TF regime), that occurs when the interactions are sufficiently large, and quantum pressure can be considered negligible in comparison. The time-independent GPE then reduces to

$$V_{\text{ext}}(\mathbf{r}) + gn(\mathbf{r}) = \mu. \qquad (1.3.19)$$

For a harmonic trap with $V_{\text{ext}} = \frac{1}{2}m\omega^2\mathbf{r}^2$ where ω is the isotropic trapping frequency we get the solution

$$n(\mathbf{r}) = \frac{\mu}{g}\left(1 - \frac{\mathbf{r}^2}{R_{\text{TF}}^2}\right)\Theta(R_{\text{TF}} - |\mathbf{r}|), \qquad (1.3.20)$$

where $R_{\text{TF}}^2 = \frac{2\mu}{m\omega^2}$ is the so-called *Thomas-Fermi radius*, and Θ is the Heaviside step function.

As mentioned above, the TF regime demands sufficiently large interactions. More precisely, we can introduce the idea of *healing length* ξ, as the typical length scale for which quantum pressure would equilibrate the interactions energy:

$$\frac{\hbar^2\left(\frac{1}{\xi}\right)^2}{2m} = gn \qquad \rightsquigarrow \qquad \xi = \frac{\hbar}{\sqrt{2mgn}}. \qquad (1.3.21)$$

This length is the minimum distance over which the condensate wave-function can "heal", meaning that it can adapt to boundary conditions. If $R_{\text{TF}} \gg \xi$, then the quantum pressure, which is proportional to $1/R_{\text{TF}}^2$ will be negligibly small compared to the interaction energy. In turn this means that $\mu \gg \hbar\omega$. These two equivalent conditions define the TF regime.

1.4 Lee-Huang-Yang correction to the condensate energy

As already mentioned, the weakly-interacting regime is typically very well described within mean-field theory. Higher-oder terms resulting from quantum fluctuations are negligibly small, and do not change the qualitative physics. As we will discuss in detail in this Thesis this may change under appropriate conditions. In this section, we derive the first correction to the ground-state energy of the condensate, assuming a three-dimensional system with solely contact interactions.

Let us start with the Hamiltonian of a weakly interacting Boson gas described by Eq. (1.3.12) with no trapping. By assuming a uniform gas in a volume V, we can write down the field operator as a summation over $\mathbf{k}$ in Fourier space,

$$\hat{\Psi}(\mathbf{r}) = \sum_{\mathbf{k}} \frac{e^{i\mathbf{k}\cdot\mathbf{r}}}{(2\pi)^{3/2}\sqrt{V}} \hat{a}_{\mathbf{k}} \,, \qquad (1.4.22)$$

where $\hat{a}_{\mathbf{k}}$ annihilates and $\hat{a}_{\mathbf{k}}^{\dagger}$ creates a particle with momentum $\mathbf{p} = \hbar\mathbf{k}$. These operators follow the bosonic commutation relations. Substituting (1.4.22) into the many-body Hamiltonian we obtain

$$\hat{H} = \sum_{k} \frac{\hbar^2 k^2}{2m} \hat{a}_k^{\dagger} \hat{a}_k + \frac{1}{2V} \sum_{k_1,k_2,q} \tilde{V}_{\text{int}}(\mathbf{q}) \hat{a}_{\mathbf{k}_1+\mathbf{q}}^{\dagger} \hat{a}_{\mathbf{k}_2-\mathbf{q}}^{\dagger} \hat{a}_{\mathbf{k}_2} \hat{a}_{\mathbf{k}_1} \,, \qquad (1.4.23)$$

where $\tilde{V}_{\text{int}}(\mathbf{q})$ is the Fourier-transformed interaction potential. Since only small momenta contribute we use the approximation $\tilde{V}_{\text{int}}(\mathbf{q}) \approx \tilde{V}_{\text{int}}(0) =: \tilde{V}_{\text{int}}$.

We apply the Bogoliubov approximation and replace the $\hat{a}_0^{\dagger}$, $\hat{a}_0$ with $\sqrt{N_0}$, yielding

$$\hat{H} = \hat{H}_{\text{kin}} + \frac{\tilde{V}_{\text{int}}}{2V} \sum_{\mathbf{k}\neq 0} \left(N_0^2 + 4N_0 \hat{a}_{\mathbf{k}}^{\dagger} \hat{a}_{\mathbf{k}} + N_0 \hat{a}_{\mathbf{k}}^{\dagger} \hat{a}_{-\mathbf{k}}^{\dagger} + N_0 \hat{a}_{\mathbf{k}} \hat{a}_{-\mathbf{k}} + \mathcal{O}\big((\hat{a}^{\dagger}\hat{a})^2\big) \right), \qquad (1.4.24)$$

where $\hat{H}_{\text{kin}} = \sum_{\mathbf{k}} \frac{\hbar^2 |\mathbf{k}|^2}{2m} \hat{a}_{\mathbf{k}}^{\dagger} \hat{a}_{\mathbf{k}}$. Note that due to momentum conservation, terms with only one particle operator with $\mathbf{k} \neq 0$ do not contribute to the Hamiltonian. We should remember from Eq. (1.2.3) how N is composed of and rewrite N_0 as $N - \sum_{\mathbf{k}\neq 0} \hat{a}_{\mathbf{k}}^{\dagger} \hat{a}_{\mathbf{k}}$ and hence $N_0^2 = N^2 - 2N \sum_{\mathbf{k}\neq 0} \hat{a}_{\mathbf{k}}^{\dagger} \hat{a}_{\mathbf{k}} + \mathcal{O}\big((\hat{a}^{\dagger}\hat{a})^2\big)$.

In this section we are interested in the first non-vanishing correction to the mean-field energy. This means that we can omit higher order terms. But for the term

with the lowest order we need to incorporate the second-order Born approximation for the potential $V_{\text{int}} = g\left(1 + \frac{g}{V}\sum_{\mathbf{k}\neq 0}\frac{m}{\hbar^2|\mathbf{k}|^2}\right)$. We end up with the following Hamiltonian:

$$\hat{H} = \hat{H}_{\text{kin}} + E_0^{(0)} + \frac{gn}{2}\sum_{\mathbf{k}\neq 0}\left(\frac{mgn}{\hbar^2 k^2} + 2\hat{a}_{\mathbf{k}}^\dagger\hat{a}_{\mathbf{k}} + \hat{a}_{\mathbf{k}}^\dagger\hat{a}_{-\mathbf{k}}^\dagger + \hat{a}_{\mathbf{k}}\hat{a}_{-\mathbf{k}}\right). \qquad (1.4.25)$$

where $E_0^{(0)}/V = \frac{1}{2}gn^2$ is the ground-state energy in first approximation.

Note that the third term is not diagonal and contains terms like $\hat{a}_{\mathbf{k}}^\dagger\hat{a}_{-\mathbf{k}}^\dagger$ and $\hat{a}_{\mathbf{k}}\hat{a}_{-\mathbf{k}}$. We can diagonalize it by introducing the canonical *Bogoliubov transformation* [Bog47]

$$\hat{a}_{\mathbf{k}}^\dagger = u_{\mathbf{k}}\hat{\beta}_{\mathbf{k}}^\dagger + \overline{v_{-\mathbf{k}}}\hat{\beta}_{-\mathbf{k}}, \qquad \hat{a}_{\mathbf{k}} = \overline{u_{\mathbf{k}}}\hat{\beta}_{\mathbf{k}} + v_{-\mathbf{k}}\hat{\beta}_{-\mathbf{k}}^\dagger, \qquad (1.4.26)$$

where the newly introduced $\hat{\beta}^\dagger, \hat{\beta}$ create or annihilate a quasi particle, respectively, and follow the same Bose commutation relation $\left[\hat{\beta}_{\mathbf{k}}, \hat{\beta}_{\mathbf{k}'}^\dagger\right] = \delta_{\mathbf{k},\mathbf{k}'}$ as the real particle operators $\hat{a}^\dagger, \hat{a}$. One can easily check that this implies the condition

$$|u_{\mathbf{k}}|^2 - |v_{-\mathbf{k}}|^2 = 1. \qquad (1.4.27)$$

The problem of finding a diagonalized form of the Hamiltonian is now reduced to the problem of finding the $u_{\mathbf{k}}, v_{\mathbf{k}}$ such that the non-diagonal term vanishes while keeping the condition (1.4.27) fulfilled. Carefully done, this yields [PS04]

$$\hat{H} = E_0^{(0)} + E_0^{(1)} + \sum_{\mathbf{k}}\epsilon(k)\hat{\beta}_{\mathbf{k}}^\dagger\hat{\beta}_{\mathbf{k}}, \qquad (1.4.28)$$

where $\epsilon(k)$ is the *Bogoliubov dispersion law* for *elementary excitations*

$$\epsilon(k) = \left[\frac{\hbar^2 k^2}{2m}\left(\frac{\hbar^2 k^2}{2m} + 2gn\right)\right]^{1/2}. \qquad (1.4.29)$$

For completeness and future reference, the explicit form of the eigenfunctions is [PS04]

$$u_{\mathbf{k}}, v_{-\mathbf{k}} = \pm\left(\frac{\frac{\hbar^2 k^2}{2m} + gn}{2\epsilon(k)} \pm \frac{1}{2}\right). \qquad (1.4.30)$$

The first correction $E_0^{(1)}$ to the condensate energy resulting from quantum fluctuations is hence of the form:

$$\frac{E_0^{(1)}}{V} = \frac{E_{\text{LHY}}}{V} = \frac{1}{2V}\sum_{\mathbf{k}\neq 0}\left(\epsilon(k) - gn - \frac{\hbar^2 k^2}{2m} + \frac{m(gn)^2}{\hbar^2 k^2}\right)$$

$$\xrightarrow[n\text{ fixed}]{N,V\to\infty} \frac{64}{15\sqrt{\pi}}gn^{5/2}a^{3/2}. \qquad (1.4.31)$$

This correction was first derived by Lee, Huang and Yang in 1957 and hence it is called *Lee-Huang-Yang correction* or just *LHY correction* [LHY57]. Note that $E_0^{(1)}/E_0^{(0)} \propto \sqrt{na^3}$, and hence, for dilute weakly-interacting systems, the LHY correction is typically very small compared to the mean-field energy. As we discuss later in this Thesis, this may be remarkably different in both binary Bose mixtures and dipolar gases.

1.5 Local-density approximation

The results from the previous section were derived for a uniform gas and hence are only valid in this rather unrealistic regime. However, one can expect that "locally" it can be applied to "slowly" varying inhomogeneous distributions. The question of the applicability is discussed in the following, based on Ref. [TTH97].

We introduce the spatial-dependent Bogoliubov transformation as a general linear transformation relating the fluctuation operators $\hat{\delta\psi}(\mathbf{r})$, $\hat{\delta\psi}^\dagger(\mathbf{r})$ from Eq. (1.3.14) to the new quasi-particle operators $\hat{\xi}(\mathbf{r})$ and $\hat{\xi}^\dagger(\mathbf{r})$,

$$
\begin{aligned}
\hat{\delta\psi}(\mathbf{r}) &= \int \mathrm{d}^3 r' \left[U(\mathbf{r},\mathbf{r}')\hat{\xi}(\mathbf{r}') - V(\mathbf{r},\mathbf{r}')\hat{\xi}^\dagger(\mathbf{r}') \right], \\
\hat{\delta\psi}^\dagger(\mathbf{r}) &= \int \mathrm{d}^3 r' \left[\overline{U(\mathbf{r},\mathbf{r}')}\hat{\xi}^\dagger(\mathbf{r}') - \overline{V(\mathbf{r},\mathbf{r}')}\hat{\xi}(\mathbf{r}') \right].
\end{aligned}
\tag{1.5.32}
$$

As expected, this transformation is in general non-local. Similarly to Eq. (1.4.27) we require the new quasiparticle operators to be canonical, so we demand for U and V the condition

$$
\int \mathrm{d}^3 \alpha \left[U(\mathbf{r},\boldsymbol{\alpha})U(\boldsymbol{\alpha},\mathbf{r}') - V(\mathbf{r},\boldsymbol{\alpha})V(\boldsymbol{\alpha},\mathbf{r}') \right] = \delta^{(3)}(\mathbf{r} - \mathbf{r}').
\tag{1.5.33}
$$

Since we consider systems, which have sufficiently slow spatial variations, it is helpful to switch to the Wigner representation, which is defined for a function $A(\mathbf{r},\mathbf{r}')$ as [TTH97; Wig32]

$$
A_W(\mathbf{R},\mathbf{k}) = \int \mathrm{d}^3 \bar{r}\, A\left(\mathbf{R} + \frac{\bar{\mathbf{r}}}{2}, \mathbf{R} - \frac{\bar{\mathbf{r}}}{2} e^{\mathrm{i}\mathbf{k}\cdot\bar{\mathbf{r}}} \right).
\tag{1.5.34}
$$

Both of the integrals in Eq. (1.5.33), of the form $C(\mathbf{r},\mathbf{r}') = \int \mathrm{d}^3 \alpha\, U(\mathbf{r},\boldsymbol{\alpha})U(\boldsymbol{\alpha},\mathbf{r}')$,

can be rewritten in terms of a gradient expansion in Wigner representation as

$$
\begin{aligned}
C_W(\mathbf{R}, \mathbf{p}) = U_W(\mathbf{R}, \mathbf{p})^2 \\
- \frac{1}{8} \sum_j \left(\frac{\partial^2 U_W}{\partial R_j^2} \frac{\partial^2 U_W}{\partial p_j^2} + \frac{\partial^2 U_W}{\partial p_j^2} \frac{\partial^2 U_W}{\partial R_j^2} - 2 \frac{\partial^2 U_W}{\partial R_j \partial p_j} \frac{\partial^2 U_W}{\partial R_j \partial p_j} \right) + \cdots .
\end{aligned}
\tag{1.5.35}
$$

Hence, we obtain up to first order in the spatial derivatives a similar constrain as in Eq. (1.4.27)

$$
U_W^2(\mathbf{R}, \mathbf{p}) - V_W^2(\mathbf{R}, \mathbf{p}) \approx 1,
\tag{1.5.36}
$$

leading to the LHY-correction in *local-density approximation*

$$
\frac{E_{\mathrm{LHY}}(\mathbf{r})}{V} = \frac{64}{15\sqrt{\pi}} g n^{5/2}(\mathbf{r}) a^{3/2}.
\tag{1.5.37}
$$

This expression is valid when the main contribution of the LHY correction stems from modes with wavelengths much smaller than the condensate's size, and hence the spatial variation of the density is small over one wavelength of these modes. Hence, it resembles the description of a locally homogeneous system. This condition is always satisfied in the Thomas-Fermi regime [LP11; LP12]. The local-density approximation will be used in the following chapters when deriving an effective equation for the study of both binary mixtures and dipolar condensates.

Part II

Binary Mixtures

Chapter 2

Binary mixtures

Shortly after the first realizations of single-component condensates, scientists moved to the next level of complexity by achieving condensates of two components. There are several ways to achieve a multi-component BEC. It can be built up by different atomic elements or isotopes. Another approach was used in the first dual-component BEC in the group of C. E. Wieman in 1996 [Mya+97], in which ^{87}Rb atoms were condensed into two different hyperfine states. This chapter introduces some important concepts of binary mixtures. The question of stability is addressed in Sec. 2.1 from the mean-field point of view. As in the previous chapter, we extend our discussion beyond mean-field. The derivation of the corresponding LHY correction is presented in Sec. 2.2, whereas the so-called quantum stabilization is discussed in Sec. 2.3. The chapter ends with an overview of the current experimental status in Sec. 2.4.

2.1 Mean-field stability of a binary Bose mixture

In order to properly describe two-body contact interactions in gases with two or more components, we introduce the coupling constants $g_{ii} = \frac{4\pi\hbar^2 a_{ii}}{m_i}$ and $g_{ij} = \frac{4\pi\hbar^2 a_{ij}}{m_{ij}}$ with $i \neq j$ where m_{ij} is the reduced mass of m_i and m_j, and a_{ij} is the corresponding scattering length.

Let us consider a homogeneous binary Bose system with densities n_1 and n_2. The free energy density is of the form [Tim98]

$$F = \frac{1}{2}g_{11}n_1^2 + \frac{1}{2}g_{22}n_2^2 + g_{12}n_1 n_2 - \mu_1 n_1 - \mu_2 n_2. \tag{2.1.1}$$

To find stable solutions, the free energy density needs to have a minimum. The derivative of F with respect to the densities needs to be zero, which demands

$$\begin{aligned}
\mu_1 &= g_{11}n_1 + g_{12}n_2, \\
\mu_2 &= g_{22}n_2 + g_{12}n_1.
\end{aligned} \tag{2.1.2}$$

Since it should be a minimum, both eigenvalues of the corresponding Jacobian matrix $\frac{\partial^2 F}{\partial n_i \partial n_2}$ should be positive. This demands that the trace is positive, i.e.

$$\frac{\partial^2 F}{\partial n_1^2} + \frac{\partial^2 F}{\partial n_2^2} = g_{11} + g_{22} > 0 \tag{2.1.3}$$

and the determinant of the Jacobian matrix is also positive, i.e.

$$\left(\frac{\partial^2 F}{\partial n_1^2}\right)\left(\frac{\partial^2 F}{\partial n_2^2}\right) - \left(\frac{\partial^2 F}{\partial n_1 \partial n_2}\right)^2 = g_{11}g_{22} - g_{12}^2 > 0. \tag{2.1.4}$$

Equations (2.1.3) and (2.1.4) determine the conditions under which the binary mixture reaches a stable ground state. Note that instability may occur due to two different reasons, either the mixture becomes unstable against collapse, or against spatial phase separation.

2.2 Lee-Huang-Yang correction of a binary mixture

Let us consider both $g_{11}, g_{22} > 0$. As discussed in the previous section, one expects a stable homogeneous system if $|g_{12}| < \sqrt{g_{11}g_{22}}$. This however just concerns mean-field stability, since the free energy (2.1.1) was obtained in the mean-field approximation. As we will discuss in this and the next section, the effects of quantum fluctuations may become surprisingly relevant in the vicinity of the stability threshold (against collapse) $g_{12} \approx -\sqrt{g_{11}g_{22}}$. In this section, we discuss in detail the derivation of the LHY correction.

We consider in the following a homogeneous binary mixture. Let $\hat{\Psi}_1^\dagger, \hat{\Psi}_1$ be the creation/annihilation operators for component 1, and $\hat{\Psi}_2^\dagger, \hat{\Psi}_2$ be those for

component 2. They need to follow the usual bosonic commutation relations $\left[\hat{\Psi}_i^\dagger(\mathbf{r}), \hat{\Psi}_j^\dagger(\mathbf{r}')\right] = \left[\hat{\Psi}_i(\mathbf{r}), \hat{\Psi}_j(\mathbf{r}')\right] = 0$ and $\left[\hat{\Psi}_i^\dagger(\mathbf{r}), \hat{\Psi}_j(\mathbf{r}')\right] = \delta_{ij}\delta^{(3)}(\mathbf{r} - \mathbf{r}')$. In second quantization, the Hamiltonian for the binary system acquires the form:

$$\hat{H} = \int \mathrm{d}^3 r \left\{ \hat{\Psi}_1^\dagger \hat{h}_1 \hat{\Psi}_1 + \hat{\Psi}_2^\dagger \hat{h}_2 \hat{\Psi}_2 + \frac{1}{2} \sum_{i,j \in \{1,2\}} g_{ij} \hat{\Psi}_i^\dagger \hat{\Psi}_j^\dagger \hat{\Psi}_i \hat{\Psi}_j \right\} \tag{2.2.5}$$

where $\hat{h}_i = \frac{-\hbar^2}{2m_i}\nabla^2$ is the single-particle Hamiltonian for component i.

We may now Fourier-transform both field operators, expressing them in terms of the corresponding bosonic operators in momentum space, $\hat{a}_{\mathbf{k},i}$ and $\hat{a}_{\mathbf{k},i}^\dagger$. We may then re-write the Hamiltonian in the form:

$$\hat{H} = \sum_{i,\mathbf{k}} \hat{a}_{\mathbf{k},i}^\dagger \frac{\hbar^2 k^2}{2m_i} \hat{a}_{\mathbf{k},i} + \frac{1}{2V} \sum_{i,j} \left\{ g_{ij} \sum_{\mathbf{k}_1,\mathbf{k}_2,\mathbf{q}} \left(\hat{a}_{\mathbf{k}_1+\mathbf{q},i}^\dagger \hat{a}_{\mathbf{k}_2-\mathbf{q},j}^\dagger \hat{a}_{\mathbf{k}_2,j} \hat{a}_{\mathbf{k}_1,i} \right) \right\}. \tag{2.2.6}$$

We use the Bogoliubov approximation, i.e. $\hat{a}_{0,i}^\dagger, \hat{a}_{0,i} \cong N_{0,i}$, where $N_{0,i}$ is the number of condensed particles of type i. Developing up to second-order, and taking into account that up to that order

$$\hat{a}_{0,i}^\dagger \hat{a}_{0,j}^\dagger \hat{a}_{0,j} \hat{a}_{0,i} \cong N_{0,i} N_{0,j} \cong N_i N_j - N_j \sum_{\mathbf{k} \neq 0} \hat{a}_{\mathbf{k},i}^\dagger \hat{a}_{\mathbf{k},i} - N_i \sum_{\mathbf{k} \neq 0} \hat{a}_{\mathbf{k},j}^\dagger \hat{a}_{\mathbf{k},j}, \tag{2.2.7}$$

we obtain the Hamiltonian

$$\begin{aligned}
\hat{H} = {}& \sum_{i,\mathbf{k}} \hat{a}_{\mathbf{k},i}^\dagger \frac{\hbar^2 k^2}{2m_i} \hat{a}_{\mathbf{k},i} + \frac{1}{2V} \sum_{i,j} \left\{ g_{ij} N_{ij}^2 \right. \\
& \left. + g_{ij} \sum_{\mathbf{k}_1,\mathbf{k}_2,\mathbf{q}} \left(N_{ij} \hat{a}_{\mathbf{k},i}^\dagger \hat{a}_{\mathbf{k},j} + N_{ij} \hat{a}_{\mathbf{k},j}^\dagger \hat{a}_{\mathbf{k},i} + N_{ij} \hat{a}_{\mathbf{k},i}^\dagger \hat{a}_{-\mathbf{k},j}^\dagger + N_{ij} \hat{a}_{\mathbf{k},i} \hat{a}_{-\mathbf{k},j} \right) \right\},
\end{aligned}$$
$$\tag{2.2.8}$$

where $N_{ij} = \sqrt{N_i N_j}$.

In the following, we want to diagonalize the Hamiltonian, which is clearly not in a diagonal form because of the off-diagonal terms, like $\hat{a}_{\mathbf{k},i}^\dagger \hat{a}_{-\mathbf{k},j}^\dagger$. In 1963 D. Larsen first applied a transformation in which the two components were unmixed in a new set of operators. Then, a similar diagonalization as for a single-component may be applied for the two blocks of the remaining matrix [Lar63].

We use here the Bogoliubov transformation directly:

$$\hat{a}_{\mathbf{k},i} = u_{\mathbf{k},i} \hat{\beta}_{\mathbf{k},i} + \overline{v_{\mathbf{k},i}} \hat{\beta}_{-\mathbf{k},i}^\dagger, \qquad \hat{a}_{\mathbf{k},i}^\dagger = \overline{u_{\mathbf{k},i}} \hat{\beta}_{\mathbf{k},i}^\dagger + v_{\mathbf{k},i} \hat{\beta}_{-\mathbf{k},i}. \tag{2.2.9}$$

We then introduce the operators

$$\hat{\gamma}_{\mathbf{k}}^{\dagger} = \hat{\beta}_{\mathbf{k},1}^{\dagger} + \hat{\beta}_{\mathbf{k},2}^{\dagger} = \sum_i \left(u_{\mathbf{k},i} \hat{a}_{\mathbf{k},i}^{\dagger} - v_{\mathbf{k},i} \hat{a}_{-\mathbf{k},i} \right), \qquad (2.2.10)$$

demanding the commutation relation

$$[\hat{\gamma}_{\mathbf{k}}, \hat{\gamma}_{\mathbf{k}'}^{\dagger}] = \delta_{k,k'}, \qquad (2.2.11)$$

which results in

$$\sum_i \left(|u_{\mathbf{k},i}|^2 - |v_{\mathbf{k},i}|^2 \right) = 1. \qquad (2.2.12)$$

For each $\mathbf{k}$ and a certain set of $u_{\mathbf{k},i}$ and $v_{\mathbf{k},i}$, the cross-terms like $\hat{\beta}_{\mathbf{k},i}^{\dagger} \hat{\beta}_{-\mathbf{k},j}$ vanish and the Hamiltonian is in its diagonal form, i.e.

$$\hat{H} = E^{(0)} + E_{\mathrm{LHY}} + \sum_{\pm} \sum_{\mathbf{k}} \varepsilon_{\pm}(k) \hat{\gamma}_{\mathbf{k},\pm}^{\dagger} \hat{\gamma}_{\mathbf{k},\pm}. \qquad (2.2.13)$$

The energies $\varepsilon_{\pm}(k)$ and the LHY correction E_{LHY} can be easily obtained from the Heisenberg equation of the new quasi-particle operators:

$$i\hbar \partial_t \hat{\gamma}_{\mathbf{k},i} = \varepsilon_k \hat{\gamma}_{\mathbf{k},i} = \sum_i \left(u_{\mathbf{k},i} \left[\hat{a}_{\mathbf{k},i}, \hat{H} \right] - v_{\mathbf{k},i} \left[\hat{a}_{-\mathbf{k},i}^{\dagger}, \hat{H} \right] \right). \qquad (2.2.14)$$

Sorting the terms with respect to their operators $\hat{a}_{\mathbf{k},i}^{\dagger}, \hat{a}_{\mathbf{k},i}$ we get the four *Bogoliubov-de Gennes* equations

$$\begin{cases} \varepsilon_k u_{\mathbf{k},i} = \sum_j \left\{ \left(\delta_{ij} \frac{\hbar^2 k^2}{2m_i} + g_{ij} \sqrt{n_i n_j} \right) u_{\mathbf{k},i} + g_{ij} \sqrt{n_i n_j} v_{\mathbf{k},i} \right\} \\ -\varepsilon_k v_{\mathbf{k},i} = \sum_j \left\{ \left(\delta_{ij} \frac{\hbar^2 k^2}{2m_i} + g_{ij} \sqrt{n_i n_j} \right) v_{\mathbf{k},i} + g_{ij} \sqrt{n_i n_j} u_{\mathbf{k},i} \right\} \end{cases} \qquad (2.2.15)$$

After a cumbersome, but straightforward, calculation, one may obtain the two excitation branches [Pet15]

$$\varepsilon_{\pm}(k) = \sqrt{ \frac{\epsilon_1^2(k) + \epsilon_2^2(k)}{2} \pm \sqrt{ \frac{(\epsilon_1^2(k) - \epsilon_2^2(k))^2}{4} + \frac{g_{12}^2 n_1 n_2 k^4}{m_1 m_2} } }, \qquad (2.2.16)$$

where $\epsilon_i(k) = \sqrt{ \frac{\hbar^2 k^2}{2m_i} \left(\frac{\hbar^2 k^2}{2m_i} + 2g_{ii} n_i \right) }$ is the dispersion relation for a single-component condensate, obtained in Chapter 1. With the solution of the Bogoliubov coefficients $u_{\mathbf{k},i}$ and $v_{\mathbf{k},i}$, and considering the second Born-approximation correction to

the coupling constants, we may obtain the LHY correction

$$\frac{E_{\text{LHY}}}{V} = \int \frac{\mathrm{d}^3 k}{(2\pi)^3} \frac{1}{2} \left(\varepsilon_+(k) + \varepsilon_-(k) - \frac{\hbar^2 k^2}{m_{12}} - g_{11} n_1 - g_{22} n_2 \right.$$

$$\left. + \frac{m_1 g_{11}^2 n_1^2 + m_2 g_{22}^2 n_2^2 + 2 m_{ij} g_{ij}^2 n_1 n_2}{k^2} \right) \tag{2.2.17}$$

$$= \frac{8}{15\pi^2} \left(\frac{m_1}{\hbar^2} \right)^{3/2} (g_{11} n_1)^{5/2} f\left(z = \frac{m_2}{m_1}, x = \frac{g_{12}^2}{g_{11} g_{22}}, y = \frac{g_{22} n_2}{g_{11} n_1} \right) \tag{2.2.18}$$

where $f(z, x, y) > 0$ is a dimensionless function.

2.2.1 Analytic expressions for different cases

Although no general analytical expression for $f(z, x, y)$ is known, there are particularly relevant cases in which one may obtain a closed expression.

Equal scattering lengths   The first one was described by D. M. Larsen for the case where all scattering lengths are equal and positive, i.e. $a_{11} = a_{12} = a_{22} > 0$, and where the heavy component has a much lower density than the light component, i.e. $z > 1$ and $y \ll 1$. The condition of equal scattering lengths is equivalent to $x = \frac{(1+z)^2}{4z}$ [Lar63].

$$f\left(z, \frac{(1+z)^2}{4z}, y \right)\bigg|_{z<1, y\ll 1} = 1 + y \frac{15}{16} \frac{z+1}{z-1} \left[\frac{z^2}{\sqrt{z^2-1}} \arctan(\sqrt{z^2-1}) - 1 \right]. \tag{2.2.19}$$

Since the LHY correction does not depend on a_{12} but rather on a_{12}^2 it can be extended to negative values of a_{12} as well.

At mean-field instability   Another approach is not to solve the integral from (2.2.17) directly, but rather try to find an analytic expression that describes the behavior good enough. This was done by F. Minardi *et al.* in 2019 [Min+19]. They considered the MF-stability threshold, $g_{12}^2 = g_{11} g_{22}$, and found an expression that converges for both extrema $y \ll 1$ and $y \gg 1$ to the single-component LHY correction.

$$f(z, 1, y) \approx \left(1 + z^{3/5} y \right)^{5/2}. \tag{2.2.20}$$

For a mass imbalance of $z = 41/87 \approx \frac{1}{2}$ the relative error is at most 4%.

Equal masses Another interesting and very important case where we can get an analytic expression is when all masses are equal. D. Petrov derived the LHY term for $m := m_1 = m_2$ in 2015 [Pet15]

$$f(1, x, y) = \frac{1}{2^{5/2}} \sum_{\pm} \left(1 + y \pm \sqrt{(1 - y)^2 + 4xy} \right)^{5/2}. \qquad (2.2.21)$$

This case turns out to be particularly relevant for experiments, as discussed below.

2.2.2 Extended Gross-Pitaevskii equations

In the previous section we have discussed the LHY correction for an homogeneous binary mixture. Following similar arguments as those discussed in Sec. 1.5, we may use the knowledge of the previous section to study in local-density approximation the effects of quantum fluctuations for an inhomogeneous condensate, obtaining the local LHY energy. As in the discussion of Sec. 1.5 this is typically motivated by the fact that the momenta that contribute at most to the LHY correction are actually much larger than the inverse of the typical spatial scale of the density variation of the condensate. We add the local LHY energy to the energy functional, and then obtain a set of two coupled modified Gross-Pitaevskii equations, which we call in the following extended Gross-Pitaevskii equations (eGPEs):

$$\mu \psi_1(\mathbf{r}) = \left(-\frac{\hbar^2 \nabla^2}{2m} + V_{\text{ext}}(\mathbf{r}) + g_{11} N_1 |\psi_1(\mathbf{r})|^2 + g_{12} N_2 |\psi_2(\mathbf{r})|^2 \right.$$
$$\left. + \mu_1^{\text{LHY}} \left[|\psi_{1,2}(\mathbf{r})|^2 \right] \right) \psi_1(\mathbf{r})$$
$$\qquad (2.2.22)$$
$$\mu \psi_2(\mathbf{r}) = \left(-\frac{\hbar^2 \nabla^2}{2m} + V_{\text{ext}}(\mathbf{r}) + g_{22} N_2 |\psi_2(\mathbf{r})|^2 + g_{12} N_1 |\psi_1(\mathbf{r})|^2 \right.$$
$$\left. + \mu_2^{\text{LHY}} \left[|\psi_{1,2}(\mathbf{r})|^2 \right] \right) \psi_2(\mathbf{r}),$$

were we note the presence of the LHY local chemical potential $\mu_i^{\text{LHY}}[n_{1,2}] = \frac{\mathrm{d}}{\mathrm{d}n_i} \frac{E_{\text{LHY}}}{V}[n_{1,2}]$, evaluated in local-density approximation.

2.3 Quantum stabilization

Let us come back to the stability discussion from Sec. 2.1. The mean-field instability condition $g_{12}^2 < g_{11}g_{22}$ gives us two possible values of g_{12} for the stability threshold, corresponding to the above-mentioned instability against collapse and against phase separation. In the following, we concentrate on the regime around the negative one, i.e. $|g_{12}|^2 \approx g_{11}g_{22}$ and $g_{12} < 0$, i.e. at the instability against collapse. An equivalent formulation is that the value $\delta g = g_{12} + \sqrt{g_{11}g_{22}} \approx 0$. We assume that $\delta g < 0$, and hence the system will collapse in mean-field. The mean-field energy density can be written in the form:

$$\frac{E^{\mathrm{MF}}}{V} = \lambda_+ n_+^2 + \lambda_- n_-^2, \tag{2.3.23}$$

with

$$\lambda_+ \simeq \frac{g_{11} + g_{22}}{2}, \qquad \lambda_- \simeq \frac{\delta g \sqrt{g_{11}g_{22}}}{g_{11} + g_{22}}, \tag{2.3.24}$$

and

$$
\begin{aligned}
n_+ &= \frac{n_1\sqrt{g_{22}} - n_2\sqrt{g_{11}}}{\sqrt{g_{11} + g_{22}}}, \\
n_- &= \frac{n_1\sqrt{g_{11}} + n_2\sqrt{g_{22}}}{\sqrt{g_{11} + g_{22}}}.
\end{aligned}
\tag{2.3.25}
$$

Note that λ_- is small and negative. In contrast $\lambda_+ > 0$ and potentially much larger. It is hence energetically favorable for the system to minimize n_+^2 and maximize n_-^2. This implies increasing both densities, while keeping a constant polarization $P = \frac{n_2}{n_1} = \sqrt{\frac{g_{11}}{g_{22}}}$. We may then write the mean-field energy density in the form:

$$\frac{E^{\mathrm{MF}}}{V} = \delta g \, \frac{P}{(1+P)^2} n^2, \tag{2.3.26}$$

with $n = n_1 + n_2$ the overall density. Note that the mixture hence behaves as a single-component condensate with a negative coupling constant $\propto \delta g$.

As it is known from single-component condensates, a negative coupling constant eventually leads to a collapse unless there is a second repulsive term preventing it. For a small number of particles in a harmonic trap this can be the quantum pressure, but since it scales linearly with the number of particles and the contact interaction term scales quadratically, the latter drives the collapse for large N.

Interestingly, quantum fluctuations may prevent the collapse of the mixture. Recall that the LHY correction (2.2.18) is repulsive and scales as $n^{5/2}$, i.e. steeper than the mean-field n^2 scaling.

Note as well that in the vicinity of the mean-field instability threshold, the mean-field energy, which is proportional to δg, is very small. Crucially, the LHY energy does not have the same dependence with the coupling constants as the mean-field term. As a result, whereas for a single-component condensate the ratio between LHY correction and mean-field energy is always very small, this is not any more the case in a binary mixture, in which the LHY term may become comparable to the mean-field energy. Note that, crucially, this relies on the competition of intra- and inter-component interactions, which quasi-cancel the mean-field term. We will see later on in this Thesis, that a similar quasi-cancellation occurs as well in single-component dipolar condensates.

When the mean-field term drives the collapse, the density n grows, but this increases the LHY repulsion more than the mean-field attraction. As a result, there is an optimal density n_{opt} at which the overall energy (mean-field plus LHY) is minimal. Note, however, that this density could be large. Large densities favor three-body losses, and hence reduce the lifetime. This is a relevant point for experiments, as discussed below.

Interestingly, the interplay between mean-field attraction and LHY repulsion allows for a self-bound cloud, a so-called *quantum droplet*, which constitutes a peculiar new type of ultra-dilute quantum liquid. Note also that the optimal density is fixed for a given set of interaction strengths. Once the number of particles in the system is large enough to reach this optimal density, further particles will be added at the surface, increasing the droplet size, keeping the density fixed, and a flat-top density profile, as that shown in Fig. 2.1, forms.

2.4 Experimental realizations

In 2017 the groups of L. Tarruell [Cab+18] at ICFO (Barcelona) and M. Fattori [Sem+18] at LENS (Florence) independently realized the regime of quantum stabilization in a homonuclear mixture of ^{39}K in the two different hyperfine states $|F = 1, m_F = 0\rangle =: |1\rangle$ and $|F = 1, m_F = -1\rangle =: |2\rangle$. Subsequently, it was also shown in heteronuclear mixtures of ^{41}K and ^{87}Rb [DEr+19; Bur+20] and also in a mixture of ^{23}Na and ^{87}Rb [Guo+20].
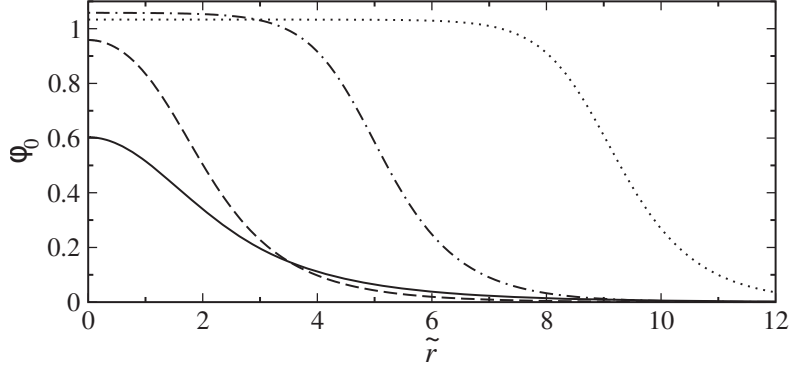
Figure 2.1: Droplet wave-function for various particle numbers with respect to the rescaled radial distance $\tilde{r} = r/\xi$ with $\xi = \sqrt{\frac{3}{2} \frac{\sqrt{g_{22}/m_1} + \sqrt{g_{22}/m_2}}{|\delta g|^2 \sqrt{g_{11}} n_1^{\text{peak}}}}$ where n_1^{peak} is the peak density of component 1. Note that when a sufficiently large number of particles is surpassed, additional particles do not increase the density, but are rather added at the condensate wings, keeping the central density fixed, as determined by the interplay between the mean-field and LHY energies. As a result a flat-top profile forms. Reprinted from [Pet15]
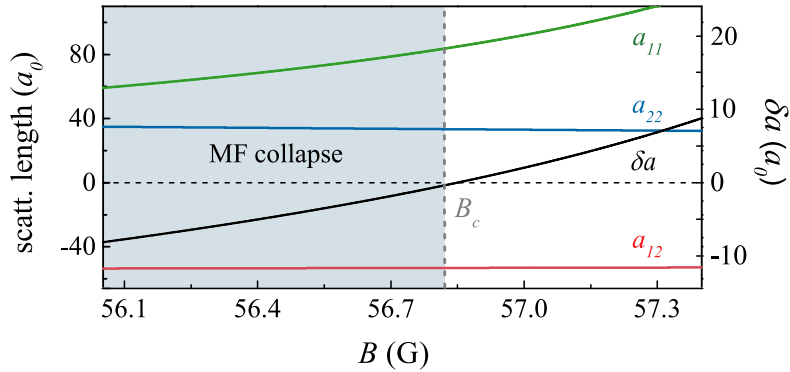
Figure 2.2: Scattering lengths a_{11} (green), a_{22} (blue) and a_{12} (red) (left scale) for the ^{39}K experiments discussed in the text. On the right scale are the values for the scattering δa. Both are in multiples of the Bohr radius a_0 and are plotted against the applied magnetic field B in Gauss. The vertical dashed line at $B_c = 56.85$ G separates the MF-stable regime $\delta a > 0$ (right white area) from the MF-unstable one $\delta a < 0$ (left grey area). Reprinted from [Sem+18].

27
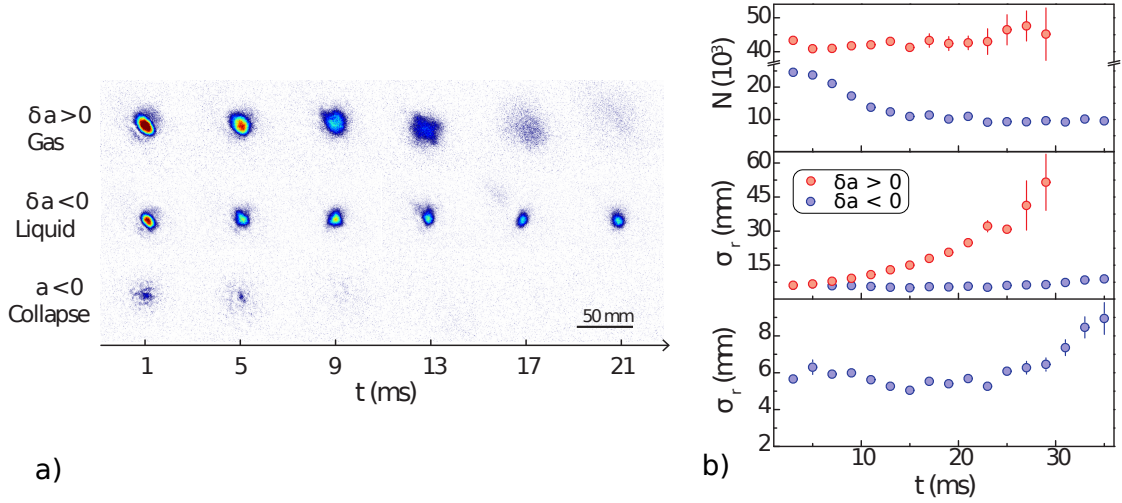
Figure 2.3: a) Images of the ^{39}K experiments at different times t for different values of δa. The top row shows the expansion of a gaseous mixture for a repulsive δa. In the central row one sees a self-bound mixture droplet. The bottom row shows the collapse of an attractive single-component system in the $|1\rangle$ state. b) Time evolution of the number of particles (top row) and system width (center and bottom row). The blue (red) points correspond to the droplet (gaseous) case. After around 25 ms the droplet lost so many particles such that it enters the gaseous state and spreads in space. Adapted from [Cab+18].

We focus in the following in the above-mentioned homonuclear ^{39}K experiments. Since both masses are hence equal, we only consider the scattering lengths, rather than the coupling constants (and instead of δg we consider the corresponding δa). At a magnetic field $B_{\mathrm{crit}} = 56.85\,\mathrm{G}$, a_{11} presents a Feshbach resonance, whereas a_{12} and a_{22} are basically constant at around $-53\,a_0$ and $33\,a_0$, respectively (see Fig. 2.2). Note that there is a window around $B = 56.7 - 56.8\,\mathrm{G}$ at which $\delta a < 0$ and small.

In the experiments, they first prepared the system in the $|2\rangle$ state in the MF-stable regime. By applying an RF-pulse, half of the mixture was transferred to the $|1\rangle$ state, following a ramp of the magnetic field to the desired value of δa. Finally, the traps, which were necessary in the MF-regime for the preparation, were switched off except for the confinement that compensated gravity.

The cloud was imaged in-situ at different times t after the removal of the radial trap and scattering lengths, see Fig. 2.3. For experiments in the mean-field stable regime with $\delta a > 0$ (top row) one sees a steady expansion of the width. This is
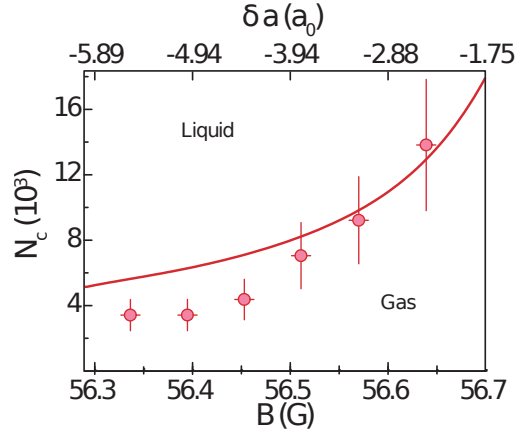
Figure 2.4: Liquid-to-gas phase diagram in the experiments. The figure shows the critical number of particles N_c as a function of the magnetic field (lower horizontal axis) or δa (upper horizontal axis). The solid line is the prediction of the extended Gross-Pitaevskii model. Adapted from [Cab+18].

the expected behavior of an un-trapped gas. In the parameter regime of small but negative δa (central row) we can see that the system does not expand, as expected for a self-bound quantum droplet. For comparison, in the case of a single-component system in $|1\rangle$, the collapse for an attractive scattering length is depicted in the bottom row.

Figure 2.3 (blue dots) shows the time evolution of the width for the droplet case, i.e. $\delta a < 0$. The width remains constant for approximately $20\,\text{ms}$. However, for a longer time, the droplet increases its radial width. This is due to a constantly decreasing particle number as a result of three-body losses, which, as already mentioned, play an important role at the relatively large densities of the quantum droplet. With the reduced particle number, the quantum pressure at the droplet border gains in importance, and eventually drives the expansion. This expansion characterizes a liquid-to-gas transition at a critical number of particles N_{crit}. Figure 2.4 depicts this transition for different values of δa. The solid line is inferred from solving the eGPEs from Eq. (2.2.2).

Chapter 3

Hugenholtz-Pines formalism

In the previous chapter, when deriving the LHY correction to the mean-field term, one faces an ultraviolet divergence which arises from the approximated relation between the coupling constant g and the s-wave scattering length a in the first Born approximation $g = \frac{4\pi\hbar^2 a}{m}$. This was solved by a proper renormalization of the coupling constant $g \to g(1 + g/V \sum_k m/(\hbar k)^2)$. The sum over momentum is then easily turned into an integral, which gave us an analytic result in the thermodynamic limit.

In this Chapter we explore a different approach, free of divergences, based on the idea of propagators and Green's functions which are known from quantum field theory. If not otherwise stated, the following derivation follows closely the publication by N. M. Hugenholtz and D. Pines from 1959 [HP59], which in turn makes use of a publication by S. T. Beliaev [Bel58], published one year earlier. This approach will be used in the case of a mixture of three components in Chapter 4, and it is crucial in the derivation of the LHY for quasi-one-dimensional dipolar systems in Chapter 7.

The chapter starts with a short discussion on the problems of the depletion of a condensate in Sec. 3.1. In Sec. 3.2 the Green's function is introduced, which eventually leads to the derivation of a general differential equation describing any higher order term. For simplicity we restrict ourselves for this derivation to the single component case. At the end, we briefly discuss the changes that need to be done for the mixture case. This derivation concludes in Sec. 3.3 with a quick

validity check by recovering the same expression of Sec. 1.4. The chapter closes in Sec. 3.4 with a discussion of the usefulness and the actual power of this method.

3.1 Hamiltonian

As in Chapter 1, we consider a system of N interacting bosons in a d-dimensional box of size V. The Hamiltonian can be written as the sum of the non-interacting $\hat{H}_0$ and the interacting $\hat{V}_{\text{int}}$ component, $\hat{H} = \hat{H}_0 + \hat{V}_{\text{int}}$, where $\hat{V}_{\text{int}}$ is defined as in (1.4.23). We move to the thermodynamic limit by introducing a continuous version of the annihilation and creation operators,

$$\hat{c}_{\mathbf{k}}^{\dagger} = \frac{1}{\sqrt{V(2\pi)^d}}\hat{a}_{\mathbf{k}}^{\dagger}, \qquad \hat{c}_{\mathbf{k}} = \frac{1}{\sqrt{V(2\pi)^d}}\hat{a}_{\mathbf{k}}. \tag{3.1.1}$$

These new operators fulfill the usual bosonic commutation relations

$$[\hat{c}_{\mathbf{k}}^{\dagger}, \hat{c}_{\mathbf{l}}^{\dagger}] = [\hat{c}_{\mathbf{k}}, \hat{c}_{\mathbf{l}}] = 0, \qquad [\hat{c}_{\mathbf{k}}, \hat{c}_{\mathbf{l}}^{\dagger}] = \delta^{(d)}(\mathbf{k} - \mathbf{l}). \tag{3.1.2}$$

The interaction part is then

$$\hat{V}_{\text{int}} = \frac{1}{4}\frac{1}{(2\pi)^d}\int_{\mathbf{k}_1,\mathbf{k}_2,\mathbf{k}_3,\mathbf{k}_4} \left(\tilde{V}_{\text{int}}(\mathbf{k}_1 - \mathbf{k}_3) + \tilde{V}_{\text{int}}(\mathbf{k}_1 - \mathbf{k}_4)\right)\delta^{(d)}(\mathbf{k}_1 + \mathbf{k}_2 - \mathbf{k}_3 - \mathbf{k}_4)$$
$$\times \hat{c}_{\mathbf{k}_1}^{\dagger}\hat{c}_{\mathbf{k}_2}^{\dagger}\hat{c}_{\mathbf{k}_3}\hat{c}_{\mathbf{k}_4}. \tag{3.1.3}$$

Since for our bosonic system the condensed part with $k = 0$ is special and macroscopically populated, we split it from the rest, as it was done in previous chapters. The Hamiltonian then reads

$$\hat{H} = \hat{H}_0 + \hat{V}_0 + \sum_{i=1}^{6}\hat{V}_i \tag{3.1.4}$$

where

$$V_0 = \frac{1}{2}\frac{1}{(2\pi)^d}\frac{(\hat{a}_0^{\dagger})^2\hat{a}_0^2}{V^2}(2\pi)^{2d}\delta^{(3)}(0)V_{\text{int}}(0)$$
$$V_1 = \frac{1}{4}\frac{1}{(2\pi)^d}\int_{\mathbf{k}_1,\mathbf{k}_2,\mathbf{k}_3,\mathbf{k}_4 \neq 0}\left(\tilde{V}_{\text{int}}(\mathbf{k}_1 - \mathbf{k}_3) + \tilde{V}_{\text{int}}(\mathbf{k}_1 - \mathbf{k}_4)\right)\delta^{(d)}(\mathbf{k}_1 + \mathbf{k}_2 - \mathbf{k}_3 - \mathbf{k}_4)$$
$$\times \hat{c}_{\mathbf{k}_1}^{\dagger}\hat{c}_{\mathbf{k}_2}^{\dagger}\hat{c}_{\mathbf{k}_3}\hat{c}_{\mathbf{k}_4}$$

$$V_2 = \frac{1}{2}\frac{1}{(2\pi)^{d/2}}\frac{\hat{a}_0}{\sqrt{V}}\int_{\mathbf{k}_1,\mathbf{k}_2,\mathbf{k}_3 \neq 0}\left(\tilde{V}_{\text{int}}(\mathbf{k}_1) + \tilde{V}_{\text{int}}(\mathbf{k}_2)\right)\delta^{(d)}(\mathbf{k}_1 + \mathbf{k}_2 - \mathbf{k}_3)\hat{c}_{\mathbf{k}_1}^\dagger\,\hat{c}_{\mathbf{k}_2}^\dagger\,\hat{c}_{\mathbf{k}_3}$$

$$V_3 = \frac{1}{2}\frac{1}{(2\pi)^{d/2}}\frac{\hat{a}_0^\dagger}{\sqrt{V}}\int_{\mathbf{k}_2,\mathbf{k}_3,\mathbf{k}_4 \neq 0}\left(\tilde{V}_{\text{int}}(\mathbf{k}_3) + \tilde{V}_{\text{int}}(\mathbf{k}_4)\right)\delta^{(d)}(\mathbf{k}_2 + \mathbf{k}_3 - \mathbf{k}_4)\hat{c}_{\mathbf{k}_2}^\dagger\,\hat{c}_{\mathbf{k}_3}\,\hat{c}_{\mathbf{k}_4}$$

$$V_4 = \frac{1}{4}\frac{\hat{a}_0^2}{V}\int_{\mathbf{k}_1,\mathbf{k}_2 \neq 0}\left(\tilde{V}_{\text{int}}(\mathbf{k}_1) + \tilde{V}_{\text{int}}(\mathbf{k}_2)\right)\delta^{(d)}(\mathbf{k}_1 + \mathbf{k}_2)\hat{c}_{\mathbf{k}_1}^\dagger\,\hat{c}_{\mathbf{k}_2}^\dagger$$

$$V_5 = \frac{1}{4}\frac{(\hat{a}_0^\dagger)^2}{V}\int_{\mathbf{k}_3,\mathbf{k}_4 \neq 0}\left(\tilde{V}_{\text{int}}(\mathbf{k}_3) + \tilde{V}_{\text{int}}(\mathbf{k}_4)\right)\delta^{(d)}(\mathbf{k}_3 + \mathbf{k}_4)\hat{c}_{\mathbf{k}_3}\,\hat{c}_{\mathbf{k}_4}$$

$$V_6 = \frac{\hat{a}_0^\dagger\hat{a}_0}{V}\int_{\mathbf{k}_2,\mathbf{k}_3 \neq 0}\left(\tilde{V}_{\text{int}}(\mathbf{k}_2) + \tilde{V}_{\text{int}}(0)\right)\delta^{(d)}(\mathbf{k}_2 - \mathbf{k}_3)\hat{c}_{\mathbf{k}_2}^\dagger\,\hat{c}_{\mathbf{k}_3} \tag{3.1.5}$$

As in previous chapters, we apply the Bogoliubov approximation, and treat the annihililation and creation operators of zero momentum as a c-number $\sqrt{N_0}$. This modifies the Hamiltonian to one that depends on the density n_0 of the condensated part, i.e. $\hat{H} \rightarrow \hat{H}(n_0) = \hat{H}_0 + \hat{V}_{\text{int}}(n_0)$. By removing this special state of $k = 0$ from the problem we violate particle number conservation. In particular this means that the new Hamiltonian does not commute with the particle operator $\hat{N}$ anymore. We need to impose the system to conserve on average the number of particles, i.e. $N = N_0 + \langle \hat{N}' \rangle$, where $\hat{N}' = \sum_{k>0} \hat{a}_{\mathbf{k}}^\dagger \hat{a}_{\mathbf{k}}$.

An alternative to solving the Hamiltonian with the additional imposed relation is to introduce the Hamiltonian

$$\hat{K}(n_0) = \hat{H}(n_0) - \mu\hat{N}' \tag{3.1.6}$$

$$= \int \frac{\mathrm{d}^d k}{(2\pi)^d}\frac{\hbar^2 k^2}{2m}\hat{c}_{\mathbf{k}}^\dagger\,\hat{c}_{\mathbf{k}} + \sum_{i=0}^6 V(n_0) - \mu\hat{N}' \tag{3.1.7}$$

where $\mu = \frac{\mathrm{d}}{\mathrm{d}n}\frac{E_0}{V}$ is the chemical potential and acts as an Lagrange multiplier to minimize the energy of the system.

3.2 Green's function

Up to now, the derivation is very similar to the one in the previous chapters. But instead of proceeding with the Bogoliubov transformation we use a way closer to quantum field theory. We define the *one-particle Green's function*, or *propagator*, by

$$G\left(\mathbf{r} - \mathbf{r}', t - t'\right) = -\mathrm{i}\left\langle \psi_0 \left| \mathcal{T}\left\{\hat{\Psi}(\mathbf{r}, t)\hat{\Psi}^\dagger(\mathbf{r}', t')\right\} \right| \psi_0 \right\rangle \tag{3.2.8}$$

where $\mathcal{T}\{\}$ is the *time ordering operator* which orders its input operators from right to left by increased time. $|\psi_0(n_0)\rangle$ is the eigenstate with the lowest eigenvalue of the Hamiltonian $\hat{H}(n_0)$. In the following we set $t < t'$.

By Fourier transforming the Green's function $G(\mathbf{r}, t) = (2\pi)^d \int \mathrm{d}^d k \, e^{\mathrm{i}\mathbf{k}\cdot\mathbf{r}} G(\mathbf{k}, t)$ we obtain

$$G(\mathbf{k}, t - t')\,\delta^{(d)}(\mathbf{k} - \mathbf{k}') = -\mathrm{i}\left\langle \psi_0 \left| \mathcal{T}\left\{\hat{c}_{\mathbf{k}}(t)\hat{c}_{\mathbf{k}'}^\dagger(t')\right\} \right| \psi_0 \right\rangle. \tag{3.2.9}$$

Then

$$\hbar\frac{\mathrm{d}}{\mathrm{d}t}G(\mathbf{k}, t - t')\,\delta^{(d)}(\mathbf{k} - \mathbf{k}') = \left\langle \psi_0 \left| \hat{c}_{\mathbf{k}'}^\dagger(t')\left[\hat{K}(t), \hat{c}_{\mathbf{k}}(t)\right] \right| \psi_0 \right\rangle \tag{3.2.10}$$

$$= -\mathrm{i}\left(\frac{\hbar^2 k^2}{2m} + \hbar\omega - \mu\right)G(\mathbf{k}, t - t')\,\delta^{(d)}(\mathbf{k} - \mathbf{k}') + \left\langle \psi_0 \left| \hat{c}_{\mathbf{k}'}^\dagger(t')\left[\hat{V}_{\mathrm{int}}, \hat{c}_{\mathbf{k}}(t)\right] \right| \psi_0 \right\rangle \tag{3.2.11}$$

where we used $\hat{c}_{\mathbf{k}}|\psi_0\rangle = 0$.

We introduce at this point the temporal Fourier transform of the $G(\mathbf{k}, t)$,

$$G(\mathbf{k}, \epsilon) = \int_{-\infty}^{\infty} \mathrm{d}t\, G(\mathbf{k}, t)\, e^{\mathrm{i}\epsilon t} \tag{3.2.12}$$

$$\Leftrightarrow G(\mathbf{k}, t - t') = \frac{1}{2\pi}\int_C \mathrm{d}\epsilon\, G(\mathbf{k}, \epsilon)\, e^{-\mathrm{i}\epsilon(t - t')}. \tag{3.2.13}$$

where C is a path in the complex plane going from $-\infty$ in the real axis to $+\infty$ and performing a semicircle in the upper half plane. We can take again the time derivative like in (3.2.10) and find in the limit of $t \to t'$

$$\frac{\mathrm{d}}{\mathrm{d}t}G(\mathbf{k}, t - t')\,\delta^{(d)}(\mathbf{k} - \mathbf{k}') = -\mathrm{i}\int_C \frac{\mathrm{d}\epsilon}{2\pi}G(\mathbf{k}, \epsilon)\,\epsilon\,\delta^{(d)}(\mathbf{k} - \mathbf{k}'). \tag{3.2.14}$$

Combining this with (3.2.10) and (3.2.13) we get

$$\left\langle \psi_0 \left| \hat{c}_{\mathbf{k}'}^\dagger(t')\left[\hat{V}_{\mathrm{int}}, \hat{c}_{\mathbf{k}}(t)\right] \right| \psi_0 \right\rangle = -\mathrm{i}\int_C \frac{\mathrm{d}\epsilon}{2\pi}\left[\epsilon - \left(\frac{\hbar^2 k^2}{2m} + \hbar\omega\right) + \mu\right]G(\mathbf{k}, \epsilon)\,\delta^{(d)}(\mathbf{k} - \mathbf{k}'). \tag{3.2.15}$$

Let us have a closer look to the left-hand side of this equation and use the shorthand notation $\langle\cdot\rangle$ for $\langle\psi_0|\cdot|\psi_0\rangle$. Remembering the bosonic commutator relations one sees that the term counts the number of occurring $\hat{c}_{\mathbf{k}}^\dagger$. When we integrate over momentum we can conclude

$$\int \mathrm{d}^d k \left\langle \hat{c}_{\mathbf{k}'}^\dagger(t')\left[\hat{V}_{\mathrm{int}}, \hat{c}_{\mathbf{k}}(t)\right]\right\rangle = 2\langle\hat{V}_1\rangle + 2\langle\hat{V}_2\rangle + \langle\hat{V}_3\rangle + 2\langle\hat{V}_4\rangle + \langle\hat{V}_6\rangle, \tag{3.2.16}$$

which, crucially, can be rewritten as follows

$$= -2 \left\langle \hat{V}_{\text{int}}(n_0) \right\rangle + n_0 \left\langle \frac{\mathrm{d}\, \hat{V}_{\text{int}}(n_0)}{\mathrm{d}n_0} \right\rangle . \qquad (3.2.17)$$

Since $\hat{H}_0$ does not depend on n_0, we can easily see that $\left\langle \frac{\mathrm{d}\hat{V}_{\text{int}}(n_0)}{\mathrm{d}n_0} \right\rangle = \mu$, the chemical potential. As a result, we can re-write Eq. (3.2.15) in the form:

$$\left\langle \hat{V}_{\text{int}}(n_0) \right\rangle = \frac{1}{2} \int \mathrm{d}^d k\, \mathrm{i} \int_C \frac{\mathrm{d}\epsilon}{2\pi} \left[\epsilon - \left(\frac{\hbar^2 k^2}{2m} + \hbar\omega \right) + \mu \right] G\left(\mathbf{k}, \epsilon\right) + \frac{1}{2} n_0 \mu . \qquad (3.2.18)$$

The ground-state expectation value of the non-interacting part $\hat{H}_0$ is

$$\left\langle \frac{\hat{H}_0}{V} \right\rangle = \frac{1}{(2\pi)^d} \int \mathrm{d}^d k\, \frac{\hbar^2 k^2}{2m} \left\langle \hat{c}_{\mathbf{k}}^\dagger \hat{c}_{\mathbf{k}} \right\rangle . \qquad (3.2.19)$$

Directly from the definition of the Green's function in Eq. (3.2.9), we can see that the expectation value on the right side of Eq. (3.2.19) can be expressed in terms of the one-particle Green's function with (3.2.13):

$$\left\langle \frac{\hat{H}_0}{V} \right\rangle = \frac{\mathrm{i}}{(2\pi)^{d+1}} \int \mathrm{d}^d k \int_C \mathrm{d}\epsilon\, \frac{\hbar^2 k^2}{2m} G\left(\mathbf{k}, \epsilon\right) . \qquad (3.2.20)$$

We can now write down an equation for the expectation value of $\hat{K}/V$, and move all expressions including a Green's function to the right-hand side of the equation:

$$\frac{E_0}{V} - \frac{1}{2} n_0 \mu = \frac{\mathrm{i}}{(2\pi)^{d+1}} \int \mathrm{d}^d k \int_C \mathrm{d}\epsilon\, \frac{\epsilon + \frac{\hbar^2 k^2}{2m} + \mu}{2} G\left(\mathbf{k}, \epsilon\right) . \qquad (3.2.21)$$

This is a rather complicated differential equation since the energy density appears not only on the left twice but also on the right in the chemical potential and the Green's function. Additionally, the parameter n_0 of the condensed density is a problem and needs to be determined. The later problem we can tackle by subtracting $\frac{1}{2} n' \mu$ on both sides of the equation which allows us to write it in terms of the total density $n = n_0 + n'$. With the Green's function definitions we can write down an expression for the density of the depleted states, i.e.

$$\frac{1}{2} \mu n' = \frac{\mathrm{i}}{(2\pi)^{d+1}} \int \mathrm{d}^d k \int_C \mathrm{d}\epsilon\, \frac{1}{2} \mu G\left(\mathbf{k}, \epsilon\right) . \qquad (3.2.22)$$

Which brings us to the differential equation

$$\frac{E_0}{V} - \frac{1}{2}n\mu = \frac{\mathrm{i}}{(2\pi)^{d+1}} \int \mathrm{d}^d k \int_C \mathrm{d}\epsilon \, \frac{\epsilon + \frac{\hbar^2 k^2}{2m}}{2} G\left(\mathbf{k}, \epsilon\right). \qquad (3.2.23)$$

But still, the $G\left(\mathbf{k}, \epsilon\right)$ depends on the energy density of the ground state.

For the proceeding steps we need to dive deeper into the theory of quantum fields, which is beyond the scope of this Thesis. Details of the derivation can be found in the paper by N. M. Hugenholtz and D. Pines [HP59], and may be supported by standard literature on the introduction of quantum field theory, e.g. [PS97]. To get an explicit expression for the Green's function we need to re-express it in terms of the non-interacting part. This process gives us a series of terms were in the following we are only interested in the second-order contribution. An important observation is that in the low-density regime the $G\left(\mathbf{k}, \epsilon\right)$ has poles in the Bogoliubov spectrum. The Green's function can be rewritten, using the results of the Bogoliubov-de Gennes equations, in the form:

$$G\left(\mathbf{k}, \epsilon\right) = \sum_\nu \left\{ \mathbf{u}_\nu \frac{1}{\epsilon - \epsilon_\nu + \mathrm{i}\delta} \mathbf{u}_\nu^T + \mathbf{v}_\nu \frac{1}{-\epsilon - \epsilon_\nu + \mathrm{i}\delta} \mathbf{v}_\nu^T \right\} \qquad (3.2.24)$$

with the Bogoliubov modes $\epsilon_\nu, \mathbf{u}_\nu, \mathbf{v}_\nu$. Integrating over the contour, and employing the residual theorem, this simplifies the differential equation to

$$\frac{E_0^{(1)}}{V} - \frac{1}{2}n\mu^{(1)} = \frac{1}{2} \int \frac{\mathrm{d}^d k}{(2\pi)^d} \sum_\nu \left(\frac{\hbar^2 k^2}{2m} - \epsilon_\nu(\mathbf{k}) \right) (v_\nu(\mathbf{k}))^2, \qquad (3.2.25)$$

where "(1)" denotes that we solve the problem up to the lowest order correction. Equation (3.2.25) will be denoted in the following as the Hugenholtz-Pines equation.

The same technique can also be applied for a mixture of M different kinds of bosons. The derivation is very similar but with additional summations over all different possible inter- and intra-component interactions. The analogue of Hugenholtz-Pines equation for a mixture acquires the form:

$$\frac{E_0^{(1)}}{V} - \frac{1}{2}n\mu^{(1)} = \frac{1}{2} \sum_i^M \int \frac{\mathrm{d}^d k}{(2\pi)^d} \sum_\nu \left(\frac{\hbar^2 k^2}{2m_i} - \epsilon_\nu(\mathbf{k}) \right) (v_{\nu,i}(\mathbf{k}))^2. \qquad (3.2.26)$$

3.3 Recovering the LHY

For a three-dimensional system with contact interactions, we should be able to recover the expression of Eq. (1.4.31) for the LHY energy correction. For that case,

we have the explicit expression for the eigenvalue and eigenvectors in Eqs. (1.4.29) and (1.4.30), respectively. Plugging this into Eq. (3.2.25) and integrating over k we get the differential equation

$$\frac{E_0^{(1)}}{V} - \frac{1}{2}n\mu^{(1)} = -\frac{2(ng)^{5/2}}{15\pi^2}. \qquad (3.3.27)$$

When we take the ansatz $\frac{E_0^{(1)}}{V} = \alpha(gn)^{5/2}$ with α to be determined, the derivative with respect to n is the chemical potential and $\mu^{(1)} = \frac{5\alpha}{2}g^{5/2}n^{3/2}$. Plugging the ansatz back into Eq. (3.3.27), we can solve for α, finding $\alpha = \frac{8}{15\pi^2}$. We hence recover the LHY-correction

$$\frac{E_0^{(1)}}{V} = \frac{64}{15\sqrt{\pi}}n^{5/2}a^{3/2}, \qquad (3.3.28)$$

as previously obtained using a different procedure in Sec. 1.4.

3.4 Conclusion

The method discussed in the chapter is powerful for various reasons. On one hand, as discussed by Hugenholtz and Pines in their paper [HP59], it provides a path for the study of even higher-order corrections beyond the LHY term. On the other hand, the method may be easily applied to lower-dimensional systems, without any problem associated to divergences. Moreover, it can be employed to quasi-low dimensional systems, in which the other dimensions are e.g. harmonically trapped. This permits the analysis of beyond-mean-field corrections in the cross-dimensional regime, which will be exceedingly difficult to describe using the more standard Bogoliubov analysis. This plays a crucial role in our discussion of Chapter 7.

Chapter **4**

Anomalous buoyancy of quantum bubbles in immiscible Bose mixtures

In Chapter 2 we discussed the stability of a binary mixture at the stability threshold $|g_{12}|^2 < g_{11}g_{22}$ with $g_{12} < 0$. There we had a first example of a system in which quantum fluctuations play a surprisingly crucial role, despite the weakly-interacting character of the mixture. In this chapter, in Sec. 4.1 we will see that at the other side of the stability regime, i.e. for $g_{12} > 0$, phase separation between the two components occurs. Additionally, the concept of buoyancy in a two-component mixture is presented.

Following the spirit of this Thesis, we look for interesting physics resulting from quantum fluctuations in weakly-interacting systems. For this, we consider a three-component mixture, where two of the components are miscible and quasi-cancel their mean-field energy, whereas the third one is immiscible and acts as a bath for the other components. Using the formalism of the previous chapter we derive in Sec. 4.2 the LHY correction for general three-component mixtures. We consider in Sec. 4.3 the properties of a quantum bubble, formed by the miscible components, in the bath provided by the third one, showing that quantum fluctuations change significantly the scaling of the bubble volume with the bath density. Section 4.4 deals with the buoyancy of the quantum bubble, showing that quantum fluctuations may result in the novel phenomenon of *arrested buoyancy*. In Sec. 4.5 we discuss a possible feasible experimental scenario for the realization of the quantum bubble.

The results of this chapter can be found in Ref. [Edl+22].

4.1 Phase separation and buoyancy

The miscibility of a binary Bose mixture depends on the nature of the inter- and intra-component interactions. Let us consider a homogeneous mixture of two contact-interacting components, 1 and 2, with coupling constants g_{ij}, with $i, j = 1, 2$. We can re-arrange the terms from Eq. (2.1.1) to obtain

$$F(\mathbf{r}) = \frac{g_{11}}{2} \left[n_1(\mathbf{r}) + n_2(\mathbf{r}) \sqrt{\frac{g_{22}}{g_{11}}} \right]^2 + (g_{12} - \sqrt{g_{11}g_{22}})\, n_1(\mathbf{r})n_2(\mathbf{r}) - \mu_1 n_1(\mathbf{r}) - \mu_2 n_2(\mathbf{r}).$$

$$(4.1.1)$$

For a system with repulsive intra-component interactions ($g_{11}, g_{22} > 0$), one clearly sees that miscibility is given by the ratio $\Gamma = g_{12}/\sqrt{g_{11}g_{22}}$, between the inter-component coupling constant g_{12} and the intra-component ones g_{11} and g_{22}. If $\Gamma > 1$ the system enters the immiscible regime characterized by spatial phase separation [Tim98].

The presence of external confinement significantly affects the miscibiliity and spatial distribution of binary mixtures [HS96; PB98; Tim98; Hal+98; Öhb99]. In particular, for an immiscible mixture, depending on the relation between the confinement harmonic frequencies $\omega_{1,2}$ of the two components, a bubble of component 1 may sink to the center of the trap or float rather to the surface of component 2, in a process that resembles buoyancy in ordinary fluids [Tim98]. Similar to Archimedes' principle, buoyancy in a binary Bose mixture is controlled by the equilibration of the pressures inside and outside the bubble. Buoyancy sets in, approximately, when [Tim98]

$$\frac{\omega_1}{\omega_2} = \left(\frac{g_{11}}{g_{22}} \right)^{1/4}.$$

$$(4.1.2)$$

4.2 Three-component system

In this Chapter we will be interested in how quantum fluctuations affect the properties and buoyancy of a quantum bubble, characterized by enhanced quantum

fluctuations. As discussed below, a possible experimentally feasible scenario for a quantum bubble in an immiscible bath is provided by a three-component system. In this section, we discuss in general the LHY correction in a three-component Bose system.

As in previous chapters, the interactions are determined by the *s*-wave scattering lengths a_{ij}, with $i, j = 1, 2, 3$. Motivated by experimental considerations (see the end of this chapter), we focus on the case in which the three components have equal mass m. The interactions are hence characterized by the coupling constants $g_{ii} = 4\pi\hbar^2 a_{ii}/m$ and $g_{ij} = 2\pi\hbar^2 a_{ij}/m_{12}$ for $i \neq j$ where m_{12} is the reduced mass.

In analogy to Eq. (2.2.5), we can write down the Hamiltonian for an unconfined system of N_i particles in the i component

$$\hat{H} = \int \mathrm{d}^3 r \left\{ \sum_i^3 \hat{\Psi}_i^\dagger \hat{h}_i \hat{\Psi}_i + \frac{1}{2} \sum_{i,j=1,2,3} g_{ij} \hat{\Psi}_i^\dagger \hat{\Psi}_j^\dagger \hat{\Psi}_i \hat{\Psi}_j \right\} \tag{4.2.3}$$

where $\hat{h}_i = \frac{-\hbar^2}{2m} \nabla^2$ is the one-particle Hamiltonian. Proceeding as in Chapters 1 and 2, we move to Fourier space, and introduce the Bogoliubov transformation (see Eq. (2.2.10)). We can define $f_{\mathbf{k},i}^- = u_{\mathbf{k},i} - v_{\mathbf{k},i}$, $f_{\mathbf{k},i}^+ = u_{\mathbf{k},i} + v_{\mathbf{k},i}$ and write down the Bogoliubov-de Gennes equations in analogy to Eq. (2.2.14) as follows

$$\begin{cases} \varepsilon_k f_{\mathbf{k},i}^- = \sum_j \left\{ \left(\delta_{ij} \hat{h} + 2g_{ij} \sqrt{n_i n_j} \right) f_{\mathbf{k},i}^+ \right\} \\ \varepsilon_k f_{\mathbf{k},i}^+ = \hat{h} f_{\mathbf{k},i}^- \end{cases} \tag{4.2.4}$$

Combining all equations in (4.2.4), the problem can be expressed in a single equation

$$\varepsilon^2(k)\mathbf{f} = \epsilon(k) \left[\epsilon(k)\mathbb{1} + 2g_{11}n_1 U(P_2, P_3) \right] \mathbf{f} \tag{4.2.5}$$

where $\epsilon(k) = \hbar^2 k^2/2m$, and

$$U(P_2, P_3) = \frac{1}{g_{11}} \begin{pmatrix} g_{11} & g_{12}\sqrt{P_2} & g_{13}\sqrt{P_3} \\ g_{12}\sqrt{P_2} & g_{22}P_2 & g_{23}\sqrt{P_2 P_3} \\ g_{13}\sqrt{P_3} & g_{23}\sqrt{P_2 P_3} & g_{33}P_3 \end{pmatrix}, \quad P_i = \frac{n_i}{n_1}, \quad \mathbf{f} = \left[f_{\mathbf{k},i}^- \right]. \tag{4.2.6}$$

Let $F_i(P_2, P_3)$ be the eigenvalues of the matrix U, then we can get an explicit expression for the eigenvalues ε_i:

$$\varepsilon_i(k) = \epsilon(k) \left[\epsilon(k) + 2g_{11}n_1 F_i(P_2, P_3) \right]. \tag{4.2.7}$$

With the known excitation branches and with the help of the formalism by Hugenholtz and Pines introduced previously (see Eq. (3.2.26)), we can write down the Hugenholtz-Pines differential equation that needs to be solved to obtain the LHY correction:

$$\frac{E_0^{(1)}}{V} - \frac{1}{2}\sum_i n_i \frac{\partial}{\partial n_i}\frac{E_0^{(1)}}{V} = -\frac{1}{2}\int \frac{\mathrm{d}^3k}{(2\pi)^3}\sum_i \frac{(\varepsilon_i(k) - \epsilon(k))^3}{4\varepsilon_i(k)\epsilon(k)}. \tag{4.2.8}$$

Plugging Eq. (4.2.7) into (4.2.8) we obtain that

$$\frac{E_{\mathrm{LHY}}}{V} - \frac{1}{2}\sum_i n_i \frac{\partial}{\partial n_i}\frac{E_{\mathrm{LHY}}}{V} = -\frac{\hbar^2}{m}(n_1 a_{11})^{5/2}\frac{64}{15}\sqrt{\pi}\sum_i F_i^{5/2} =: \chi. \tag{4.2.9}$$

Taking into account the form of the function $\chi(n_1, P_2, P_3)$, we introduce the ansatz

$$\frac{E_{\mathrm{LHY}}}{V} = \frac{\hbar^2}{m}(n_1 a_{11})^{5/2}G(P_2, P_3). \tag{4.2.10}$$

Plugging this into the differential equation (4.2.9), it simplifies to

$$\frac{1}{4}G(P_2, P_3) = \frac{64}{15}\sqrt{\pi}\sum_i F_i^{5/2}, \tag{4.2.11}$$

resulting in the LHY-correction

$$\frac{E_{\mathrm{LHY}}}{V} = \frac{256}{15}\sqrt{\pi}\frac{\hbar^2}{m}(n_1 a_{11})^{5/2}\sum_i F_i^{5/2}. \tag{4.2.12}$$

Hence the beyond-mean field correction to the chemical potential of component i reads

$$\mu_i^{\mathrm{LHY}} = \frac{\partial}{\partial n_i}\frac{E_{\mathrm{LHY}}}{V} = \frac{32}{3\sqrt{\pi}}g_{11}(n_1 a_{11})^{3/2}Q_i \tag{4.2.13}$$

with

$$\begin{aligned} Q_1 &= \sum_i F_i^{3/2}\left(F_i - P_2\frac{\partial}{\partial P_2}F_i - P_3\frac{\partial}{\partial P_3}F_i\right) \\ Q_2 &= \sum_i F_i^{3/2}\frac{\partial}{\partial P_2}F_2 \\ Q_3 &= \sum_i F_i^{3/2}\frac{\partial}{\partial P_3}F_3 \end{aligned} \tag{4.2.14}$$
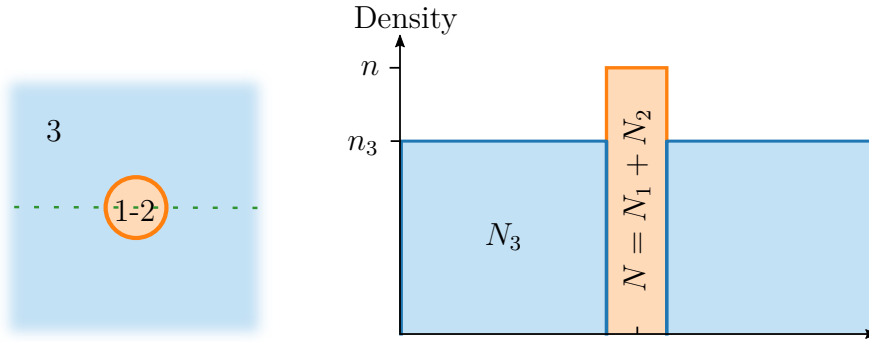
Figure 4.1: Sketch of homogeneous-bubble model. A 1-2 bubble of homogenous density n is immersed within the majority component of density n_3. The kinetic energy is hence neglected in this model.

The matrix U in Eq. (4.2.6) determines the mean-field stability of the mixture. If all its eigenvalues are positive, the mixture is fully miscible. For the purposes of this chapter, we restrict ourselves to the case where component 3 and components 1-2 are immiscible. Hence in the 1-2 region, we may assume $P_3 = 0$, and we recover the known LHY corrections for the 1-2 mixture [Pet15] obtained previously in Sec. 2.2. We simplify also the notation in the following, using $P = P_2 = N_2/N_1$.

4.3 Quantum bubble in a homogeneous bath

The coupling constants g_{11}, g_{22} and g_{12} are such that components 1 and 2 are miscible and in the regime of mean-field quasi-cancellation [Pet15] discussed previously in this Thesis. The bath is characterized by the coupling g_{33}. The inter-component coupling constants g_{13} and g_{23} are supposed to be large and repulsive, ensuring immiscibility between component 3 and the other two components. Components 1 and 2 form an effective scalar component with enhanced quantum fluctuations that we will call the 1-2 gas.

We consider at this point a spherical homogenous 1-2 bubble of volume V, with $N = N_1 + N_2$ particles of the minority component, placed in an otherwise homogeneous bath of component 3, with particle density n_3 as sketched in Fig. 4.1. The bubble density will be denoted as $n = N/V$. The value of the density is established by an equilibrium of pressures, as elaborated in the following.

4.3.1 Equilibrium of pressures

The 1-2 contribution to the bubble energy is

$$E_{12}(V) = \frac{1}{2}G(P)\frac{N^2}{V} + \gamma(P)g_{11}a_{11}^{3/2}\frac{N^{5/2}}{V^{3/2}} \qquad (4.3.15)$$

where the first and second terms correspond, respectively, to the mean-field and LHY corrections, and

$$G(P) = \frac{g_{11} + g_{22}P^2 + 2g_{12}P}{(1+P)^2}, \qquad (4.3.16)$$

$$\gamma(P) = \frac{64}{15\sqrt{\pi}} \frac{f\left(\frac{g_{12}^2}{g_{11}g_{22}}, \frac{g_{22}}{g_{11}}P\right)}{(1+P)^{5/2}} \qquad (4.3.17)$$

with $f(x,y)$ from Eq. (2.2.21).

The 1-2 gas, with a fixed polarization $P = \sqrt{\frac{g_{11}}{g_{22}}}$, acts as a scalar component with an effective scattering length $a(P)$, with $G(P) = \frac{4\pi\hbar^2 a(P)}{m}$. The enhanced quantum fluctuations are achieved in the regime of mean-field energy quasi-cancellation, which corresponds to $G(P) \approx 0$.

Due to the immiscibility between 1-2 and 3, the bubble induces a hollow spherical cavity of volume V in the bath. The change of the bath energy ΔE_3 between the cavity system C and non-cavity system NC is $\Delta E_3 = E_C(N_3) - E_{NC}(N_3)$, with $E_C(N_3)$ the energy of the cavity system of N_3 particles and $E_{NC}(N_3)$ the one for the non-cavity system.

It is to be noted that quantum fluctuations are only relevant for the 1-2 mixture. For the third component the LHY correction is assumed as negligibly small compared to the mean-field energy. The cavity energy can then be rewritten as

$$E_C(N_3) \cong E_{NC}(N_3 + \delta N_3) - \frac{E_3}{V}V, \qquad (4.3.18)$$

where $\delta N_3 = n_3 V$ and $\frac{E_3}{V} = \frac{1}{2}g_{33}n_3^2$ is the mean-field energy density of the third component. In turn, the non-cavity term for $N_3 + \delta N_3$ particles can be decomposed in the non-cavity term for N_3 particles plus the energy needed to add δN_3 more particles, i.e.

$$E_{NC}(N_3 + \delta N_3) \cong E_{NC}(N_3) + \mu_3\delta N_3, \qquad (4.3.19)$$

with $\mu_3 = g_{33}n_3$ the chemical potential of the bath. We may hence write

$$\Delta E_3(V) = \frac{1}{2}g_{33}n_3^2 V. \tag{4.3.20}$$

The energy associated to the bubble is hence $E_{12}(V) + \Delta E_3(V)$. Minimizing it with respect to V, we obtain the equation for the equilibrium between the inner pressure $\mathcal{P}_{12} = -\partial_V E_{12}$ and the outer bath pressure $\mathcal{P}_3 = -\partial_V \Delta E_3$:

$$G(P)n^2 + 3\gamma(P)g_{11}a_{11}^{3/2}n^{5/2} = g_{33}n_3^2 \tag{4.3.21}$$

4.3.2 Bubble volume scaling

Equation (4.3.21) determines, for a given bath density, the bubble density, and hence its volume. The scaling of the bubble volume with the bath density changes significantly in the different interaction regimes.

In the mean-field regime we may neglect the effect of quantum fluctuations in the bubble. The equilibrium of pressures results

$$n^{\mathrm{MF}} = \sqrt{\frac{g_{33}}{G(P)}}n_3, \tag{4.3.22}$$

as it is well-known for binary mean-field mixtures [Tim98]. Hence the bubble volume is inversely proportional to n_3.

The situation changes significantly when the 1-2 mean-field interactions quasi-cancel, i.e. $G(P) = 0$. For sufficiently large density, the LHY energy dominates the bubble energy (we call this regime the *LHY bubble regime*). The equilibrium of pressures leads to an anomalous dependence

$$n^{G=0} = \left(\frac{g_{33}}{3\gamma(P)g_{11}a_{11}^{3/2}}\right)^{2/5} n_3^{4/5}. \tag{4.3.23}$$

Consequently, the volume of the LHY bubble scales as $n_3^{-4/5}$.

In contrast, for $G(P) = 0$, if the bubble density is too low, we can neglect the effect of quantum fluctuations and the bubble energy is dominated by the single-particle kinetic contribution, associated to the inhomogeneity of the bubble wavefunction

within the bath cavity, which we have neglected up to now. Approximating that the bubble is in a spherical hard-wall cavity of volume V, the bubble energy is $E_{12,\mathrm{kin}} = \frac{\hbar^2 \pi^2}{2m} \left(\frac{4\pi}{3V} \right)^{2/3}$. As before, we can get the pressure $\mathcal{P}_{12} = -\partial_V E_{12,\mathrm{kin}}$ and equate it with the pressure $\mathcal{P}_3$ i.e.

$$\frac{1}{2} g_{33} n_3^2 = \frac{\pi^2}{3} \left(\frac{4\pi}{3} \right)^{2/3} \frac{\hbar^2 N}{mV^{5/3}} \tag{4.3.24}$$

$$V = \left[\frac{2\pi^2}{3} \left(\frac{4\pi}{3} \right)^{2/3} \frac{\hbar^2 N}{mg_{33}} \right]^{3/5} n_3^{-6/5}. \tag{4.3.25}$$

Hence for low density bubbles we expect a scaling $V \propto n_3^{-6/5}$.

Extended Gross-Pitaevskii analysis

Quantum fluctuations hence significantly modify the bubble volume, and its scaling with the bath density. In order to investigate the bubble properties we employ, as in previous chapters, local-density approximation arguments to treat the LHY correction for a spatially inhomogeneous mixture, obtaining a set of three coupled extended Gross-Pitaevskii equations:

$$\mu_i \Psi_i(\mathbf{r}) = \left[-\frac{\hbar^2 \nabla^2}{2m} + \sum_j g_{ij} n_j(\mathbf{r}) + \mu_i^{\mathrm{LHY}}(\{n_j\}) \right] \Psi_i(\mathbf{r}) \tag{4.3.26}$$

with $n_i(\mathbf{r}) = |\Psi_i(\mathbf{r})|^2$. In our numerics, we consider a cubic hard-wall numerical box of an edge length R_B, with $N_3 = n_3 R_B^3$ particles in the bath. We placed a bubble at the center of the numerical box, with $N = N_1 + N_2$ particles and $P = \sqrt{a_{11}/a_{22}}$.

Variational analysis

Although the eGPE formalism permits a good characterization of the quantum bubble, a simpler variational formalism, discussed in the following, is in very good agreement with the eGPE calculation. It allows for a quick simulation of the system, and permits additional physical insights.

We consider a spherically symmetric trial wave-function for the 1-2 bubble of the

form of a higher-order Gaussian:

$$\Psi_{1,2}(r;\sigma,s) = A_{1,2} \exp\left[-\frac{1}{2}\left(\frac{r}{\sigma}\right)^s\right], \qquad (4.3.27)$$

where the variational parameters σ and s characterize, respectively, the bubble radius, and the flatness of the bubble profile. The latter interpolates between a Gaussian ($s = 2$) and a flat-top solution for $s \gg 2$.[LB21] For the bath, we employ the ansatz:

$$\Psi_3(r;r_0,\delta r) = A_3\left[1 + \tanh\left(\frac{r - r_0}{\delta r}\right)\right], \qquad (4.3.28)$$

where the variational parameters r_0 and δr characterize, respectively, the radius of the hollow cavity in the bath, and the bath healing length back into the homogeneous density value. The amplitudes $A_{1,2,3}$ are found upon normalization to the number of particles $N_i = \int \mathrm{d}^3r\,|\Psi_i(r)|^2$.

Figures 4.2(a) and (b) depict the results for $G(P) = 0, P = \sqrt{a_{11}/a_{22}}$, $N = N_1 + N_2 = 10\,000$ in two different bath densities, $n_3 = 9 \times 10^{18}\,\mathrm{m}^{-3}$ and $7 \times 10^{20}\,\mathrm{m}^{-3}$. The simulations were performed for the experimentally feasible scattering lengths of potassium $(a_{11}, a_{22}, a_{13}, a_{23}, a_{33}) = (34.5, 82, 172, 172, 60)a_0$ (see the discussion below in this chapter). Note that the variational calculations are in excellent qualitative and to a large extent quantitative agreement with the eGPE results.

For a given number of particles N in the bubble, an increase of the bath density n_3 increases the outer pressure, which compresses the bubble. In turn, the increase of the bubble density results in an enhanced role of interactions. Hence, for an LHY bubble, i.e. $G(P) = 0$, when n_3 grows, the bubble transitions from a regime dominated by the kinetic energy (as in Fig. 4.2(a)) into a regime dominated by the LHY energy (as in Fig. 4.2(b)) where the quantum bubble acquires a flat-top profile. The change in the character of the density profile is evident from Fig. 4.3, where we plot the variational "flatness" parameter s as a function of the bath density for a fixed $N = 10\,000$. Note the transition from a Gaussian-like profile $s \cong 2$ to a flat-top, $s \gg 2$.

The progressively larger role played by the LHY energy for growing n_3 modifies, according to the discussion above, the dependence of the bubble volume with the bath density. In Fig. 4.4, we depict the volume as a function of the bath density in a system of $N = 1650$ and the same scattering lengths as mentioned earlier. Note the expected crossover between a scaling $V \propto n_3^{-6/5}$ when the kinetic energy dominates, and a scaling $V \propto n_3^{-4/5}$, when the LHY energy dominates.
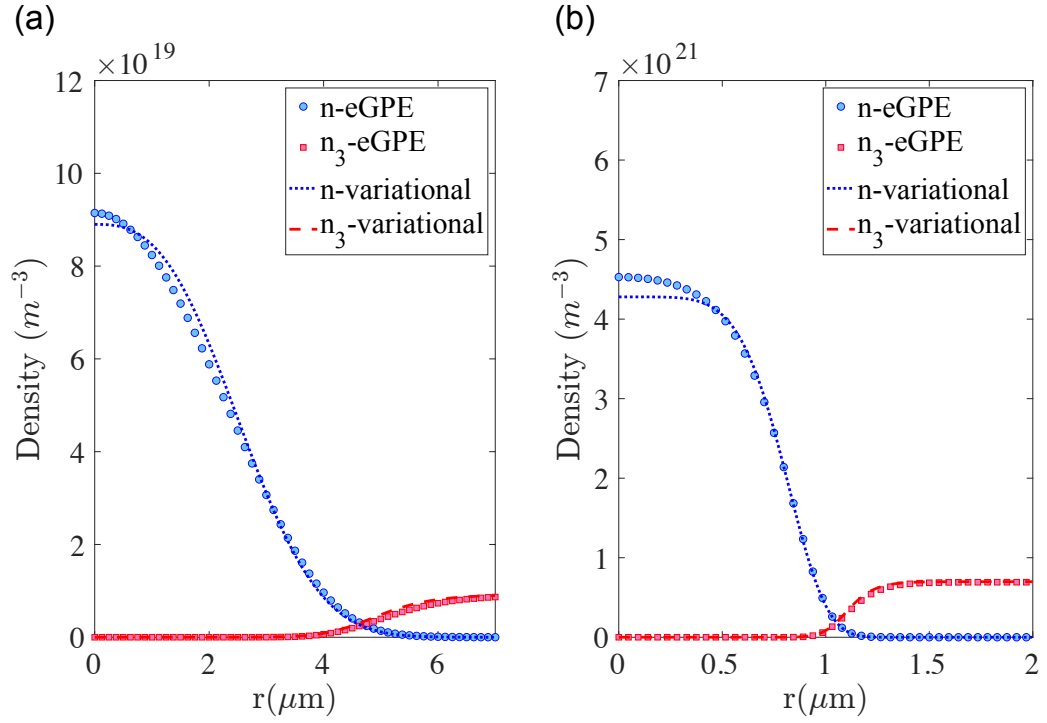
Figure 4.2: Density profile $n(r) = n_1(r) + n_2(r)$ of the 1-2 gas (circles) and of the bath (squares) obtained from the coupled eGPEs, for $(a_{11}, a_{22}, a_{13}, a_{23}, a_{33}) = (34.44, 82, 172, 172, 60)a_0$, $N = 10^4$, for two different bath densities $n_3^{\mathrm{peak}} = 9 \times 10^{18} \, \mathrm{m}^{-3}$ (a) and $7 \times 10^{20} \, \mathrm{m}^{-3}$ (b). Dashed lines indicate the corresponding variational results. Reprinted from [Edl+22]
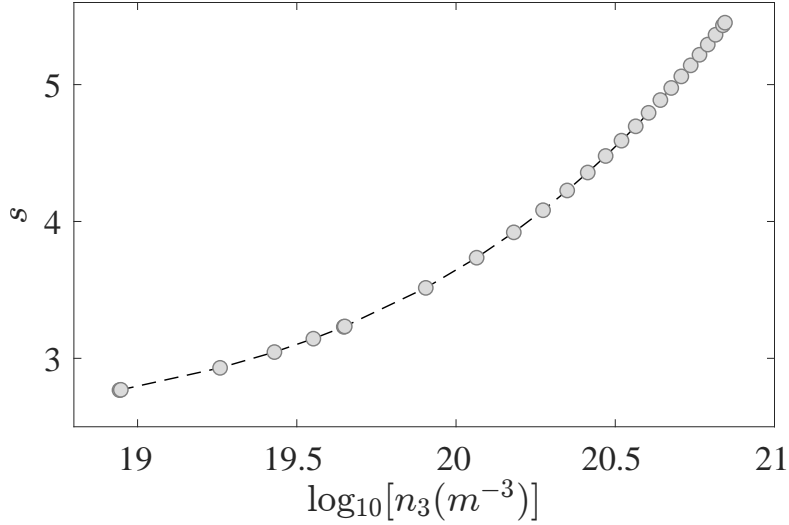
Figure 4.3: Exponent s that characterizes the profile of the droplet. $s = 2$ indicated a Gaussian-like droplet, whereas $s \gg 2$ corresponds to a flat-top profile. The calculations are performed for the same parameters as in Fig. 4.2, with $N = 10^4$. Note that when the bath density grows, the bubble profile becomes progressively more flat-top. Reprinted from [Edl+22]

Figure 4.4: Volume of the quantum bubble as a function of the bath density n_3 for the same scattering lengths as in Fig. 4.2, for $G(P) = 0$ and $N = 1650$. Note the crossover from a kinetic-energy dominated $V \propto n_3^{-6/5}$ (dashed line) dependence into a LHY-dominated $V \propto n_3^{-4/5}$ dependence (dotted line). Reprinted from [Edl+22]

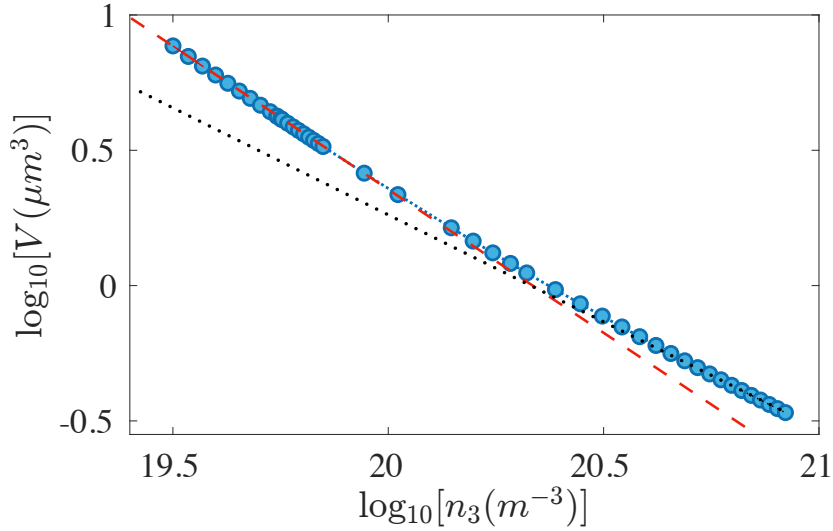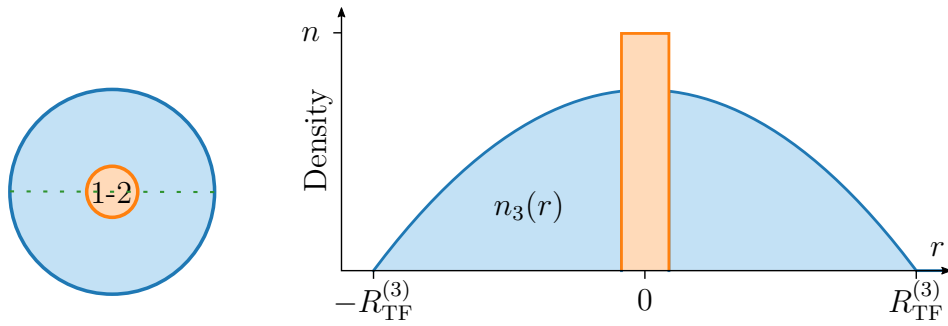Figure 4.5: Sketch of the model considered. The majority component 3 acts as a bath and has a much larger radius $R_{\mathrm{TF}}^{(3)}$ than the width of the 1-2 bubble. The 1-2 mixture is supposed to be homogeneously distributed within the bubble.

4.4 Anomalous buoyancy of a quantum bubble

In the previous section we had a look at a bubble in an otherwise homogeneous bath. In this section we want to concentrate on a more realistic situation in which the mixture is confined in an isotropic harmonic trap, characterized by a frequency ω for the 1-2 components, and a frequency ω_3 for the bath.

We assume, as before, the quantum fluctuations in the bath to be negligible and that the interactions are strong enough to be in the Thomas-Fermi regime. Both assumptions allow us for using the radial density profile $n_3(r) = n_3(0) \left(1 - \frac{r^2}{R_{\mathrm{TF}}^2}\right)$ from Eq. (1.3.20). The model is sketched in Fig. 4.5.

The presence of a trap results eventually in buoyancy [Tim98]. For a given ratio $\omega/\omega_3 > (\omega/\omega_3)_{\mathrm{cr}}$, the 1-2 bubble remains at the trap center. In contrast, when $\omega/\omega_3 < (\omega/\omega_3)_{\mathrm{cr}}$ the bubble floats to the bath surface [Tim98]. For the case of a mean-field bubble, when it reaches the surface, it is destroyed, forming a partial or complete spherical shell around the bath.

In the following, we will see that quantum fluctuations significantly modify the buoyancy condition. Moreover, they may lead to *arrested buoyancy*, i.e. the displacement of the bubble to an intermediate position between the center and the surface of the bath. Finally, for $\delta a < 0$, when the bubble moves to the surface it does not spill over the surface, but undergoes a transition into a self-bound droplet that remains compact floating at the bath surface.

4.4.1 Buoyancy condition for a uniform bubble

We first consider the simplified case in which the bubble density is homogeneous within the hollow cavity, and in which the bubble volume is much smaller than the overall bath volume (see Fig. 4.5). Under these conditions, we may neglect the kinetic energy and the boundary effects associated to inter-particle interactions between 1-2 and 3 at the domain wall.

The energy per particle of the bubble is:

$$\frac{E(r)}{N} = \frac{1}{2}m\omega^2 r^2 + \frac{1}{2}G(P)n(r) + \gamma(P)g_{11}a_{11}^{3/2}n^{3/2}(r) + \frac{1}{2}g_{33}\frac{n_3^2(r)}{n(r)} \qquad (4.4.29)$$

In the vicinity of small r we can approximate the bubble density as

$$n(r) \cong n(0)(1 + \epsilon(r)) \qquad (4.4.30)$$

with $\epsilon(r)$ acting as a small correction term, i.e. $\epsilon(r) \ll 1$. Note that we have the Thomas-Fermi relation $\frac{1}{2}m\omega_3^2 R_{\mathrm{TF}}^2 = g_{33}n_3(0)$ which allows us to replace the trapping term in Eq. (4.4.29) by

$$\frac{1}{2}m\omega^2 r^2 = g_{33}n_3(0)\left(\frac{\omega}{\omega_3}\right)^2\left(\frac{r}{R_{\mathrm{TF}}}\right)^2 \qquad (4.4.31)$$

Plugging Equations (4.4.30) and (4.4.31) into (4.4.29) and keeping up to linear terms in ϵ and $(r/R)^2$, we obtain

$$\begin{aligned}
\frac{E}{N} \cong &\ \frac{1}{2}Gn(0)(1 + \epsilon) + \gamma g_{11}a_{11}^{3/2}n(0)^{3/2}\left(1 + \frac{3}{2}\epsilon\right) \\
&+ g_{33}n_3(0)(1 + \epsilon)\left(\frac{\omega}{\omega_3}\right)^2\left(\frac{r}{R_{\mathrm{TF}}}\right)^2 + \frac{1}{2}g_{33}\frac{n_3^2(0)}{n(0)}\left[1 - 2\left(\frac{r}{R_{\mathrm{TF}}}\right)^2 - \epsilon\right]
\end{aligned}$$
$$(4.4.32)$$

The terms proportional to ϵ vanish identically due to the condition of pressure equilibrium of Eq. (4.3.21) at $r = 0$. Hence we are left with

$$\frac{E(r) - E(0)}{Ng_{33}n_3(0)} \cong \left[\left(\frac{\omega}{\omega_3}\right)^2 - \frac{n_3(0)}{n(0)}\right]\left(\frac{r}{R_{\mathrm{TF}}}\right)^2 \qquad (4.4.33)$$

We hence obtain the critical frequency ratio for buoyancy:

$$\left(\frac{\omega}{\omega_3}\right)_{\mathrm{cr}} = \sqrt{\frac{n_3(0)}{n(0)}}. \tag{4.4.34}$$

We can distinguish between different regimes. For a mean-field bubble, in which we can neglect the LHY contribution, the density ratio is given by Eq. (4.3.22), and we retrieve the known critical frequency ratio for mean-field buoyancy[Tim98]

$$\left(\frac{\omega}{\omega_3}\right)_{\mathrm{cr}}^{\mathrm{MF}} = \left(\frac{G(P)}{g_{33}}\right)^{1/4}. \tag{4.4.35}$$

For a LHY bubble, i.e. $G(P) = 0$, the equilibrium of pressures leads to a simple dependence of $n(0)$ on $n_3(0)$ given by Eq. (4.3.23). The critical frequency ratio acquires the form

$$\left(\frac{\omega}{\omega_3}\right)_{\mathrm{cr}}^{G=0} = \sqrt{\left(3\gamma(P)\right)^{2/5}\frac{a_{11}}{a_{33}}\left(n_3(0)a_{33}^3\right)^{1/5}}. \tag{4.4.36}$$

Note that it depends explicitly on the bath density. This is connected to the arrested buoyancy discussed below.

A third case of special interest is when quantum fluctuations are non-negligible but the mean-field term does not completely cancel. For this case of mean-field quasi-cancellation, when $\frac{|\delta a|}{\sqrt{a_{11}a_{22}}} \ll 1$, we can expand Eq. (2.2.21) around $x = 1$, obtaining

$$\gamma(P) \cong \gamma_0(P)\left(1 - \frac{5P}{(1+P)^2}\frac{\delta a}{\sqrt{a_{11}a_{22}}}\right) \tag{4.4.37}$$

with $\gamma_0 := \frac{64}{15\sqrt{\pi}}P^{-5/2}$. At the critical frequency for buoyancy, we may substitute the relation (4.1.2) in the equation for the equilibrium of pressures, obtaining

$$\frac{a(P)}{a_{33}}\left(\frac{\omega}{\omega_3}\right)_{\mathrm{cr}}^4 + 3\gamma(P)\left(\frac{a_{11}}{a_{33}}\right)^{5/2}\sqrt{n_3(0)a_{33}^3}\left(\frac{\omega}{\omega_3}\right)_{\mathrm{cr}}^5 = 1 \tag{4.4.38}$$

with $a(P) = \frac{2P}{(1+P)^2}\delta a$. We may then evaluate up to first order in $\frac{|\delta a|}{\sqrt{a_{11}a_{22}}}$ the critical frequency ratio for the buoyancy of a quantum bubble

$$\left(\frac{\omega}{\omega_3}\right)_{\mathrm{cr}}^{G\neq0} \cong \left(\frac{\omega}{\omega_3}\right)_{\mathrm{cr}}^{G=0}\left(1 + \frac{a(P)}{2\sqrt{a_{11}a_{22}}}\left\{1 - \frac{2}{5}\frac{\sqrt{a_{11}a_{22}}}{a_{33}}\left[\left(\frac{\omega}{\omega_3}\right)_{\mathrm{cr}}^{G=0}\right]^{-4}\right\}\right) \tag{4.4.39}$$

4.4.2 Arrested buoyancy

Interestingly, when occurring, buoyancy may differ significantly from the well-known mean-field case, due to the role played by quantum fluctuations in the 1-2 gas. Let us first consider the case of a mean-field bubble. Using the Thomas-Fermi form of $n_3(r)$, we re-write the bubble energy as:

$$\frac{E(r)/N}{g_{33}n_3(0)} = \left[\left(\frac{\omega}{\omega_3}\right)^{\mathrm{MF}}_{\mathrm{cr}}\right]^2 \left(1 - \frac{r^2}{R_{\mathrm{TF}}^2}\right) + \left(\frac{\omega}{\omega_3}\right)^2 \frac{r^2}{R_{\mathrm{TF}}^2}. \qquad (4.4.40)$$

For $\frac{\omega}{\omega_3} > \left(\frac{\omega}{\omega_3}\right)^{\mathrm{MF}}_{\mathrm{cr}}$ the bubble passes from the center directly to the bath surface since the energy becomes monotonously decreasing with increasing r/R_{TF}. At the surface the mean-field bubble, which was solely maintained by the outer bath pressure, is destroyed and it forms a partial or complete covering of the bath spherical surface.

For a LHY bubble, we may express the bubble energy as:

$$\frac{E(r)/N}{g_{33}n_3(0)} = \frac{5}{6}\left[\left(\frac{\omega}{\omega_3}\right)^{G=0}_{\mathrm{cr}}\right]^2 \left(1 - \frac{r^2}{R_{\mathrm{TF}}^2}\right)^{6/5} + \left(\frac{\omega}{\omega_3}\right)^2 \frac{r^2}{R_{\mathrm{TF}}^2}. \qquad (4.4.41)$$

In contrast to the mean-field case, when $\Lambda \equiv \frac{\omega}{\omega_3}/\left(\frac{\omega}{\omega_3}\right)^{G=0}_{\mathrm{cr}} < 1$, the bubble energy has a minimum at

$$\frac{r}{R_{\mathrm{TF}}} = \sqrt{1 - \Lambda^{10}}. \qquad (4.4.42)$$

Hence, when buoyancy sets in, the position of the bubble does not immediately jump to the surface, as in the mean-field case, but rather experiences an abrupt, but finite, position displacement, breaking spontaneously the spherical symmetry. The red dashed curve in Fig. 4.6(a) shows, as a function of ω/ω_3, the average position for an homogeneous quantum bubble, well within the quasi-cancellation regime for the parameters considered. As expected from the discussion above, there is a window of frequency ratios for which the bubble is placed at an intermediate position within the bath component.

4.4.3 Buoyancy for an inhomogeneous bubble

The previous discussion neglects the kinetic energy of the bubble, which in general may have a sizeable contribution, and assumes that the bubble size is negligible with respect to the size of the Thomas-Fermi cloud of the bath. The latter is a particularly crude approximation under typical conditions.

We have evaluated the ground-state of the mixture using the coupled eGPEs (4.3.26), adding the confinement potential. The squares in Fig. 4.6(a) show our results of the average position of the bubble for a small number of particles $N_1 = 1000$. For this case, the LHY term is negligible and the bubble proper-ties are dominated by the kinetic energy. As a result, compared to Eq. (4.4.39), a larger ω/ω_3 ratio is necessary to keep the bubble confined at the center. Also, when buoyancy sets in, there is no discernible regime of arrested buoyancy.

When the number of particles in the bubble increases (or alternatively for a growing n_3) $(\omega/\omega_3)_{\mathrm{cr}}$ decreases, and a progressively wider window of arrested buoyancy is observed (see Fig. 4.6). Although the numerical results approach the result of the homogeneous-droplet calculation, there are still sizable deviations of the critical frequency ratio compared to Eq. (4.4.39), mostly due to the non-negligible size of the bubble compared to the Thomas-Fermi cloud of the bath. Figure 4.7 shows the density profile of the mixture in the arrested buoyancy regime for $N_1 = 50\,000$ atoms. Note that, as discussed for the case of an homogeneous droplet, the inhomogeneous bubble is placed at intermediate positions (spontaneously breaking the spherical symmetry). Note as well, that in contrast to the mean-field case, when the bubble reaches the boundary, it does not spread around the spherical Thomas-Fermi surface. Since $\delta a < 0$, it rather undergoes a crossover from a bubble into a self-bound droplet, which remains compact floating at the bath surface.

4.5 Experimental considerations

A possible implementation of the quantum bubble scenario discussed in this chap-ter is provided by the multi-component ^{41}K$-^{39}$K mixture [Cab18], whose con-crete parameters have been employed in our simulations. In this implementa-tion, the 1-2 gas is composed by a ^{39}K mixture in states $|1\rangle \equiv |F = 1, m_F = -1\rangle$ and $|2\rangle \equiv |F = 1, m_F = 0\rangle$, whereas the bath is composed by the state $|3\rangle \equiv |F = 1, m_F = -1\rangle$ of ^{41}K. In this setting, the system is in the lowest energy state
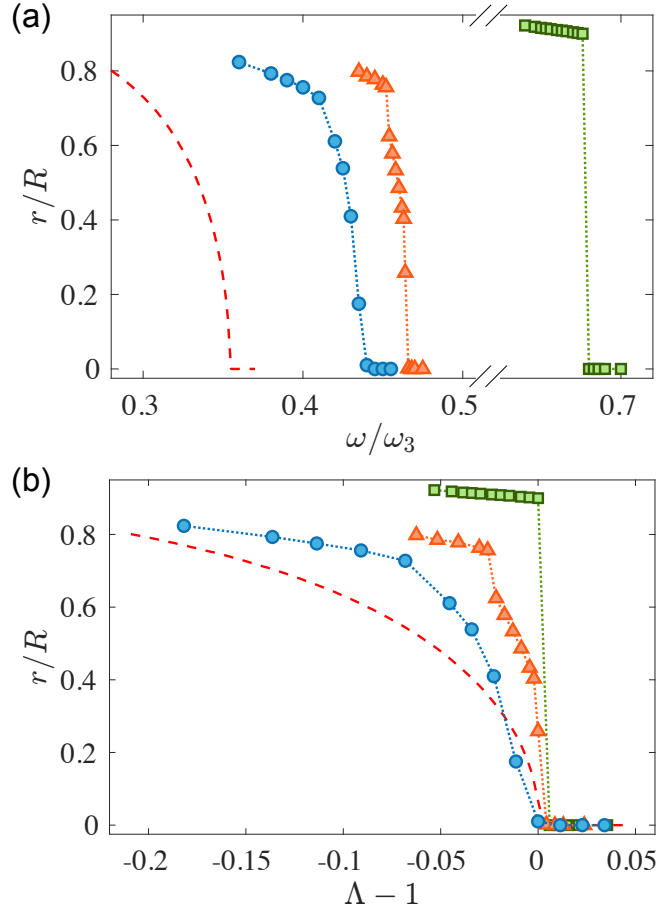
Figure 4.6: (a) Position of the quantum bubble for a Thomas-Fermi bath with $n_3(0) = 5 \times 10^{20} \, \mathrm{m}^{-3}$ (using $N_3 = 800\,000$), for the same parameters as in Fig. 4.2, for $N_1 = 1000$ (squares), $N_1 = 20\,000$ (triangles), $N_1 = 50\,000$ (circles) and $a_{33} = 100a_0$. The dashed curve indicates the position of the bubble obtained for the same $n_3(0)$ from the minimization of the energy per particle (4.4.29). Figure (b) shows in detail the arrested buoyancy regime in the vicinity of the critical frequency ratio for buoyancy, $\Lambda \equiv (\omega/\omega_3) = 1$. The $(\omega/\omega_3)_{\mathrm{cr}}$ arrested buoyancy window becomes more apparent when the LHY dominates the bubble physics. The scattering lengths considered are the same as in Fig. 4.6, except that a_{12} is slightly shifted, such that $\delta a = -5a_0$. Reprinted from [Edl+22]
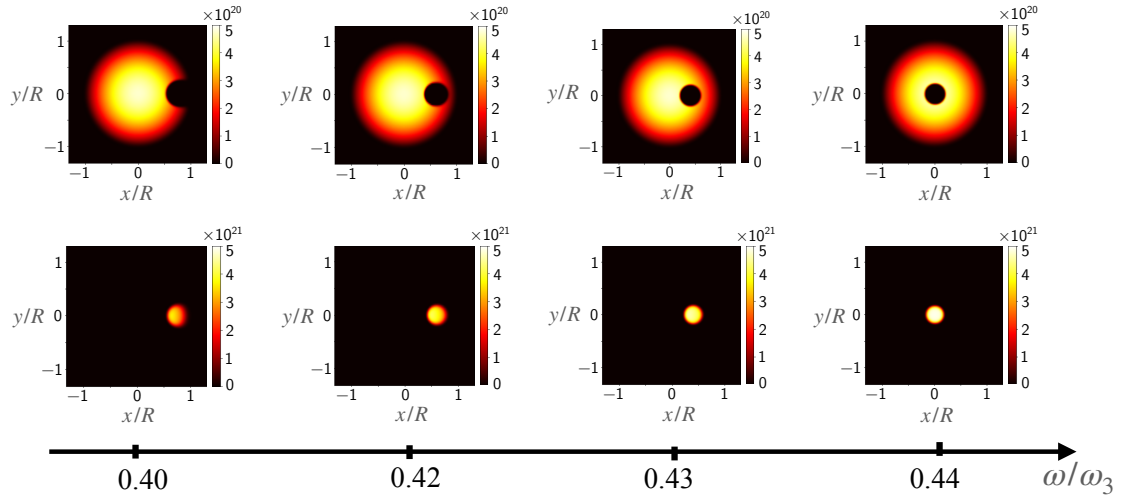
Figure 4.7: Arrested buoyancy for the same parameters as in Fig. 4.6, for $N = 8.2 \times 10^4$ and $n_3(0) = 4.7 \times 10^{20}\,\text{m}^{-3}$. The upper (lower) panels show the density profile of the bath $n_3(x, y, 0)$ (bubble $n_1(x, y, 0)$). When buoyancy sets in, and due to the effect of quantum fluctuations, the bubble does not move immediately to the bath surface, but rather remains at an intermediate distance between the center and the surface, breaking spontaneously spherical symmetry. Note also that when the bubble moves to the surface it remains compact, experiencing a crossover into a self-bound droplet. Reprinted from [Edl+22]

and inelastic spin-exchange collisions can be neglected [Tan+18b]. For the bubble, the parameter $\delta a \leq 0$ can be tuned in the vicinity of ~ 56.9 G [Cab+18; Sem+18] where the overlap of three different Feshbach resonances allows to control the values of a_{11}, a_{22}, and a_{12}. At this magnetic field, the bath-bubble interactions is set by the background ^{41}K$-^{39}$K scattering length, which is constant ($a_{13} = a_{23} \approx 172a_0$).

Since the system is composed by two different potassium isotopes, high-resolution *in situ* imaging detection can be performed in order to extract the bubble and bath density profiles independently. Experiments may then readily monitor how the contribution of the LHY energy at $G = 0$ affects the bubble size. For typical densities of $n_3 = 10^{20}\,\mathrm{m}^{-3}$, we can expect for large atom number in the bubble a discrepancy of up to 40% in its radius compared to the case where quantum fluctuations are neglected. This discrepancy becomes larger when increasing the density n_3. Hence, the analysis of the bubble size may readily reveal the effect of quantum fluctuations and the scaling features discussed in this chapter.

4.6 Conclusions

We have considered in this chapter a peculiar effective immiscible binary mixture. Two miscible components form an effective scalar condensate (1-2 gas) with enhanced quantum fluctuations due to mean-field quasi-cancellation, and a third component is immiscible with the other two. We have shown that due to quantum fluctuations, the properties of the effective mixture significantly depart from those well-known for an immiscible mean-field Bose-Bose gas. In particular, the volume of a quantum 1-2 bubble in component 3 presents a significantly modified dependence with respect to the bath density. Moreover, quantum fluctuations lead to an anomalous buoyancy criterion. Once buoyancy sets in, in contrast to the case of mean-field mixtures, the bubble may occupy an intermediate position between the center and the surface of the bath (arrested buoyancy). Furthermore, once the surface is reached the bubble may transition into a droplet, which remains compact and floating at the bath surface.

These results, which may be readily probed in e.g. Potassium mixtures, illustrate how quantum fluctuations, in addition to providing the stabilization mechanism for self-bound droplets, may significantly change other general and well established properties of Bose mixtures. We anticipate that a similar physics may be at play as well in immiscible mixtures, in which at least one of the components (forming

the quantum bubble) is dipolar within the regime of mean-field quasi-cancellation [Bla+22] (see the discussion on dipolar gases in the following chapters). However, the nonlocal anisotropic character of the dipole-dipole interaction may significantly affect the droplet properties and the buoyancy condition.

Part III

Dipolar Condensates

Chapter 5

Dipolar Bose-Einstein Condensates

In previous chapters, we restricted our discussion to short-range interacting gases, characterized by the *s*-wave scattering length. In this and the next chapter, we shall consider dipolar gases, in which magnetic or electric dipole-dipole interactions play a significant or even dominant role. The dipole-dipole interactions, being long-range and anisotropic, differ radically from the short-range isotropic interactions considered up to this point in this Thesis. As a result, the physics of dipolar gases is qualitatively different from that their non-dipolar counterparts, as we will briefly review in this chapter.

Electric or magnetic dipolar gases can be realized in a variety of systems. Electric dipoles have been studied in the context of polar molecules [Ni+08; Ni+10; Osp+10a] and Rydberg gases [Ton+04; Hei+08; GP08; SWM10]. However, most of the physics that we shall discuss in the following, and in particular quantum stabilization of droplets,has been realized using highly magnetic atoms.

In 2005 the group of T. Pfau reported the first dipolar BEC, achieved with Chromium atoms [Gri+05], a highly magnetic species with a magnetic dipole moment of $\mu = 6\mu_B$, with μ_B the Bohr magneton. This must be compared with that of alkali atoms, with a magnetic dipole moment of maximally $1\mu_B$. Dipolar effects in chromium gases were first reported in Stuttgart [Stu+05; Lah+07], and later in Paris Nord [Bis+10], followed by the observation of geometrical stabilization of a Chromium BEC [Koc+08], and dipole-induced *d*-wave collapse [Lah+08]. More recently, experiments with magnetic lanthanides have opened up new avenues for
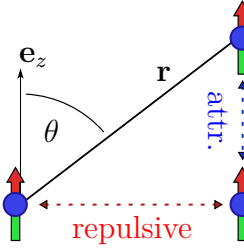
Figure 5.1: Dipoles polarized along the z direction. Due to the anisotropy of the dipole-dipole interaction potential, the interaction strength and its sign depends on the interparticle distance $r = |\mathbf{r}|$, and on the angle θ between $\mathbf{r}$ and $\mathbf{e}_z$. When staying side-by-side ($\theta = \frac{\pi}{2}$) the potential is repulsive and the dipoles repel each other, whereas in a head-to-tail configuration ($\theta = 0$) the interaction is attractive.

the study of dipolar physics with highly-magnetic atoms. Dysprosium ($\mu = 10\,\mu_B$) has been Bose-condensed in Stanford [Lu+11] and later on in Stuttgart, Innsbruck and Pisa, whereas an erbium ($\mu = 7\,\mu_B$) condensate has been realized in Innsbruck [Aik+12].

The chapter starts with a discussion on general properties of dipoles and their interaction potential in Sec. 5.1. The GPE with incorporated dipolar interactions is introduced in Sec. 5.2. The chapter continues with the presentation of the condensation of a dipolar gas in 5.3. Section 5.4 concentrates on the geometric stability of dipolar BEC in different trap geometries. The chapter closes in Sec. 5.5 with a discussion on phonon and roton instabilities.

5.1 Dipole-dipole interaction

Let us consider two dipoles, whose dipole moments are aligned along the unit vectors $\mathbf{e_1}$ and $\mathbf{e_2}$, respectively. Denoting the relative position vector as $\mathbf{r}$, and the relative distance as $r = |\mathbf{r}|$, the dipole-dipole interaction potential reads

$$V_{\mathrm{dd}}(\mathbf{r}) = \frac{C_{\mathrm{dd}}}{4\pi} \frac{(\mathbf{e}_1 \cdot \mathbf{e}_2)r^2 - 3(\mathbf{e}_1 \cdot \mathbf{r})(e_2 \cdot \mathbf{r})}{r^5} \tag{5.1.1}$$

where the constant C_{dd} is the *dipolar interaction strength*. For magnetic dipoles, $C_{\mathrm{dd,mag}} = \mu_0 \mu^2$, with μ_0 the vacuum permeability, and μ the magnetic dipole moment. For electric dipoles, the interaction strength is equal to $C_{\mathrm{dd,el}} = d^2/\varepsilon_0$, where d is the electric dipole moment, and ε_0 the vacuum permittivity.

One can compare the usual interaction strengths for magnetic atoms and polar molecules. Typical values for the magnetic dipole in highly magnetic atoms are of the order of $\mu \sim 1\,\mu_B$, with $\mu_B = 9.27 \times 10^{-24}\,\mathrm{J\,T^{-1}}$ [Cod] being the *Bohr magneton*. In bi-alkali polar molecules, once brought into the lowest ro-vibrational state and properly polarized by an external electric field, it is $d \sim 1\,\mathrm{D}$ where D is a more convenient Gauß unit called "Debye", $\mathrm{D} \approx 3.36 \times 10^{-30}\,\mathrm{C\,m}$. Note that $C_{\mathrm{dd,mag}}/C_{\mathrm{dd,el}} \approx 10^{-4}$, and hence the dipolar interactions are much weaker in magnetic systems. Highly magnetic atoms are, however, much easier to operate with. Indeed, whereas, as discussed below, experiments on magnetic dipolar gases are quite advanced in what concerns the study of many-body physics, experiments on polar molecules have been up to now significantly hindered by inelastic processes. These processes include exothermic chemical reactions [Osp+10b], and the so-called sticky collisions [MRB12], a process yet not fully understood. Recent experimental breakthroughs on shielding open, however, exciting perspectives for near-future developments concerning many-body physics in gases of polar molecules [Li+21; And+21; Sch+22].

In the following, we assume that the dipoles are polarized by an external field (as sketched in Fig. 5.1). Hence, the expression in Eq. (5.1.1) simplifies to

$$V_{\mathrm{dd}}(\mathbf{r}) = \frac{C_{\mathrm{dd}}}{4\pi} \frac{1 - 3\cos^2\theta}{r^3} \tag{5.1.2}$$

where θ describes the angle between the polarization axis and the relative position of the particles. The dipole-dipole interaction is most attractive when dipoles are in a head-to-tail configuration ($\theta = 0$). In contrast, when they are in a a side-by-side configuration ($\theta = \pi/2$), the interaction is most repulsive. At the so-called *magic angle*, $\theta = \arccos(1/\sqrt{3}) \approx 54.7°$, the interaction vanishes.

Interestingly, the dipolar interactions may be tuned if the polarization axis is not fixed in time, but rather rotates with a frequency Ω around an axis [GGP02]. For definiteness we will call this axis z, and consider magnetic dipoles in the time-dependent magnetic field $\mathbf{B} = B\{\cos\varphi\,\mathbf{e}_z + \sin\varphi[\cos(\Omega t)\mathbf{e}_x + \sin(\Omega t)\mathbf{e}_y]\}$ where the rotation forms a cone of aperture 2φ (see Fig. 5.2). The angular rotation frequency Ω must be chosen much smaller compared to the Larmor frequency $\Omega_L = \frac{\mu B}{\hbar}$ and much larger than the external trapping frequencies ω_i. With this proper choice of Ω the time-average potential of (5.1.1) reads [Lah+09]

$$\langle V_{\mathrm{dd}}(\mathbf{r}, t)\rangle = \frac{C_{\mathrm{dd}}}{4\pi} \frac{1 - 3\cos^2\theta}{r^3} \left(\frac{3\cos^2\varphi - 1}{2}\right). \tag{5.1.3}$$

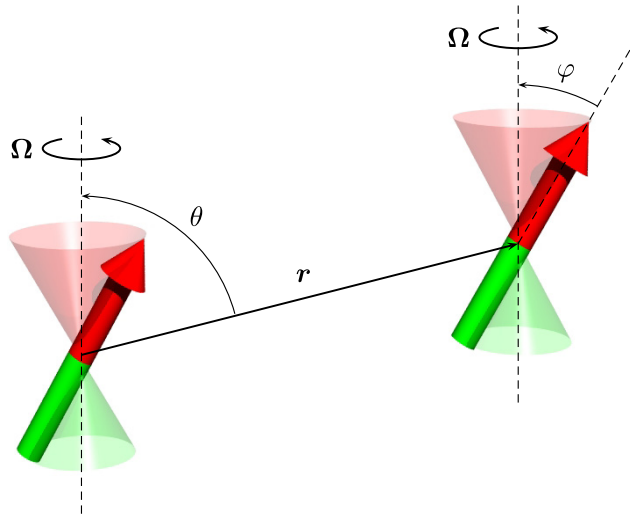The term in the brackets in Eq. (5.1.3) can take values from 1 at $\varphi = 0$ (no tilting)

Figure 5.2: Modifying the time-average dipole-dipole interaction by precessing the dipoles around the z-axis on a cone of angle 2φ. The picture was reprinted from [Lah+09]

to $-1/2$ at $\varphi = \pi$. At the *magic angle* $\varphi \approx 54.7°$ it changes its sign. This tuning was experimentally realized in recent experiments [Tan+18a].

5.2 Mean-field description of a dipolar condensate

The mean-field description for a dipolar BEC can be derived in a similar way as for the contact-interacting case. A first rigorous theoretical treatment was laid by L. You and S. Yi [YY00; YY01]. They constructed a pseudo-potential for a general anisotropic interaction. This result can be used to derive the time-independent GPE, which incorporates the dipole-dipole interactions as follows

$$\mu\Psi(\mathbf{r}) = \left(-\frac{\hbar^2\nabla^2}{2m} + V_{\text{ext}}(\mathbf{r}) + gn(\mathbf{r}) + \int \mathrm{d}^3r'\, V_{\text{dd}}(\mathbf{r} - \mathbf{r}')n(\mathbf{r}') \right) \Psi(\mathbf{r}). \quad (5.2.4)$$

Note that the dipolar pseudo-potential contains also a contact part proportional to $\delta^{(3)}(\mathbf{r})$ which is absorbed into the regular contact term. This makes the coupling constant $g = g(C_{\text{dd}})$ in principle dependent on the dipole strength.

For the calculation of the dipole term in (5.2.4) one can make use of the *convolution theorem*. It states that the Fourier transform of two convoluted functions is equal

to the product of the individually Fourier transformed functions, i.e.

$$\mathcal{F}\left[\int \mathrm{d}^3 r' \, V_{\mathrm{dd}}(\mathbf{r} - \mathbf{r}')n(\mathbf{r}')\right](\mathbf{k}) = \mathcal{F}\left[V_{\mathrm{dd}}(\mathbf{r})\right](\mathbf{k})\mathcal{F}\left[n(\mathbf{r})\right](\mathbf{k}) \tag{5.2.5}$$

where $\mathcal{F}[\cdot](\mathbf{k})$ is the Fourier transform operator to k-space. A detailed derivation of the Fourier transformed dipole-dipole interaction potential $\mathcal{F}[V_{\mathrm{dd}}](\mathbf{k}) = \tilde{V}_{\mathrm{dd}}(\mathbf{k}) = \frac{C_{\mathrm{dd}}}{3}\left(3\cos^2\theta_{\mathbf{k}} - 1\right)$ can be found in the literature [SSC12] or in the Appendix A.1. Unlike the real-space potential $V_{\mathrm{dd}}(\mathbf{r})$, the Fourier transformed potential does not diverge or posses any singular points, although it still exhibits a non-continuous behavior at the origin.

5.3 Condensate aspect ratio

Let us consider the case of a dipolar BEC, polarized along z, in an isotropic harmonic potential. We define the *trap aspect ratio* λ as the ratio of the axial and radial trapping frequencies, i.e. $\lambda = \frac{\omega_z}{\omega_\rho}$, which is in this case equal to one. Following the discussions of the dipolar anisotropy in Sec. 5.1 it is evident that for a sufficiently large relative dipolar strength

$$\varepsilon_{\mathrm{dd}} = \frac{C_{\mathrm{dd}}}{3g}, \tag{5.3.6}$$

a more prolate (cigar-like) cloud is energetically favorable, since on average more dipoles are in a head-to-tail configuration, hence reducing the energy. When we introduce the *cloud aspect ratio* $\kappa = \frac{\sigma_\rho}{\sigma_z}$, where σ_i is the cloud width in the i's direction, we expect it to be smaller than one, $\kappa < 1$. Figure 5.3 shows the results of experiments on condensed ^{52}Cr atoms performed in 2007 in the group of T. Pfau. Via a Feshbach resonance they changed the scattering length, and hence the coupling constant. By this, they were able to tune the relative dipolar strength $\varepsilon_{\mathrm{dd}}$ up to 0.5, where a clear distortion from a spherical cloud ratio is visible.

5.4 Geometric stability

Due to the anisotropic nature of the dipolar interaction, the stability of a dipolar condensate depends strongly on the trapping geometry [San+00]. In an oblate (pancake-like) cloud geometry, the dipoles are mostly in a side-by-side configuration, which results in a repulsive dipolar interaction. On the other hand, in
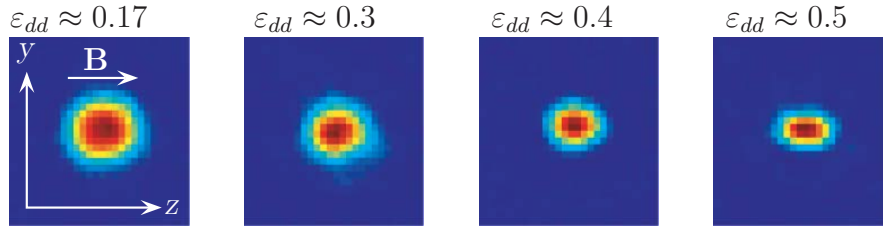
Figure 5.3: Absorption images in ^{52}Cr after $5\,\mathrm{ms}$ of expansion for different dipolar strengths $\varepsilon_{\mathrm{dd}}$. The change is due to a Feshbach resonance which modifies the contact interaction, and hence the ratio between contact and dipole-dipole interactions, i.e. $\varepsilon_{\mathrm{dd}}$. The stronger the relative dipole strength, the more prolate the cloud gets. Reprinted from [Lah+07].

a prolate (cigar-like) cloud, the interactions are in average attractive due to the mainly head-to-tail position of the dipoles. This attractive character may result in condensate collapse, unless the dipolar interactions are properly compensated by sufficiently repulsive contact-like interactions.

This geometrical stability was experimentally studied in 2008 in the group of T. Pfau [Koc+08]. First, they prepared their condensate of ^{52}Cr atoms, polarized along z, in the regime of dominant repulsive contact interactions. Afterwards, the contact interaction strength was reduced via a Feshbach resonance, which increased the relative dipolar strength $\varepsilon_{\mathrm{dd}}$. At a critical scattering length a_{crit} the condensate got unstable. This procedure can be repeated for various different trapping geometries λ, which can be seen in Fig. 5.4. The markers indicate the experimental observation whereas the lines are the numerical findings for $N = 20\,000$ particles of the border of stability. The thin line corresponds to the solution of the GPE. The thick line was achieved with a variational approach, where the wave-function was assumed to be a Gaussian, and its widths were varied to minimize the system energy [Koc+08; Lah+09]. Note that for a cigar-shape trap, a sufficiently large positive scattering length is needed to prevent collapse, whereas in a pancake trap the condensate is stable down to a critical negative scattering length.

5.4.1 Collapse of a dipolar condensate

In later experiments that year they studied the dynamics of that collapse in more detail [Lah+08]. As before, they first prepared the condensate in the stable regime, followed by a rapid ramp of the scattering length into the unstable regime, i.e. $a_f < a_{\mathrm{crit}}$. Subsequently, the system evolved for an adjustable time t_{hold}. The traps
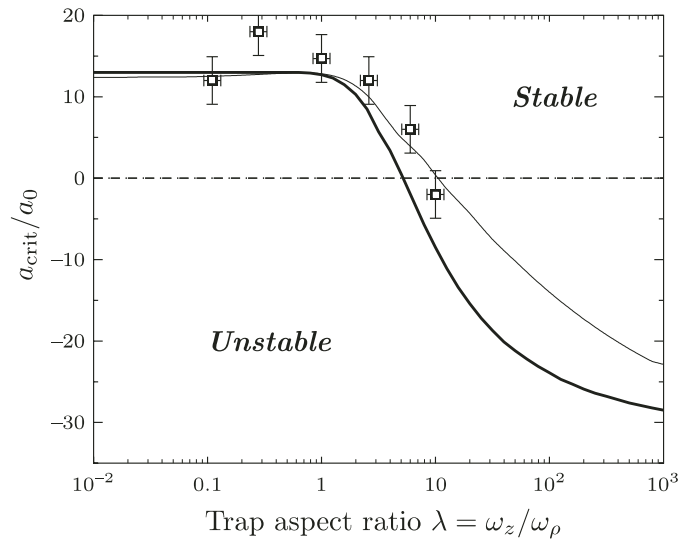
Figure 5.4: Stability diagram of a dipolar BEC of 20 000 ^{52}Cr atoms in a cylindrically-symmetric harmonic trap with $\lambda = \omega_z/\omega_\rho$. Note the logarithmic scale in the trap ratio. The squares indicate the experimental results for the stability threshold whereas the lines are inferred from a theoretical simulation. The thin lines correspond to solutions of the GPE, whereas the thick one results from a variational Gaussian ansatz. Reprinted from [Lah+09].
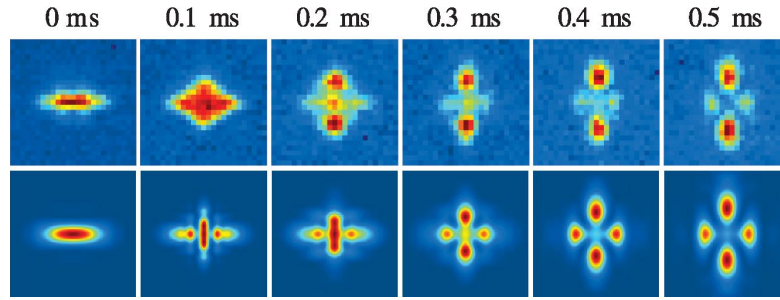
Figure 5.5: Experimental images (top row) of a condensate of ^{52}Cr atoms after collapse for various holding times t_{hold}. The numerical images (bottom row) are the solutions of Eq. (5.4.7). We see an excellent agreement with the experiment. Note the d-wave geometry of the exploding cloud resulting from the dipolar collapse, and subsequent three-body losses. Reprinted from [Lah+08].

were switched off, and the system was imaged after a time-of-flight of $t_{\text{TOF}} = 8\,\text{ms}$. The results for different holding times are depicted in Fig. 5.5. During the collapse, the cloud width reduces in radial direction and its density increases. This is due to the anisotropic nature of the dipolar interaction as the collapsed mean-field state is an infinitely thin cylinder. The condensate collapses until inelastic three-body losses dominate at large densities, which leads to particle losses, driving the subsequent explosion.

5.4.2 Collapse in Chromium

To incorporate the losses in the numerics one may add a non-unitary three-body loss term of the form $(-i\hbar L_3 n^2/2)\Psi$ to the time-dependent GPE, i.e.

$$i\hbar\frac{\partial\Psi(\mathbf{r},t)}{\partial t} = \left(-\frac{\hbar^2\nabla^2}{2m} + V_{\text{ext}}(\mathbf{r}) + gn(\mathbf{r},t) + \int \mathrm{d}^3r'\, V_{\text{dd}}(\mathbf{r}-\mathbf{r}',t)n(\mathbf{r}',\mathbf{t})\right.$$
$$\left. -i\frac{\hbar L_3}{2}n^2(\mathbf{r},t)\right)\Psi(\mathbf{r},t),$$
$$(5.4.7)$$

where, for chromium experiments, $L_3 \sim 2\times 10^{-40}\,\text{m}^6\,\text{s}^{-1}$ describes the three-body losses that occur close to the Feshbach resonance [Lah+08]. The simulations are in the bottom row of Fig. 5.5 and are in an excellent agreement with the experiment. We will see below in this Thesis, that these results, obtained in chromium

experiments, radically differ from those in lanthanide atoms, as dysprosium and erbium.

5.4.3 Thomas-Fermi regime

Similar to the non-dipolar case in Sec. 1.3.2 we may neglect the quantum pressure as long as the interactions are strong enough, entering the Thomas-Fermi regime, where one can obtain an analytic solution.

Remarkably, although we are facing a non-trivial interaction potential, the Thomas-Fermi solution for a trapped dipolar BEC still exhibits a similar inverted parabolic-shaped density distribution as that of a non-dipolar case [PO08]. In particular, for a cylindrically-symmetric trap around the dipole direction z, with axial harmonic frequency ω_z and radial frequency ω_ρ, the ground-state density profile reads

$$n(\mathbf{r}) = \begin{cases} n_{\text{peak}} \left(1 - \frac{r_\rho^2}{R_\rho^2} - \frac{r_z^2}{R_z^2} \right), & 0 \le \frac{r_\rho^2}{R_\rho^2} + \frac{r_z^2}{R_z^2} \le 1 \\ 0, & \text{else} \end{cases} \tag{5.4.8}$$

with the dipolar Thomas-Fermi radii [Lah+09; EGO05]

$$R_\rho = \left\{ \frac{15gN\kappa}{4\pi\omega_\rho} \left[1 + \varepsilon_{\text{dd}} \left(\frac{3}{2} \frac{\kappa^2 f(\kappa)}{\kappa^2 - 1} - 1 \right) \right] \right\}^{1/5}, \qquad \kappa = \frac{R_\rho}{R_z} \tag{5.4.9}$$

where

$$f(\kappa) = \frac{1 + 2\kappa^2}{1 - \kappa^2} - \frac{\kappa^2 \operatorname{artanh} \sqrt{1 - \kappa^2}}{(1 - \kappa^2)^{3/2}}. \tag{5.4.10}$$

In the Thomas-Fermi regime, one can obtain a closed transcendental equation, which provides a relation between the cloud aspect ratio κ, the trap aspect ratio $\lambda = \frac{\omega_z}{\omega_\rho}$, and the relative dipolar strength ε_{dd}:[Lah+09; EGO05]

$$3\kappa\varepsilon_{\text{dd}} \left[\left(\frac{\lambda^2}{2} + 1 \right) \frac{f(\kappa)}{\kappa^2 - 1} - 1 \right] + (\varepsilon_{\text{dd}} - 1)(\kappa^2 - \lambda^2) = 0. \tag{5.4.11}$$

The equation may be evaluated for different values of λ. The results are depicted in Fig. 5.6. Interestingly, Eq. (5.4.11) results in more than one solution κ for a given value of the trap ratio λ. One can see that in the regime of $0 < \varepsilon_{\text{dd}} < 1$ the cloud aspect ratio κ decreases monotonously with increasing relative dipolar strength ε_{dd}. In other words, the cloud is more prolate than the trap. For $\varepsilon_{\text{dd}} > 1$ we get two possible solutions for κ. The more oblate solution is meta-stable whereas the more prolate one is unstable.
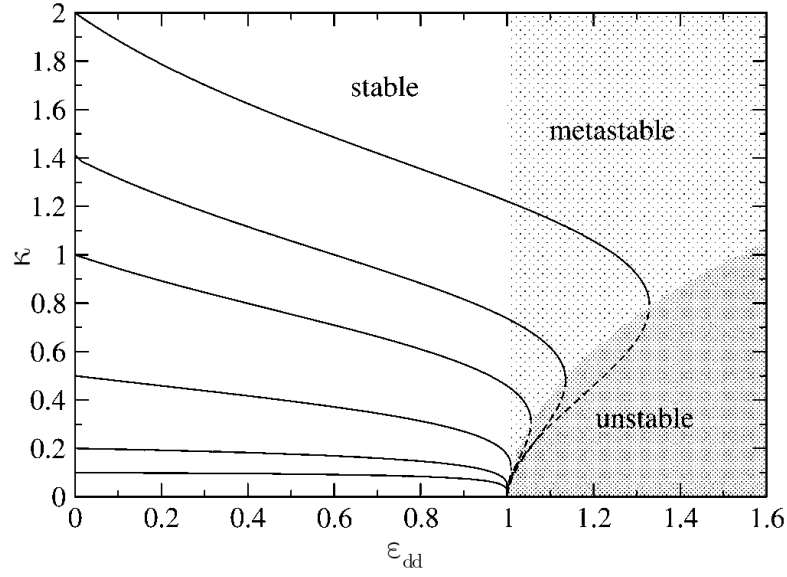
Figure 5.6: Condensates aspect ratio $\kappa = \frac{\sigma_\rho}{\sigma_z}$ as a function of the dipolar strength $\varepsilon_{\mathrm{dd}}$. Each line is for fixed trapping ratio $\lambda = \frac{\omega_z}{\omega_\rho}$. Reprinted from [EGO05].

5.5 Instability mechanisms in a dipolar condensate

5.5.1 Phonon instability

The elementary excitations of a dipolar condensate can be calculated in a similar way as we discussed in previous chapters for their non-dipolar counterparts. Note, that the interaction potential is now composed of a contact interaction and a dipole-dipole interaction part, i.e. $\tilde{V}_{\mathrm{int}}(\mathbf{q}) = g + \tilde{V}_{\mathrm{dd}}(\mathbf{q})$. In the case of a homogeneous three-dimensional system, the dispersion relation can be calculated analytically, obtaining [SSC12]

$$\varepsilon(\mathbf{k}) = \sqrt{\frac{\hbar^2 k^2}{2m} \left[\frac{k^2 k^2}{2m} + 2gn \left(1 + \varepsilon_{\mathrm{dd}}(3\cos^2\theta_k - 1) \right) \right]}. \tag{5.5.12}$$

To analyse and understand the dispersion relation, first, we should have a look to the case of small momenta, i.e. in the limit of $k \to 0$. In that case the expression in Eq. (5.5.12) reduces to [SSC12]

$$\varepsilon(\mathbf{k})\Big|_{k \to 0} = \hbar k c_s \sqrt{1 + \varepsilon_{\mathrm{dd}}(3\cos^2\theta_k - 1)} \tag{5.5.13}$$

where $c_s = \sqrt{\frac{gn}{m}}$ is the *sound velocity*. In absence of dipole-dipole interactions, i.e. $\varepsilon_{\text{dd}} = 0$, one recovers the usual linear *phononic* relation $\varepsilon(k) = \hbar k c_s$.

Due to the anisotropic nature of the dipole-dipole interactions, the spectrum is in turn also anisotropic. The energy of modes with $\theta_k < \arccos(1/\sqrt{3}) = \theta_{\text{magic}}$ increases when ε_{dd}. We shall call these modes the *hard modes*. For $\theta_k > \theta_{\text{magic}}$ the energy decreases for increasing ε_{dd}. We shall call these modes the *soft modes*. The softer modes occur for $\theta_k = \pi/2$, i.e. for momenta perpendicular to the dipolar orientation. Then we get the dispersion relation

$$\varepsilon(k, \theta_k = \pi/2)\big|_{k \to 0} = \hbar k c_s \sqrt{1 - \varepsilon_{\text{dd}}}. \tag{5.5.14}$$

When the interaction strength ε_{dd} surpasses one, the excitation modes become purely imaginary. Consequently, the dipolar condensate becomes dynamically unstable against long-wave length excitation. This instability at small momentum is also called *phonon instability*. This instability problem resembles that of homogeneous, purely contact interacting BECs, i.e. $V_{\text{dd}} = 0$, with a negative scattering length [PS04].

5.5.2 Roton instability

Interestingly, dipolar condensates present yet another form of instability. Let us consider a harmonically confined dipolar condensate in the z-direction, trapped by ω_z, and uniformly distributed on the xy-plane. The corresponding non-local time-dependent GPE reads

$$i\hbar \frac{\partial}{\partial t} \psi(\mathbf{r}, t) = \left[-\frac{\hbar^2}{2m} \nabla^2 - \mu + \frac{m\omega_z^2 z^2}{2} + gn(\mathbf{r}, t) + \int \mathrm{d}^3 r' \, V_{\text{dd}}(\mathbf{r} - \mathbf{r}') n(\mathbf{r}', t) \right] \psi(\mathbf{r}, t)$$
$$\tag{5.5.15}$$

Here, the groundstate wave-function decomposes into two parts. Hence, the integration of the dipole-dipole interaction term over the in-plane coordinates can be performed and we can obtain a one-dimensional equation which has the form of a GPE for a one-dimensional system with short-range interactions:

$$\left[\frac{-\hbar^2}{2m} \frac{\mathrm{d}^2}{\mathrm{d}z^2} + \frac{m\omega_z^2 z^2}{2} + (g + g_d) n_0 - \mu \right] \psi_0(z) = 0 \tag{5.5.16}$$

where $g_d = 8\pi C_{\text{dd}}/3$. We shall concentrate on the case of positive $g + g_d$ where $\mu > 0$. When we assume $\mu \gg \hbar\omega_z$ the BEC is in the Thomas-Fermi regime
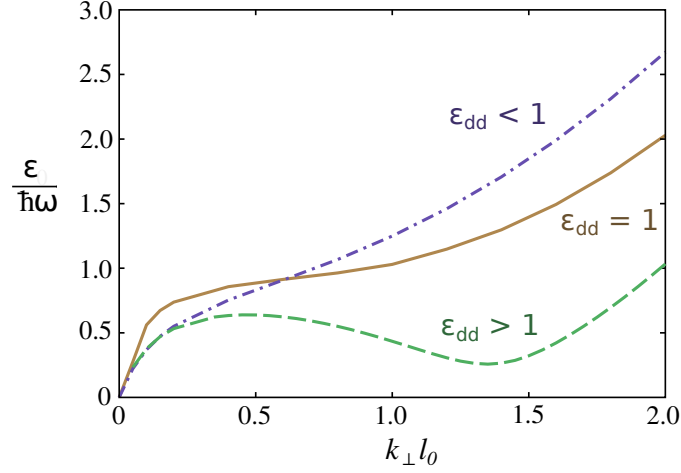
Figure 5.7: Dispersion relation of a dipolar BEC trapped in the dipole direction and uniformly distributed on the xy-plane. The momentum is units of $k_\perp l_0$ where $l_0 = \sqrt{\hbar/m\omega_z}$. The dash-dotted and solid lines show a monotonous spectrum for $\varepsilon_{dd} < 1$ and $\varepsilon_{dd} = 1$, respectively. In contrast, the dashed line features the roton-maxon spectrum. Adapted from [SSL03].

with a density profile $n_0(z) = n_{\text{peak}}(1 - \frac{z^2}{R_{\text{TF}}^2})$ with peak density $n_{\text{peak}} = \frac{\mu}{g+g_d}$ and Thomas-Fermi radius $R_{\text{TF}} = \sqrt{\frac{2\mu}{m\omega^2}}$.

Santos *et al.* [SSL03] showed in 2003 that the energy spectrum of a dipolar BEC can be non-monotonic, in stark contrast to the non-dipolar case.

The elementary excitations on top of ψ_0 may be studied by means of a Bogoliubov-de Gennes analysis. As the system considered is translational invariant on the xy plane, the in-plane momentum $\mathbf{k}_\perp$ can be used as a proper quantum number, and one may look for solutions of the form:

$$\psi(\mathbf{r}, t) = \psi_0(z) + u(z)e^{i\mathbf{k}_\perp \cdot \boldsymbol{\rho}}e^{-i\omega t} + \overline{v(z)}e^{-i\mathbf{k}_\perp \cdot \boldsymbol{\rho}}e^{-i\omega t}. \tag{5.5.17}$$

Introducing $f_\pm = u \pm v$ the Bogoliubov-de Gennes equations become of the form:

$$\begin{aligned} \hbar\omega f_-(z) &= \hat{H}_{\text{kin}} f_+(z), \\ \hbar\omega f_+(z) &= \hat{H}_{\text{kin}} f_-(z) + \hat{H}_{\text{int}}[f_-(z)], \end{aligned} \tag{5.5.18}$$

where

$$\hat{H}_{\text{kin}} = \frac{\hbar^2}{2m} \left[-\frac{\mathrm{d}^2}{\mathrm{d}^2 z} + k_\perp^2 + \frac{\nabla^2 \psi_0}{\psi_0} \right], \tag{5.5.19}$$

$$\hat{H}_{\text{int}}[f_-] = 2(g + g_d)\psi_0^2(z)f_-(z)$$
$$- \frac{3}{2} k_\perp g_d \psi_0(z) \int_{-\infty}^{\infty} \mathrm{d}z' \, \psi_0(z') e^{-k_\perp |z-z'|} f_-(z'). \tag{5.5.20}$$

For each $k_\perp$ one may determine the lowest energy $\omega_0(k_\perp)$, which provides the dispersion law.

For small momenta $k_\perp R \ll 1$ the phonon excitations are basically two-dimensional, and since the dipoles interact in average side-by-side the phonon spectrum is stable, i.e. there is no phonon instability. In contrast, for large-enough momenta $k_\perp R \gg 1$ the excitations acquire a three-dimensional character. Since the dipole-dipole interaction is attractive along z, the repulsive character of the total interaction is reduced, leading to a decrease of the eigenenergy. Eventually for even larger momentum, the kinetic term dominates and the spectrum resembles the one of a free-particle solution. As a result, under proper conditions, the Bogoliubov spectrum of a trapped dipolar condensate may present a local minimum, see Fig. 5.7, which resembles the celebrated roton minimum in Helium [Lan47; Fey54]. One should point however that the physics behind both rotons is of course very different. Recently, breakthrough experiments in erbium atoms have finally proved the existence of dipolar rotons in quasi-one-dimensional geometries [Cho+16; Pet+19].

For large-enough momenta, i.e. $k_\perp R \gg 1$, where the excitations have a three-dimensional character, one can derive an analytic expression for the excitation spectrum in the vicinity of the roton momentum (i.e. the momentum at the roton minimum) k_{roton} [SSL03]

$$\varepsilon^2(k_\perp) = E_{k_\perp}^2 - 2E_{k_{\text{roton}}} E_{k_\perp} + \hbar^2 \omega_z^2, \tag{5.5.21}$$

with $E_{k_\perp} = \frac{\hbar^2 k_\perp^2}{2m}$, and where the equation

$$E_{k_{\text{roton}}} = \frac{2}{3} \frac{(\varepsilon_{\text{dd}} - 1)(5\varepsilon_{\text{dd}} + 1)}{(2\varepsilon_{\text{dd}} + 1)(4\varepsilon_{\text{dd}} + 1)} \mu \tag{5.5.22}$$

provides the roton momentum. Note that

$$\varepsilon^2(k_\perp) = (E_{k_\perp} - E_{k_{\text{roton}}})^2 + \hbar^2 \omega_z^2 - E_{k_{\text{roton}}}^2, \tag{5.5.23}$$

and the roton minimum occurs for an energy

$$\Delta E = \sqrt{\hbar^2 \omega_z^2 - E_{k_{\text{roton}}}^2}. \tag{5.5.24}$$

When this energy reaches zero, the condensate develops a new form of instability, the so-called roton-instability. In contrast to the phonon instability which occurred at low momenta, the roton instability occurs for intermediate momenta. Roton instability results in a dynamical instability against the formation of a density modulation with the roton wavelength. This instability was observed in 2018 in a breakthrough experiment with ^{166}Er by F. Ferlaino's group (see Fig. 5.8), were they reported the first observation of the roton excitation [Cho+18]. Later experiments in the same group mapped conclusively the roton dispersion [Pet+19].

In mean-field theory the roton instability leads eventually to the formation of local collapses. The situation, under proper conditions, may be very different in the presence of quantum fluctuations, as we discuss in the following chapter.
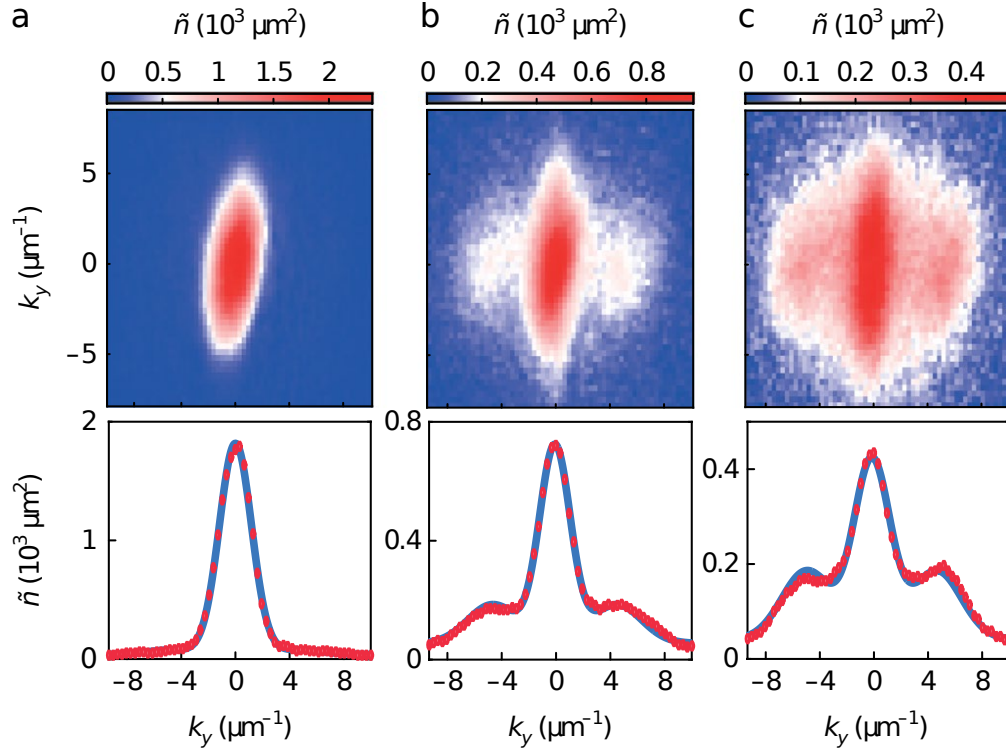
Figure 5.8: Experimental results at F. Ferlaino's group reporting for the first time the observation of roton excitations in an elongated dipolar condensate, along a direction perpendicular the dipole orientation. A quench of the scattering length leads to roton instability, which triggers a modulation that results in side peaks observable in the momentum distributions $\tilde{n}(k_x, k_y)$ obtained in time-of-flight experiments. The average results over 15-25 single-shot images is shown in the top row. The bottom row shows the corresponding cuts at $k_x \approx 0$. Reprinted from [Cho+18].

Chapter 6

Dipolar quantum droplets

In the preceding Chapter 5, we introduced the physics of dipolar systems. We discussed their geometry-dependent stability, and in particular the d-wave collapse observed in Chromium experiments. In this chapter, we shall see that this collapsing behavior is not a general feature of dipolar condensates. In particular, as discussed in Sec. 6.1, experiments in dysprosium and erbium do not show such a collapse, but rather the emergence of ultra-dilute liquid-like droplets. The mean-field theoretical model introduced in the previous chapter is clearly insufficient to explain this phenomenon. Thus, in Sec. 6.2, and following ideas already introduced in previous chapters, the theory of dipolar condensates is extended in order to include the surprisingly relevant role played by quantum fluctuations. This chapter closes in Sec. 6.4 with a brief discussion on *dipolar supersolids*, a new state of matter recently observed in experiments, which results from the combined effect of the enhanced role of quantum fluctuations and external confinement.

6.1 Dipolar quantum droplets

Dysprosium atoms have one of the largest magnetic moments of all elements in the periodic table, with a magnetic moment of around $10\,\mu_{\mathrm{B}}$. Additionally, the background scattering length is relatively small, which makes it possible to achieve, even without the use of Feshbach resonances, a large relative dipole strength $\varepsilon_{\mathrm{dd}}$.
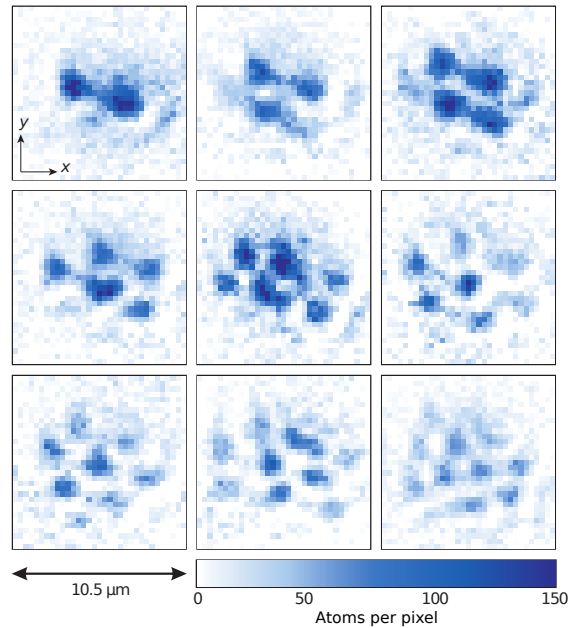
Figure 6.1: Experimental in-situ images showing the formation of droplets in Dysprosium experiments after a quench of the scattering length into the mean-field unstable regime. Reprinted from [Kad+16]

Hence, once condensation is achieved, dysprosium constitutes an optimal system for studying dipolar condensates.

In 2015, the group of T. Pfau performed experiments with ultra-cold dysprosium [Kad+16] in which they approximately repeated the procedure performed on chromium atoms in Ref. [Lah+08], in which they observed the d-wave collapse discussed in Sec. 5.4. They created a stable condensate of approximately $15\,000$ particles in an oblate trap with dipoles aligned along the z direction. With the help of a Feshbach resonance they modified the scattering length such that $\varepsilon_{\text{dd}} \approx 1$. Subsequently, the scattering length was further lowered to achieve $\varepsilon_{\text{dd}} > 1$, for values in which the mean-field theory discussed in the preceeding chapter predicted instability against collapse. Surprisingly, the experiment revealed something very different (see Fig. 6.1). The dipole-driven collapse instead was arrested at densities of $n \gtrsim 5 \times 10^{20}\,\text{m}^{-3}$, still well within the ultra-dilute, weakly interacting, regime, resulting in the formation of droplets. Similar results were subsequently reported in Erbium experiments in F. Ferlaino's group in Innsbruck [Cho+16].

The obvious immediate question was to find the stabilization mechanism that prevented collapse. Such a mechanism had to be density-dependent, to have a higher

order with density than the mean-field term, and to be repulsive to compensate the attractive mean-field interaction. First attempts tried to explain the phenomenon with large conservative, i.e. non particle loosing, three-body interactions. The conservative part must have been two to three orders of magnitude larger than the non-conservative ones [BB15]. However, no conclusive explanation for these values could be given. It became however quickly clear that quantum fluctuations were responsible for the observed stabilization, in a process analogous to that discussed in Sec. 2.3 for non-dipolar binary mixtures.

6.2 Lee-Huang-Yang correction for a dipolar condensate

Using the Hugenholtz-Pines formalism introduced in Chapter 3, we can obtain the equation for the LHY energy density correction $\mathcal{E}_{\text{LHY}} = E_{\text{LHY}}/V$:

$$\mathcal{E}_{\text{LHY}}(n) - \frac{1}{2}n\frac{\partial}{\partial n}\mathcal{E}_{\text{LHY}}(n) = \chi(n) \tag{6.2.1}$$

with

$$\chi(n) = -\frac{1}{2}\int \mathrm{d}^3k \, \frac{1}{(2\pi)^3}\frac{[\varepsilon(\mathbf{k}) - \epsilon(k)]^3}{4\varepsilon(\mathbf{k})\epsilon(k)} \tag{6.2.2}$$

where we have the free particle energy $\epsilon(k) = \frac{\hbar^2 k^2}{2m}$ and the Bogoliubov modes

$$\varepsilon(\mathbf{k}) = \sqrt{\epsilon(k)[\epsilon(k) + \tilde{V}_{\text{int}}(\theta_k)]} \tag{6.2.3}$$

with

$$\tilde{V}_{\text{int}}(\theta_k) = 2n\gamma(\theta_k), \qquad \gamma(\theta_k) := g + \frac{C_{\text{dd}}}{3}(3\cos^2\theta_k - 1). \tag{6.2.4}$$

In Sec. 1.4 we already derived the LHY-correction for a three dimensional system with only contact interactions. We found that such the LHY energy density scales with the particles density as $n^{5/2}$. Although, now we have additional dipole-dipole interactions, from the potential in Eq. (6.2.4) we can see that this should not change the power-law dependence. Hence, we can introduce a function $G(\mathbf{k})$ and employ the ansatz $\mathcal{E}_{\text{LHY}} = n^{5/2}G(\mathbf{k})$. We can apply the derivative and plug it into the differential equation (6.2.1):

$$n^{5/2}G(\mathbf{k}) - \frac{1}{4}n^{5/2}G(\mathbf{k}) = -\frac{1}{4}\mathcal{E}_{\text{LHY}} = \chi(n). \tag{6.2.5}$$

This gives us an expression for the LHY correction energy density

$$\mathcal{E}_{\text{LHY}}(n) = \frac{64}{15\sqrt{\pi}} gn(na)^{3/2} \mathcal{Q}_5(\varepsilon_{\text{dd}}), \qquad \mathcal{Q}_5(\varepsilon_{\text{dd}}) := \int_0^1 \mathrm{d}u \left[1 + \varepsilon_{\text{dd}}(3u^2 - 1) \right]^{5/2}$$

(6.2.6)

and the corresponding chemical potential

$$\mu_{\text{LHY}} = \frac{32}{3\sqrt{\pi}} gn\sqrt{na^3} \mathcal{Q}_5(\varepsilon_{\text{dd}}).$$

(6.2.7)

The $\mathcal{Q}_5(\varepsilon_{\text{dd}})$ can be even further evaluated as [Pol+21]

$$\mathcal{Q}_5(\varepsilon_{\text{dd}}) = \frac{(3\varepsilon_{\text{dd}})^{5/2}}{48} \left[(8 + 26\alpha + 33\alpha^2)\sqrt{1 + \alpha} + 15\alpha^2 \ln\left(\frac{1 + \sqrt{1 + \alpha}}{\sqrt{\alpha}} \right) \right] \quad (6.2.8)$$

with $\alpha = (1 - \varepsilon_{\text{dd}})/(3\varepsilon_{\text{dd}})$. The function $\mathcal{Q}_5(\varepsilon_{\text{dd}})$ increases monotonously for $0 < \varepsilon_{\text{dd}} < 1$, taking values in the closed interval from 1 to $\frac{3}{2}\sqrt{3} \approx 2.6$. It becomes complex for $\varepsilon_{\text{dd}} > 1$. The imaginary part signals a dynamical instability, as discussed in the previous chapter. For values of ε_{dd} in the vicinity of the instability, i.e. $\varepsilon_{\text{dd}} \gtrsim 1$, the imaginary part of $\mathcal{Q}_5(\varepsilon_{\text{dd}})$ is several orders of magnitude smaller than its real part, and hence it may be neglected.

In 2011, A. Lima and A. Pelster derived the very same term in Eq. (6.2.6) but using a different approach [LP11; LP12]. Instead of the presented method, based on the Hugenholtz-Pines formalism [HP59], they used a similar method as that discussed in Chapter 1.4, where one needs to cure the ultraviolet divergence. One can quickly verify that in the case of a non-dipolar system, i.e. $\varepsilon_{\text{dd}} = 0$, the expression recovers the equation (1.4.31) from the first chapter. Interestingly, despite the anisotropic dipole-dipole interaction in the mean-field term, the LHY corrections are isotropic.

6.2.1 Quantum stabilization

Note that at the boundary of mean-field collapse instability, the contact and dipolar contributions to the mean-field energy are of comparable size but opposite sign, and hence the mean-field energy quasi-cancels. This is indeed a very similar scenario as that of non-dipolar binary mixtures in Sec. 2.3, in which intra- and inter-component interactions also quasi-cancelled at the mean-field level.

The overall mean-field contribution is slightly attractive, and hence energy is minimized for increasing densities. This caused the mean-field collapse of a dipolar

condensate discussed in the previous chapter. However, as for non-dipolar binary mixtures, with the included LHY-correction, with a density proportional to $\propto n^{5/2}$, we can see that with increased density the repulsive LHY-correction becomes more relevant. Hence, at sufficiently large densities the LHY-correction eventually balances the mean-field term, which stabilizes the system and prevents collapse. This mechanism, as for the case of binary mixtures, explains the observation of quantum droplets in a dipolar condensate. We note at this point that due to the anisotropy of the dipole-dipole interactions, dipolar droplets differ from those of binary mixtures in the fact that they are elongated along the dipole direction, instead of being spherical as in binary mixtures.

6.3 Extended Gross-Pitaevskii equation for a dipolar condensate

In Sec. 2.2.2 we introduce the idea of extended Gross-Pitaevskii equation. In 2016, F. Wächtler and L. Santos introduced a non-local extended Gross-Pitaevskii equation for the study of dipolar condensates, that includes both the mean-field interplay between contact and dipole-dipole interactions, and the effects of quantum fluctuations in local density approximation. The eGPE acquires the form:

$$i\hbar\frac{\mathrm{d}\Psi(\mathbf{r})}{\mathrm{d}t} = \left[\frac{-\hbar^2\nabla^2}{2m} + V_{\text{ext}}(\mathbf{r}) + gn(\mathbf{r}) + \int \mathrm{d}^3r'\, V_{\text{dd}}(\mathbf{r}-\mathbf{r}')n(\mathbf{r}') \right.$$
$$\left. +\frac{32}{3\sqrt{\pi}}gn(\mathbf{r})\sqrt{n(\mathbf{r})a^3}\mathcal{Q}_5(\varepsilon_{\text{dd}})\right]\Psi(\mathbf{r}). \quad (6.3.9)$$

We note that this equation is obtained from the minimization of the energy functional, in which one includes the effect of quantum fluctuations using local-density approximation and the above-mentioned expression of the LHY correction in an homogeneous dipolar condensate [WS16b]. We stress at this point that, as already mentioned in previous chapters, the local-density approximation is generally correct if the main contribution to the LHY correction stems from short-wavelength excitations. It was previously shown for typical values in the Thomas-Fermi regime and the error was proven to be negligible [LP11]. However, in typical experiments as the seminal ones of T. Pfau's group [Kad+16], the quantum droplet is only in Thomas-Fermi regime along the axial, z, direction. In the case of small droplets the density profile was rather a Gaussian in radial direction. To check the validity, Wächtler and Santos compared an adjusted LHY correction with a low momentum cut-off with the full LHY and found, for typical values in the experiments,
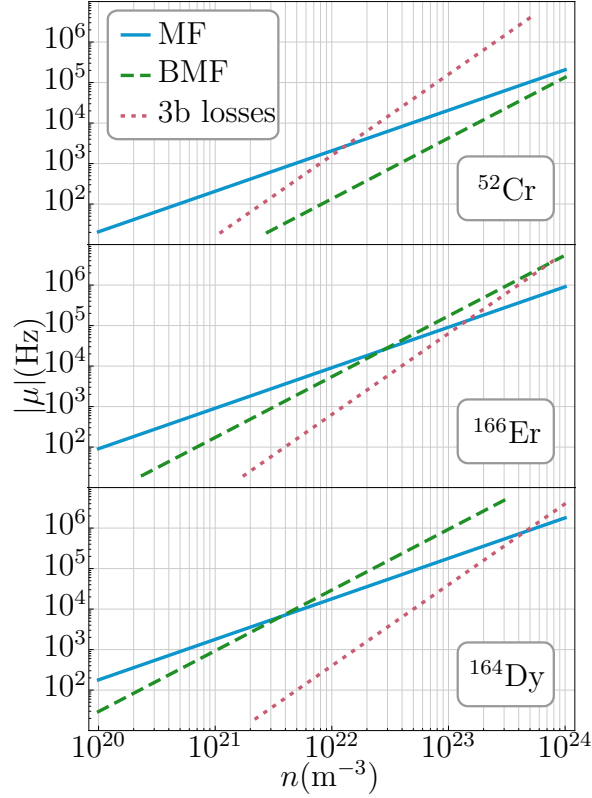
Figure 6.2: Different contributions to the extended Gross-Pitaevskii equation in absolute value $|\mu|$, considering a homogeneous density and $\varepsilon_{\mathrm{dd}} = 1.5$ in all cases. In the log-log-plot, the attractive mean-field contribution (blue solid line) has a slope of 1 and dominates at low densities. Whereas for ^{52}Cr the three-body loss rate (grey dotted line) crosses the curve of the mean-field energy before the beyond mean-field (BMF) contribution (green dashed line) does, in ^{166}Er and ^{164}Dy the BMF crosses first. This is crucial to understand why droplets have been observed in ^{166}Er and ^{164}Dy, whereas collapse occurred in ^{52}Cr. Reprinted from [Cho+22].

that the adjusted LHY correction is still $\sim 80\,\%$ of the total LHY correction. As briefly discussed at the end of Chapter 7, the local-density approximation is in general a very good approximation for typical experiments, even for relatively small droplets. We finally note that numerical results based on Path Integral Monte Carlo techniques have confirmed the validity of Eq. (6.3.9) for the description of the droplets created in quench experiments [Sai16].

As for the case of binary mixtures, quantum stabilization allows for the realization of self-bound dipolar droplets, and indeed their theoretical prediction based on the eGPE 6.3.9 [Bai+16; WS16a] was quickly followed by their experimental observation in T. Pfau's group [Sch+16].

6.4 Dipolar supersolids

The presence of a sufficiently strong confinement along the dipole direction changes the physics of dipolar droplets, resulting in a surprisingly rich physics, which is absent in non-dipolar binary mixtures.

When we consider an ordinary liquid droplet and apply a compressional force along a specific axis, e.g. the gravitational force, the droplet deforms and spreads in perpendicular direction in order to maintain its density and volume. The same happens in quantum droplets in binary mixtures. However, in the case of a polarized dipolar system, we need to take the anisotropic character of the dipole-dipole interaction into account. As mentioned above, quantum droplets acquire an elongated shape along the dipole direction. The more particles enter the system, the more elongated it gets while simultaneously keeping an optimal peak density. The presence of a strong-enough confinement along the dipole direction changes this picture. For a sufficiently large number of particles it becomes energetically unfavorable to pile up particles in a progressively more elongated droplet. As a result, the system minimizes its energy by creating more than one droplet. Moreover, in an elongated trap (with its axis perpendicular to the dipole orientation) the droplets arrange in a regular array due to the inter-droplet dipolar repulsion. The formation of an array of quantum droplets was first reported by T. Pfau's group in Ref. [Wen+17].

The observation of a dipolar array opened naturally intriguing questions about the possibility to observe a supersolid phase in dipolar condensates. Supersolids constitute an intriguing state of matter that combines superfluidity and the crys-

talline order characteristic of a solid [BP12]. Despite early success in the creation of superfluidity in Helium this long-sought phase has remained elusive in these systems [CHR13]. However, recent developments on ultra-cold gases have opened new possibilities for its realization. Bose-Einstein condensates with spin-orbit coupling [Li+17] and in cavities [Léo+17] have revealed supersolid features, although with an externally imposed crystalline order. In contrast, recent breakthrough experiments on dipolar condensates have opened an intriguing novel path for the observation of supersolidity [Böt+20].

The first dipolar arrays with transient supersolid features were realized in dysprosium experiments in G. Modugno's group in Pisa in 2019 [Tan+19a], and quickly after that by T. Pfau's [Böt+19b] and F. Ferlaino's [Cho+19] groups. In these experiments the supersolid was formed in an elongated geometry (along a direction perpendicular to the dipole orientation) after a quench of the scattering length from a stable condensate into a mean-field unstable regime. Quenching the scattering length to sufficiently low values results in the roton instability discussed in Sec. 5.5.2. Whereas in mean-field theory such an instability leads to collapse, quantum stabilization results in the formation of the droplet array discussed above. If the scattering length is quenched to too low values, the induced droplets become completely separated from each other, and hence an incoherent droplet array occurs. This is the so-called individual droplet regime. However, for an intermediate, relatively narrow, window of values of the final scattering length after the quench, the droplets remain phase linked, and hence acquire supersolid-like features. Subsequent experiments at F. Ferlaino's group have realized the supersolid regime directly by evaporative cooling, without the need of quenching [Soh+21]. Later experiments studied the intriguing properties of the excitation spectrum at the boundary between unmodulated condensates and supersolids [Guo+19; Nat+19; Tan+19b]. The very recent creation of two-dimensional dipolar supersolids [Nor+21; Bla+21] opens further fascinating perspectives for the study of exotic supersolid pattern formation [ZMP19; ZPM21; Her+21; Pol+21] and quantum vortices [Gal+20; Roc+20].

Chapter **7**

Quasi one-dimensional dipolar gas

In Chapters 2, 4 and 6 we have discussed how competing mean-field terms may elevate the LHY correction to a crucial or even dominating term, while still being in the weakly interacting regime. In Bose-Bose mixtures and in dipolar condensates, quantum stabilization stems from the compensation between the attractive residual mean-field interaction, proportional to the three-dimensional density n_{3D}, and the repulsive LHY correction, which in both systems is proportional to $n_{3D}^{3/2}$ [Pet15; LP11]. As a result, there is a critical density at which both contributions compensate.

Quantum fluctuations play an even more intriguing role in lower dimensions. In particular, droplets are stabilized for a sufficiently low density in one-dimensional Bose-Bose mixtures [PA16], against melting rather than collapse, by the competition of a residual repulsive mean-field term, proportional to the one-dimensional density n_{1D}, and the attractive LHY correction, proportional to $-n_{1D}^{1/2}$. Note the crucial change of sign of the LHY term in one-dimensional systems.

Whereas beyond-mean-field effects in three-dimensional Bose-Bose mixtures and dipolar condensates are very similar due to the almost identical density dependence of the quantum correction, we show in Sec. 7.2 that quantum fluctuations lead in quasi one-dimensional dipolar condensates to a strikingly different physics compared to their non-dipolar counterparts. This difference stems from the peculiar momentum dependence of the dipole-dipole interactions in quasi one-dimensional geometries [SS07]. As a result, not only is the density dependence of the quantum

corrections very different, but even its sign may change due to the remarkable role played by transversal directions in dipolar gases, even if the condensate is well within the quasi-one-dimensional regime. We also show in Sec. 7.3 that, whereas three-body correlations present the same density dependence in three-dimensional dipolar and non-dipolar condensates [KSS85], they display in one-dimension a radically different dependence.

The results of this chapter can be found in Ref. [Edl+17].

7.1 Quasi one-dimensional geometry

In the following, we consider dipolar bosons confined in the xy-plane by a harmonic trap of frequency $\omega_\perp$, as sketched in Fig. 7.1. The axial direction, i.e. z, coincide with the dipole polarization and remains un-trapped. The transversal confinement is strong-enough, such that the absolute value of the chemical potential of the system remains much smaller than the energy level spacing in the radial direction, i.e. $|\mu| \ll \hbar\omega_\perp$. As a result, the condensate remains kinematically one-dimensional. Consequently, we can assume that the condensate wave-function $\Psi(\mathbf{r})$ is of the form:

$$\Psi(\mathbf{r}) = \psi(z)\phi_0(\boldsymbol{\rho}) \tag{7.1.1}$$

where

$$\phi_0(\boldsymbol{\rho}) = \frac{e^{-\frac{\rho^2}{2\ell_\perp}}}{\sqrt{\pi}\ell_\perp} \tag{7.1.2}$$

is the ground state of the transversal trap, with $\ell_\perp = \sqrt{\frac{\hbar}{m\omega_\perp}}$ the harmonic oscillator length in the radial direction.

The condition $|\mu|/\hbar\omega_\perp \ll 1$ demands $|1 - \varepsilon_{\mathrm{dd}}| \ll 1/2n_{\mathrm{1D}}a$. This condition is satisfied in all the calculations below.

7.1.1 Interactions

Let us recall the form of the interaction Hamiltonian (1.3.12)

$$\hat{H}_{\mathrm{int}} = \frac{1}{2}\int \mathrm{d}^3 r \int \mathrm{d}^3 r'\, \hat{\Psi}^\dagger(\mathbf{r})\hat{\Psi}^\dagger(\mathbf{r}')V_{\mathrm{int}}(\mathbf{r} - \mathbf{r}')\hat{\Psi}(\mathbf{r}')\hat{\Psi}(\mathbf{r}). \tag{7.1.3}$$
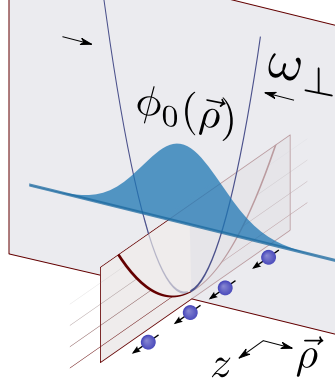
Figure 7.1: Sketch of the system under consideration. A Bose gas is confined in the radial direction ρ by a harmonic trapping with frequency $\omega_\perp$. The chemical potential is much smaller than the energy level spacing in radial direction, e.g. $|\mu| \ll \hbar\omega_\perp$. The dipoles are polarized along the axial direction.

Using Eq. (7.1.1) we can re-write:

$$\hat{H}_\text{int} = \frac{1}{2} \int \mathrm{d}z \int \mathrm{d}z'\, \hat{\psi}^\dagger(z)\hat{\psi}^\dagger(z')V_\text{int,1D}(z,z')\hat{\psi}(z')\hat{\psi}(z), \qquad (7.1.4)$$

where $V_\text{int,1D}$ is the interaction potential integrated over the radial directions, i.e.

$$V_\text{int,1D}(z,z') = \int \mathrm{d}^2\rho \int \mathrm{d}^2\rho'\, V_\text{int}(\mathbf{r}-\mathbf{r}')|\phi_0(\mathbf{r}')|^2|\phi_0(\mathbf{r})|^2. \qquad (7.1.5)$$

Using the concrete from of $\phi_0(\boldsymbol{\rho})$ from Eq. (7.1.2), the integration for the contact interaction is straightforward and equals to $g_\text{1D} = g/2\pi\ell_\perp^2$. The dipole-dipole interaction term is less obvious but can be found in the literature[SS07; Edl+17]. The complete quasi one-dimensional interaction potential in Fourier space then reads[SS07; Edl+17]

$$\tilde{V}_\text{int,1D}(k_z) = g_\text{1D} \left\{ 1 + \varepsilon_\text{dd}\left[3F(0,(k_z\ell_\perp)^2/2) - 1 \right] \right\} \qquad (7.1.6)$$

where $F(j,\sigma) = \sigma^{j+1}e^\sigma\Gamma(-j,\sigma)$, where $\Gamma(-j,\sigma)$ is the incomplete Gamma function. The function $F(0, k_z\ell_\perp)$ is monotonically increasing and takes values from 0 to 1. The momentum dependence of the dipolar term will play a crucial role in the discussion below.
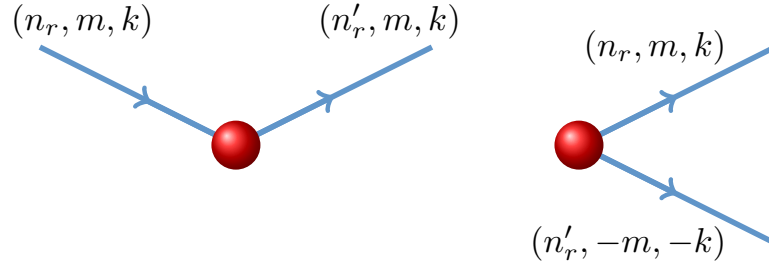
Figure 7.2: Relevant collisional processes for the LHY correction. At the left, an excited particle collides with a condensate particle changing its radial quantum number. At the right, two condensate particles collide and give two excited-state particles with opposite angular momentum, opposite axial linear momentum, and possibly different radial quantum numbers.

7.2 Quantum fluctuations

Single-particle excited states are characterized by three quantum numbers (n_ρ, m, k_z) where n_ρ is the radial quantum number, m the angular momentum, and the axial linear momentum is denoted by k_z. Although, in quasi one-dimensional contact-interacting systems, the transversal excitations with $(n_\rho, m) \neq (0, 0)$ play a negligible role, in dipolar systems it may be crucially different. There are two relevant types of interactions between particles in the condensate and excited states we need to consider. They are sketched in Fig. 7.2. One relevant collision is when a particle in (n_ρ, m, k_z) collides with a particle in the condensate $(0, 0, 0)$ and ends in (n'_ρ, m, k_z). Here the angular momentum quantum number m and the linear momentum k_z are preserved, but not necessarily the quantum number n_ρ. However, as we will see later, processes where $|n_\rho - n'_\rho|$ is large have only a small contribution. The other dominant type of collision occur when two particles in the condensate collide and form two particles in (n_ρ, m, k_z) and $(n'_\rho, -m, -k_z)$. The total angular moment and axial linear momentum remain zero, but the quantum number n_ρ does not need to be conserved.

7.2.1 Interaction potentials for collisions with the condensate

For the derivation of the first-order energy correction we need to consider all modes in the radial direction. The creation and annihilation operators in Eq. (7.1.3) can

be re-expressed as a function of the Bose operators in the single-particle basis as follows:

$$\hat{\Psi}^{\dagger}(\mathbf{r}) = \sum_{k_z} \sum_{n_\rho, m} R_{n_\rho m}(\rho) e^{im\phi} e^{ik_z z} \hat{a}_{n_\rho m}(k_z) \qquad (7.2.7)$$

where the radial wave-functions are

$$R_{n_\rho, m}(\rho) = \frac{(-1)^{n_\rho}}{\ell_\perp \sqrt{\pi}} \sqrt{\frac{n_\rho!}{(n_\rho + m)!}} \left(\frac{\rho}{\ell_\perp}\right)^m L_{n_\rho}^m \left(\frac{\rho^2}{\ell_\perp^2}\right) e^{-\frac{\rho^2}{2\ell_\perp^2}}, \qquad (7.2.8)$$

with L_n^m being the generalized Laguerre polynomials.

To obtain the LHY correction, we proceed as in previous chapters. We apply the Bogoliubov approximation and write down the second order contribution of the interacting part of the Hamiltonian:

$$\frac{\hat{H}_{\text{int}}^{(2)}}{L} = \frac{(2\pi\ell_\perp)^2}{2} \int \frac{dq}{2\pi} \sum_m \sum_{n_\rho, n_\rho'} U_{n_\rho, n_\rho', m}(q) \Big[2\hat{a}_{n_\rho, m}^{\dagger}(q) \hat{a}_{n_\rho', m}(q)$$

$$+ \hat{a}_{n_\rho, m}^{\dagger}(q) \hat{a}_{n_\rho', -m}^{\dagger}(-q) + \hat{a}_{n_\rho, m}(q) \hat{a}_{n_\rho', -m}(-q) \Big], \qquad (7.2.9)$$

with

$$U_{n_\rho, n_\rho', m}(k) = \int dk_\rho \, k_\rho \tilde{V}_{\text{int}}(\mathbf{k}) \mathcal{H}_m \Big[R_{n_\rho, m}(\rho) R_{00}(\rho) \Big] \mathcal{H}_m \Big[R_{n_\rho', m}(\rho) R_{00}(\rho) \Big] \quad (7.2.10)$$

where we have introduced the m-th order Hankel transform $\mathcal{H}_m$, defined as:

$$\mathcal{H}_m[f(\rho)](k_\rho) = \int d\rho \, \rho f(\rho) J_m(k_\rho \rho) \qquad (7.2.11)$$

with J_m the Bessel function of the first kind. We can find an analytic solution of these Hankel transformed expressions:

$$\lambda_{n_\rho m}(k_\rho) := \mathcal{H}_m \Big[R_{n_\rho, m}(\rho) R_{00}(\rho) \Big](k_\rho) = \frac{(-1)^{n_\rho}(k_\rho \ell_\perp)^{2n_\rho + m} e^{-(k_\rho \ell_\perp)^2/4}}{2^{2n_\rho + m + 1} \pi \sqrt{n_\rho!(n_\rho + m)!}} \quad (7.2.12)$$

The derivation is shown in the Appendix A.2. We should note here that two functions $\lambda_{n_\rho m}$, $\lambda_{n_\rho' m}$ with largely differing quantum numbers $|n_\rho - n_\rho'|$ share very little overlap. This justifies the claim we made earlier.

Since calculations are performed near the mean-field stability threshold of $\varepsilon_{\text{dd}} = 1$ in the following, for simplicity, we set it explicitly to this value and evaluate the

integral in Eq. (7.2.10) with the help of Eq. (3.383.10) from [GR94]

$$
U_{n_\rho, n'_\rho, m}(k_z) = g_{1\mathrm{D}} n_{1\mathrm{D}} \frac{6(-1)^{n_\rho + n'_\rho}}{2^{n_\rho + n'_\rho + m + 1}} \sqrt{\binom{n_\rho + n'_\rho + m}{n_\rho}\binom{n_\rho + n'_\rho + m}{n'_\rho}}
$$
$$
\times F\left(n_\rho + n'_\rho + m, \frac{(k_z \ell_\perp)^2}{2}\right). \quad (7.2.13)
$$

When we consider $\varepsilon_{\mathrm{dd}} = 1$ in Sec. 7.1.1 we obtain an ideal, one-dimensional condensate where the dipolar and contact interactions perfectly cancel each other, i.e. $\tilde{V}_{\mathrm{dd}}(0) = U_{000}(0) = 0$. Note, that this does not imply that there are no contributions stemming from transversal excitations. In fact, they may be of the order of $g_{1\mathrm{D}} n_{1\mathrm{D}}$ and hence non-negligible.

7.2.2 Deriving the LHY correction

Following the technique discussed in Chapter 3, the LHY correction of the ground-state energy, ΔE_{LHY}, can be obtained by solving the differential equation

$$
\mathcal{E}_{\mathrm{LHY}} - \frac{1}{2} c \frac{\mathrm{d}}{\mathrm{d}c} \mathcal{E}_{\mathrm{LHY}} = \chi(c) \quad (7.2.14)
$$

where $\mathcal{E}_{\mathrm{LHY}} = \frac{\Delta E_{\mathrm{LHY}}}{L}$ is the one-dimensional LHY energy density and $c := n_{1\mathrm{D}} a = g_{1\mathrm{D}} n_{1\mathrm{D}} / 2\hbar\omega_\perp$. Following the same procedure as in Chapter 3 we obtain the following expression

$$
\chi(c) = \frac{1}{2} \sum_m \int \frac{\mathrm{d}k_z}{2\pi} \sum_{\nu, n_\rho} \left(\frac{\hbar^2 k_z^2}{2m} + \hbar\omega_\perp (2n_\rho + m) - \varepsilon_\nu\right) v_{n_\rho, \nu}^2. \quad (7.2.15)
$$

We obtain the eigenenergies and eigenfunctions of the elementary excitations for each value of m and k_z from the Bogoliubov-de Gennes equations:

$$
\varepsilon_\nu \begin{pmatrix} \mathbf{u}_\nu \\ \mathbf{v}_\nu \end{pmatrix} = \begin{pmatrix} \hat{E}_m(k_z) + \hat{U}_m(k_z) & \hat{U}_m(k_z) \\ -\hat{U}_m(k_z) & -\hat{E}_m(k_z) - \hat{U}_m(k_z) \end{pmatrix} \begin{pmatrix} \mathbf{v}_\nu \\ \mathbf{u}_\nu \end{pmatrix} \quad (7.2.16)
$$

where we introduced the matrices

$$
\left[\hat{E}_m(k_z)\right]_{n_\rho, n'_\rho} = \left(\frac{\hbar^2 k_z^2}{2m} + \hbar\omega_\perp (2n_\rho + m)\right) \delta_{n_\rho, n'_\rho}, \quad (7.2.17)
$$

and

$$\left[\hat{U}_m(k_z)\right]_{n_\rho, n'_\rho} = U_{n_\rho, n'_\rho, m}(k_z). \tag{7.2.18}$$

To solve the differential equation in (7.2.14), we use the ansatz $\mathcal{E}_{\text{LHY}} = c^2 G(c)$. Inserting this ansatz into Eq. (7.2.14) we obtain a simplified equation for the function $G(c)$:

$$G'(c) = -2\frac{\chi(c)}{c^3} \tag{7.2.19}$$

where $G'(c)$ is the derivative with respect to c. Integrating Eq. (7.2.19) we get

$$G(c) = G(c_0) - \int_{c_0}^{c} \mathrm{d}c' \, \frac{2\chi(c')}{(c')^3}, \tag{7.2.20}$$

for a given c_0. Plugging this back into the ansatz for $\mathcal{E}_{\text{LHY}}$ we obtain

$$\mathcal{E}_{\text{LHY}}(c) = c^2 \left[G(c_0) - 2\int_{c_0}^{c} \mathrm{d}c' \, \frac{\chi(c')}{(c')^3} \right]. \tag{7.2.21}$$

Note that, as discussed above, we can evaluate the function $\chi(c)$ from the Bogoliubov modes. However, the integration constant $G(c_0)$ cannot be determined from that calculation. This constant, which eventually results in a regularization of the mean-field coupling constant (note that it provides an energy density proportional to n_{1D}^2), is established by comparing the LHY correction with that expected for large densities. For growing c, the interactions couple more and more transversal modes, and highly excited transversal modes eventually dominate the LHY correction. As a result, the LHY correction necessarily tends to its three-dimensional form, and one may safely assume local-density approximation along the radial Gaussian profile of the condensate. Hence, for $c \gg 1$, the LHY correction approaches the form $\mathcal{E}_{\text{LHY}\infty}(c) = \gamma_{\text{3D}} c^{5/2}$, where $\gamma_{\text{3D}} = \frac{256\sqrt{3\pi}}{5} \frac{\hbar\omega_\perp}{\ell}$ was obtained from the prefactor of the LHY-correction in three-dimensions integrated over the radial directions. Hence the asymptotic form of $G(c)$ is $G_\infty(c) = \gamma_{\text{3D}} c^{1/2}$, and that of $\chi(c)$ is therefore:

$$\chi_\infty(c) = -\frac{\gamma_{\text{3D}}}{4} c^{5/2}. \tag{7.2.22}$$

We obtain indeed this asymptotic result from our numerical determination of $\chi(c)$ from Eq. (7.2.15). In order to determine $G(c_0)$, we re-express $G(c)$ in the form:

$$G(c) = G(c_0) - 2\int_{c_0}^{c} \mathrm{d}c' \left[\frac{\chi(c') - \chi_\infty(c')}{(c')^3} \right] - 2\int_{c_0}^{c} \mathrm{d}c' \, \frac{\chi_\infty(c')}{(c')^3} \tag{7.2.23}$$

$$= G(c_0) - \gamma_{\text{3D}} c_0^{1/2} - 2\int_{c_0}^{c} \mathrm{d}c' \left[\frac{\chi(c') - \chi_\infty(c')}{(c')^3} \right] + \gamma_{\text{3D}} c^{1/2}. \tag{7.2.24}$$

Since $G(c \to \infty) = \gamma_{\mathrm{3D}} c^{1/2}$, then

$$G(c_0) = \gamma_{\mathrm{3D}} c_0^{1/2} + 2 \int_{c_0}^{c \to \infty} \left[\frac{\chi(c') - \chi_\infty(c')}{(c')^3} \right] \mathrm{d}c', \qquad (7.2.25)$$

where the last integral is evaluated from our numerical determination of $\chi(c)$. Note that this evaluation is particularly challenging since it involves evaluating the effect of many radial modes. This in practice demands a careful extrapolation of results to an infinite number of transversal modes. Once the constant $G(c_0)$ is determined in this way, we may express the LHY correction as a term proportional to n_{1D}^2 plus terms of higher order in n_{1D}.

The term proportional to n_{1D}^2, as mentioned above, amounts for a correction of the mean-field coupling constant g. This correction has been calculated using a different method in Ref. [PP21]. As pointed in that paper, the correction of the mean-field coupling constant is of the form: $g \to g \left(1 + 0.36 a/\ell_\perp \right)$, i.e. the LHY correction of the mean-field term is repulsive. We should mention at this point that in the published version of our work this correction was improperly determined as attractive $g \left(1 - 4.24 a/\ell_\perp \right)$ due to an error in the determination of $G(c_0)$. However, as pointed in Ref. [PP21] this does not compromise our main results, since the error in the determination of the n_{1D}^2 term in the LHY correction may be easily compensated by properly shifting the mean-field term. Hence, instead of considering the case $\varepsilon_{\mathrm{dd}} = 1$ for which the mean-field cancels, we will consider in the following a slightly shifted value, $\varepsilon_{\mathrm{dd}} \simeq 1 + 4.6 a/\ell_\perp$, such that the residual mean-field energy compensates the error in the determination of the n_{1D}^2 term of the LHY correction. With this regularization (which does not affect the LHY correction itself, since it would contribute to higher orders), we recover the results of our publication, which are slightly reworked below taking into account the new definition of $\varepsilon_{\mathrm{dd}}$.

Figure 7.3 shows the chemical potential, $\Delta\mu_{\mathrm{LHY}} + \mu_{\mathrm{MF}} = \frac{\mathrm{d}}{\mathrm{d}n_{\mathrm{1D}}} \frac{E_{\mathrm{LHY}} + E_{\mathrm{MF}}}{L}$, as a function of $n_{\mathrm{1D}}a$. For low densities, $n_{\mathrm{1D}}a \ll 1$, the LHY correction, in addition to the n_{1D}^2 dependence, which for the shifted value of $\varepsilon_{\mathrm{dd}}$ is attractive, presents a repulsive term with a steeper power law (dominantly n_{1D}^3 at low densities) given by the progressively more relevant role played by the transversal degrees of freedom. As a result the chemical potential reaches a minimal value at $n_{\mathrm{1D}}a \cong 0.2$. It then increases further and becomes positive for $n_{\mathrm{1D}}a \gtrsim 0.45$. Note that, as expected from our discussion above, for $n_{\mathrm{1D}}a \gg 1$ the chemical potential acquires the $n_{\mathrm{1D}}^{3/2}$ characteristic of the three-dimensional LHY correction.
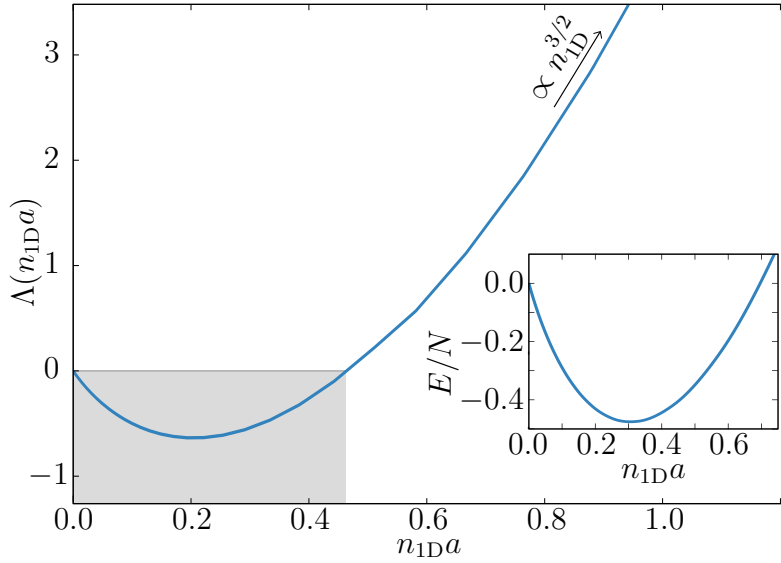
Figure 7.3: Dimensionless function $\Lambda = \frac{\mu}{\hbar\omega_\perp}\frac{\ell_\perp}{a}$ showing the change of the chemical potential caused by the LHY correction as a function of $n_{1D}a$. The inset shows the energy per particle as a function of $n_{1D}a$.

7.2.3 Self-bound droplets

The inset of Fig. 7.3 shows the energy per particle for different $n_{1D}a$. It features a minimum at $(n_{1D}a)^{\text{opt}} \cong 0.3$. It is hence energetically favorable for the system to posses densities at this value. We stress that this energy minimum results from the compensation of the residually attractive n^2 term (resulting from the regularized mean-field term) and LHY terms of higher-order in n_{1D} (most notably a n_{1D}^3 dependence). The existence of this minimum results in the formation of self-bound droplets, which constitute the one-dimensional equivalent of the three-dimensional ones discussed in previous chapters. Note the crucial difference of this mechanism to that previously discussed in Ref. [PA16] for 1D Bose-Bose mixtures, where droplets were stabilized against melting rather than collapse due to the competition between a residual repulsive mean-field term, proportional to n_{1D}^2, and an attractive LHY correction, proportional to $-n_{1D}^{3/2}$.

In the following, we study the formation of these one-dimensional quantum droplets, considering an axially un-trapped, but possibly self-bound, condensate with axial width $R \gg \ell_\perp$. In this case, the use of the local density approximation (along the axial direction) is well justified, since the momenta contributing most to the LHY correction fulfill $kR \gg 1$. The extended Gross-Pitaevskii equation in this quasi
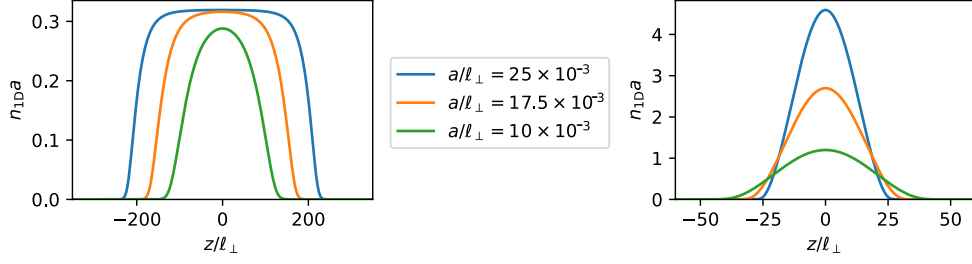
Figure 7.4: (a) Ground-state density profile obtained for $N = 5000$ and $a/\ell_\perp = 0.01, 0.0175, 0.025$ from an eGPE analysis (left) and with a GPE in absence of LHY correction (right). In the left panel one clearly sees the saturation of the density resulting from the minimum of the energy per particle minimum shown in the inset of Fig. 7.3.

one-dimensional geometry reads

$$\mu\psi(z) = \left\{ \frac{-\hbar^2}{2m} \frac{\mathrm{d}^2}{\mathrm{d}z^2} + \int \frac{\mathrm{d}k_z}{2\pi} \tilde{V}_{\mathrm{int},1\mathrm{D}}(k_z) \tilde{n}_{1\mathrm{D}}(k_z) e^{\mathrm{i}k_z z} + \Delta\mu_{\mathrm{LHY}}[n_{1\mathrm{D}}(z)] \right\} \psi(z).$$

$$(7.2.26)$$

where $\tilde{n}_{1\mathrm{D}}(k_z)$ is the Fourier transform of $n_{1\mathrm{D}}(z)$.

Figure 7.4 show our results for $N = 5000$ particles, and $a/\ell_\perp = 0.01, 0.0175, 0.025$, with $\varepsilon_{\mathrm{dd}} = 1 + 4.6a/\ell_\perp$. As seen in the left panel of Fig. 7.4, as soon as the system has enough particles to reach the optimal peak density, $(n_{1\mathrm{D}}a)^{\mathrm{opt}}$, any additional particle will rather be put at the sides of the density distribution than in the center, leading to a flat-top density profile. The right panel of Fig. 7.4 shows our results when one neglects the effects of quantum fluctuations. Note that, for the same parameters, the situation is dramatically different. In that case, since for $\varepsilon_{\mathrm{dd}} = 1 + 4.6a/\ell_\perp$ the mean-field term is slightly attractive. As expected for one-dimensional systems, the condensate does not collapse, as it would in three dimensions, but rather forms a bright soliton, with a density profile given by the equilibration of mean-field attraction and kinetic energy. The density profile is hence radically modified, and instead of a flat-top one observes a Gaussian-like distribution.

In the left panel of Fig. 7.5 we evaluate the peak density of the droplet for different values of $\varepsilon_{\mathrm{dd}} \gtrsim 1$ and small $a/\ell_\perp$, by solving the extended Gross-Pitaevskii equation (7.2.26), for a number of particles $N = 5000$. Note that the peak density $n_{1\mathrm{D}}^{\mathrm{peak}}a$ is plotted in a logarithmic scale. As discussed above, the LHY correction regularizes the mean-field $n_{1\mathrm{D}}^2$ term, such that for low densities the overall energy becomes of
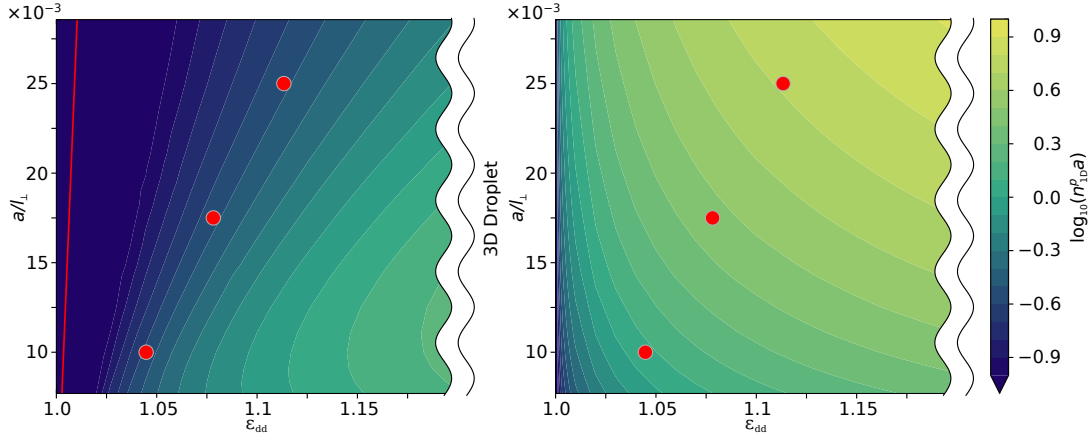
Figure 7.5: Peak density as a function of $a/\ell_\perp$ and $\varepsilon_{\mathrm{dd}}$ obtained for $N = 5000$ particle from an eGPE analysis (left) and a GPE without LHY correction (right). The red curve shows the stability threshold, at which the n_{1D}^2 energy dependence changes sign. For values of $\varepsilon_{\mathrm{dd}}$ at the left of that curve no self-bound solution is possible. The red circles correspond to the cases depicted in Fig. 7.4.

the form:

$$\frac{E_{\mathrm{tot}}}{L} \stackrel{n_{\mathrm{1D}} \to 0}{\cong} \frac{1}{2} \left[1 - \varepsilon_{\mathrm{dd}} + 0.3645 \frac{a}{\ell_\perp} \right] g_{\mathrm{1D}} n_{\mathrm{1D}}^2. \qquad (7.2.27)$$

Due to the repulsive character of the rest of the LHY energy, the existence of self-bound solutions requires an attractive n_{1D}^2 term, which clearly demands $\varepsilon_{\mathrm{dd}} > 1 + 0.3645 \frac{a}{\ell_\perp}$ (red line in Fig. 7.5), which is a slight correction to the mean-field condition $\varepsilon_{\mathrm{dd}} > 1$.

For values of $\varepsilon_{\mathrm{dd}} = 1 + \alpha a/\ell_\perp$ for a given value of α, the energy per particle (recall the inset of Fig. 7.3) presents a minimum for the same value of $n_{\mathrm{1D}}a$, and hence the optimal density $(n_{\mathrm{1D}}a)^{\mathrm{opt}}$ is the same. This is exemplified by the red circles in the left panel of Fig. 7.5, which corresponds to the density profiles depicted in the left panel of Fig. 7.4. Note that for a sufficiently large $a/\ell_\perp$ the peak density reaches the optimal value, and it becomes independent of $a/\ell_\perp$ as long as the points lie on the same $\varepsilon_{\mathrm{dd}} = 1 + \alpha a/\ell_\perp$ line. We stress that this optimal density is eventually independent of the number of particles, if that number is sufficiently large. Of course, for a sufficiently large $\varepsilon_{\mathrm{dd}} > 1$ the transversal energy level spacing becomes comparable to the chemical potential, $\mu \gtrsim \hbar\omega_\perp$, and the condensate crossovers into the 3D regime, where the repulsive LHY prevents collapse. This would correspond to the elongated 3D macro-droplet regime, which has been already studied experimentally [Cho+16].

As mentioned above, the situation is radically different in the absence of LHY corrections. The right panel of Fig. 7.5 depicts the peak density obtained from purely mean-field calculations. One clearly sees a much higher peak density, which has a completely different scaling with $\varepsilon_{\mathrm{dd}}$ and $a/\ell_\perp$. In particular, one clearly looses the universality of the peak density along the $\varepsilon_{\mathrm{dd}} = 1 + \alpha a/\ell_\perp$ lines, as seen from the different peak densities experiences for the three cases indicated with red circles. Moreover, the peak density does depend on N, since the flat-top feature is lost.

7.3 Local three-body correlation

The lifetime of cold-gases experiments is typically limited at sufficiently large densities by three-boy losses. These losses result from three-body interactions in which two of the partners form a dimer and the third one carries the excess energy. As a result all three particles are lost [Hal+11]. Three-body losses scale with the cube of the density, and may be modeled by a rate equation of the form:

$$\dot{n} = -\alpha K^{(3)} g^{(3)} n^3 \tag{7.3.28}$$

where α is equal to three when in the process all three involved particles escape the system [Hal+11]. The parameter $K^{(3)}$ contains information about the few-body physics during the process and hence depends on the scattering length [Chi+10].

The last term $g^{(3)}$ is the *local three body-correlation*,

$$g^{(3)} = \frac{\left\langle (\hat{\Psi}^\dagger)^3 \hat{\Psi}^3 \right\rangle}{n^3}. \tag{7.3.29}$$

In mean-field approximation the three-body correlation for a Bose-condensed system fulfills $g^{(3)} = 1$. Including quantum fluctuations may introduce a significant change $\Delta g^{(3)}$, hence modifying the three-body loss rate. For a homogeneous three-dimensional non-dipolar condensate with density n_{3D} the correction to the three-body correlation behaves like $\Delta g^{(3)} = \frac{64}{\sqrt{\pi}} \sqrt{n_{\mathrm{3D}} a^3}$ [KSS85]. This correction has been probed in cold-atom experiments [Hal+11].

When dipoles are included, the correlation is similar, namely $\Delta g^{(3)} = \frac{64}{\sqrt{\pi}} \sqrt{n_{\mathrm{3D}} a^3}(1 + C\varepsilon_{\mathrm{dd}}^2)$, with $C \cong 0.3$ [Edl+17]. The dipoles introduce a shift which can be tuned via $\varepsilon_{\mathrm{dd}}$. Note, that the correction has the same density dependence as for the non-dipolar case.

Three-body correlations are radically different in a quasi-one dimensional geometry. For a non-dipolar system, the correction follows the dependence:

$$\Delta g^{(3)} = \frac{-6}{\pi} \sqrt{\frac{2a}{n_{1D}\ell_\perp^2}} \tag{7.3.30}$$

where $\sqrt{\frac{2a}{n_{1D}\ell_\perp^2}}$ is chosen such that it is much smaller than one [GS03]. Note that the correction is now negative, i.e. in quasi-one dimensional systems quantum effects reduce three-body correlations. This must be compared to the three-dimensional case, where the correction term had a positive sign. A second relevant feature to note is that the quantum correction increases with a decreasing density. This is a peculiar feature of one-dimensional systems, which are more strongly-correlated when the density decreases. This results directly from the comparison between the kinetic energy, which scales with n_{1D}^2, and the interaction energy, which scales with n_{1D}. As a result, the system gets more interacting when n_{1D} decreases.

The correction of $g^{(3)}$ averaged over the transversal degree of freedom may be evaluated from the LHY correction using Hellmann-Feynman theorem

$$\Delta g^{(3)} = \int \frac{\mathrm{d}^3 r}{L} \frac{\phi^4(x,y)}{\int \mathrm{d}x' \, \mathrm{d}y' \, \phi^4(x',y')} \frac{\left\langle \left(\hat{\Psi}^\dagger(\mathbf{r})\right)^3 \hat{\Psi}^3(\mathbf{r})\right\rangle}{n^3(\mathbf{r})}. \tag{7.3.31}$$

By applying the Bogoliubov approximation from Eq. (1.3.14) and keeping only the first non-vanishing quantum fluctuation term, we can re-express the three-body correlation, i.e.

$$\left. \begin{array}{l} \left\langle (\hat{\Psi}^\dagger)^2(\mathbf{r})\hat{\Psi}^2(\mathbf{r})\right\rangle \cong n^2(\mathbf{r}) + n(\mathbf{r})W(\mathbf{r}) \\ \left\langle (\hat{\Psi}^\dagger)^3(\mathbf{r})\hat{\Psi}^3(\mathbf{r})\right\rangle \cong n^3(\mathbf{r}) + 3n^2(\mathbf{r})W(\mathbf{r}) \end{array} \right\} \Rightarrow \frac{\left\langle (\hat{\Psi}^\dagger)^3\hat{\Psi}^3\right\rangle}{n} = 3\left\langle (\hat{\Psi}^\dagger)^2\hat{\Psi}^2\right\rangle - 2n^2 \tag{7.3.32}$$

where $W(\mathbf{r}) = \left\langle (\delta\hat{\psi})^2 + \delta\hat{\psi}^2 + 2\delta\hat{\psi}\delta\hat{\psi}\right\rangle$ contains all terms with two fluctuation operators. Inserting this into the integral of (7.3.31) and employing the Hellmann-Feynman theorem we get the correction to the correlation function:

$$\Delta g^{(3)} = \frac{6}{n_{1D}^2} \frac{\partial \Delta E_{LHY}/L}{\partial g_{1D}} = -\frac{6}{\pi}\sqrt{\frac{2a}{n_{1D}\ell_\perp^2}} \beta(\varepsilon_{dd}, n_{1D}a) \tag{7.3.33}$$

where $\beta(\varepsilon_{dd}, n_{1D}a)$ is depicted in Fig. 7.6 [Edl+17]. For all values of $n_{1D}a$ it is negative and hence the local three-body correlation correction $\Delta g^{(3)}$ is positive, as
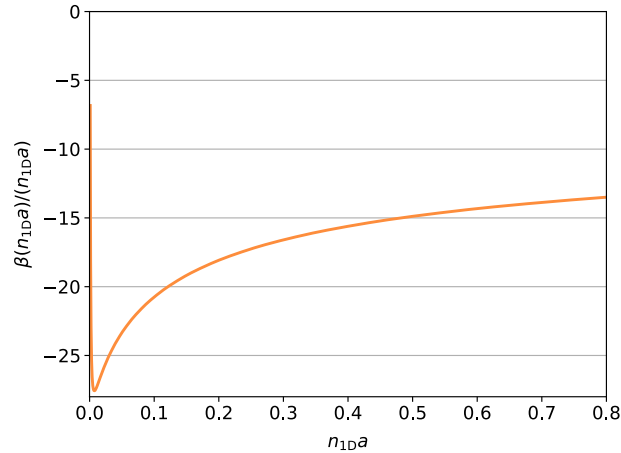
Figure 7.6: Correction of the three-body correlations β (see text) for $\varepsilon_{\rm dd} = 1$. For larger values of $n_{\rm 1D}a$ the depicted $\beta/(n_{\rm 1D}a)$ is converging to a constant value. Hence β has a linear dependence on $n_{\rm 1D}a$ featuring the same behavior for the correlation as in a three dimensional system.

for a three-dimensional system. It is to be noted that this functional behavior for small values of $n_{\rm 1D}a$ occurs despite the fact that the condensate remains in the quasi one-dimensional regime. Note, finally, that for growing $n_{\rm 1D}a$ the correction of $\beta(\varepsilon_{\rm dd}, n_{\rm 1D}a)$ converges to that expected for a 3D system, and hence $\Delta g^{(3)}$ scales as $\sqrt{n_{\rm 1D}}$.

7.4 Radially-untrapped systems

In this final section of the chapter we discuss a calculation, in which we employ a formalism similar to that discussed above in order to estimate the validity of the local density approximation for the description of quantum droplets. In 2019 experiments analyzed the critical atom number for a self-bound droplet as a function of the scattering length [Böt+19a]. The experimental data presented a sizable discrepancy with the theoretical curve obtained by means of simulation of the corresponding three-dimensional eGPE. Several reasons could explain the observed discrepancy. One of these reasons could be the lack of validity of the local density approximation along the radial direction of the droplet. Note that dipolar droplets are significantly elongated along the dipole direction. As a result, whereas one may expect that the local-density approximation could be justifiable along the droplet

axis, it may be less valid across the transversal directions. We discuss this possibility in this section. We do it relatively briefly, since the final result is actually that the local density approximation works for typical parameters very well, also in the transversal direction of the droplet.

In order to address this issue, we considered the following model. We assume a dipolar condensate uniform along the dipole direction z, but Gaussian-like on the xy plane. We assume no trapping, also not on the xy plane, but we impose the Gaussian-like transversal profile anyway, since that profile will be similar to that of a droplet. We may then proceed in a similar way as above for the calculation of the LHY correction, but we need to take into account that there is no trapping on the xy plane. Wheres the interaction part is unaffected, the non-interacting part of the Hamiltonian, $\hat{H}_0$, needs some adjustments:

$$
\frac{\hat{H}_0}{L} = \sum_{\substack{n_\rho,n_\rho' \\ m,m'}} \int \frac{\mathrm{d}k_z}{2\pi} \int \frac{\mathrm{d}k_z'}{2\pi} e^{\mathrm{i}(k_z-k_z')z} \int \mathrm{d}\rho \int \mathrm{d}\phi \, e^{\mathrm{i}(m-m')\phi}
$$

$$
\overline{R_{n_\rho',m'}(\rho)} \left[\frac{\hbar^2 {k_z}^2}{2m} - \frac{-\hbar^2 \nabla_\rho^2}{2m} \right] R_{n_\rho,m}(\rho) \hat{a}^\dagger_{n_\rho' m'}(k_z) \hat{a}_{n_\rho m}(k_z) \tag{7.4.34}
$$

$$
= \sum_{\substack{n_\rho,n_\rho' \\ m,m'}} \int \frac{\mathrm{d}k_z}{2\pi} \left\{ \left[\frac{\hbar^2 {k_z}^2}{2m} + \hbar\omega_\perp(2n_\rho+m+1) \right] \delta_{n_\rho n_\rho'}\delta_{mm'} - \mathcal{C} \right\} \hat{a}^\dagger_{n_\rho' m'}(k_z) \hat{a}_{n_\rho m}(k_z) \tag{7.4.35}
$$

where $\mathcal{C}$

$$
\mathcal{C} = \frac{m\omega_\perp^2}{2}\ell_\perp^2 \delta_{m,m'}(-1)^{n_\rho+n_\rho'} \sqrt{\frac{n_\rho!}{(n_\rho+m)!}\frac{n_\rho'!}{(n_\rho'+m')!}} \int_0^\infty \mathrm{d}x\, x^{m+1} e^{-x} L_{n_\rho}^m(x) L_{n_\rho'}^{m'}(x) \tag{7.4.36}
$$

With the Eq. (8.971.4) and (8.971.5) from [GR94] and the orthogonality property of the Laguerre polynomials we see that we only have to deal with three non-negligible cases. The sum over all m' of $\mathcal{C}$ is

$$
\sum_{m'} \mathcal{C} = \frac{\hbar\omega_\perp}{2} \begin{cases} \sqrt{n_\rho(n_\rho+m)}, & n_\rho' = n_\rho - 1 \\ 2n_\rho+m+1, & n_\rho' = n_\rho \\ \sqrt{(n_\rho+1)(n_\rho+m+1)}, & n_\rho' = n_\rho + 1 \end{cases} \tag{7.4.37}
$$

The rest of the derivation is similar to the one in the previous section. In the end

one obtains the differential equation (7.2.14) with the function $\chi(n_{1D})$

$$\chi(n_{1D}) = \frac{1}{2}\frac{1}{2\pi} \sum_{\nu} \sum_{n_\rho,m} \int dk_z \left\{ [\epsilon_{n_\rho m}(k_z) - \varepsilon_\nu] v^2_{\nu;n_\rho,m}(k_z) \right.$$
$$- \Lambda_{n_\rho,m} v_{\nu;n_\rho,m}(k_z) v_{\nu;n_\rho+1,m}(k_z)$$
$$\left. - \Lambda_{n_\rho-1,m} v_{\nu;n_\rho,m}(k_z) v_{\nu;n_\rho-1,m}(k_z) \right\} \qquad (7.4.38)$$

where $\epsilon_{n_\rho m}(k_z) = (\frac{\hbar^2 k_z^2}{2m} + \frac{\hbar\omega_\perp}{2}(2n_\rho+m))$ and $\Lambda_{n_\rho,m} = \hbar\omega_\perp \sqrt{(n_\rho + 1)(n_\rho + m + 1)}$.

When solving the eGPE for a radially un-trapped system one needs to solve it first with an arbitrarily value of $\omega_\perp$. This needs to be re-done until the system energy (including the LHY correction) is minimized with respect to $\omega_\perp$. The comparison of the results of this analysis to those obtained from direct application of the three-dimensional LHY energy in local density approximation (i.e. as it is typically employed in the eGPE analysis of quantum droplets) shows, however, that the local density approximation is actually very good even in the transversal direction of the droplet. Moreover, the small corrections resulting from deviations from the 3D local-density approximation approach results in a shift in the critical number of particles, which is in the opposite direction as the shift observed in experiments. We hence conclude from this analysis that the discrepancy between the eGPE theory and experiments is not due to the lack of validity of the local density approximation.

7.5 Conclusions

Whereas in three-dimensional condensates the LHY correction for a dipolar condensate has a very similar form as that for a non-dipolar one (just differing in the prefactor), the momentum dependence of the dipolar interactions leads to strikingly different quantum effects in quasi one-dimensional dipolar condensates compared to their non-dipolar counterparts. In a dipolar condensate, in addition to a regularization of the mean-field energy, the coupling with transversal modes results in additional repulsive terms scaling steeper with the one-dimensional density (in particular a cubic term at low densities). In a quasi-one-dimensional non-dipolar condensate, the LHY term is attractive, and as a result a droplet may occur for a repulsive mean-field due to quantum stabilization against expansion rather than against collapse. In contrast, one-dimensional dipolar condensates present droplets which closely resemble those formed in three-dimensional scenarios. The repulsive

mean-field terms scaling with a higher power than n_{1D}^2, may compensate an attractive n_{1D}^2 term, and result in flat-top droplets that differ very significantly from the usual bright solitons expected under those circumstances in a mean-field Bose gas. As a result, we have shown that the peak density is strikingly different compared to the non-dipolar case. Quasi-one-dimensional dipolar condensates hence provide an exciting new scenario for the study of flat-top droplets, and in general for the analysis of the effects of quantum fluctuations in low-dimensional geometries, including e.g. the modification of three-body loss rates.

Part IV

Conclusion and Outlook

Chapter 8

Conclusion and Outlook

In this Thesis, we have discussed how quantum fluctuations can lead to novel intriguing physics for Bose systems well within the weakly-interacting regime. Indeed, the Lee-Huang-Yang correction results in observable phenomena that are fully missed by a purely mean-field theory. This remarkable and surprisingly important role played by quantum fluctuations results on one side from the competition of two types of mean-field interactions, which quasi-cancel each other. Those may be intra- and inter-component interactions in binary mixtures, or contact and dipole-dipole interactions in dipolar condensates. In this Thesis, we have considered both scenarios, non-dipolar mixtures and dipolar gases.

In the first part of the Thesis we focused on the physics of binary mixtures. In addition to the by now well-known stabilization mechanism for a self-bound droplets in a bosonic mixture, we showed that quantum fluctuations may also significantly change other general and well established properties of Bose mixtures. We consider in particular, a peculiar immiscible binary mixture, in which one of the components has enhanced quantum fluctuations, whereas the other is well described in mean-field. We discussed that such a peculiar mixture may be attained in three-component Bose systems, in which two of the components form a miscible mixture (forming an effective scalar condensate) in the regime of mean-field quasi-cancellation. This effective scalar component is immersed in a bath formed by a third component, immiscible with the other two. The system then behaves as the desired effective binary immiscible system, in which one of the components presents an enhanced role of quantum fluctuations. We the showed that the prop-

erties of this effective binary mixture significantly departs from those known in standard immiscible Bose-Bose mixtures. We considered in particular the behavior of a quantum bubble formed by the miscible components immersed in the bath of the other component. We showed that quantum fluctuation alter the equilibrium of pressures, leading to a modified dependence of the volume of the quantum bubble as a function of the bath density. Moreover, the criterion for buoyancy of the bubble is very significantly modified by quantum fluctuations. Interestingly, once buoyancy sets in, there is an intermediate regime in which buoyancy is arrested, i.e. the bubble occupies an intermediate position between the center and the surface of the trapped bath, in stark contrast to the immediate buoyancy from the center to the surface occurring in mean-field mixtures. Finally, once the bubble reaches the surface it remains compact floating there, since it transitions into a quantum droplet, rather than spreading over the bath surface as in standard mean-field immiscible Bose-Bose mixtures.

The second part of the Thesis, was devoted to the study of the effect of quantum fluctuations in dipolar Bose-Einstein condensates. We have focused in particular on the role of those fluctuations in quasi-one-dimensional geometries. Interestingly, due to the peculiar momentum dependence of the dipole-dipole interactions in those geometries, the effects of quantum fluctuations in dipolar condensates differ radically from those expected in their non-dipolar counterparts, including Bose-Bose mixtures. The coupling with transversal modes leads to a crossover of the Lee-Huang-Yang energy from its one-dimensional dependence into its three-dimensional one (assuming local density approximation along the transversal directions). We showed that such a crossover, which cannot be described using the standard Bogoliubov approach due to difficulties related to the cure of ultraviolet divergences, may be accomplished using the Hugenholz-Pines technique. Our results show that the LHY correction determined in this way changes radically the physics of quasi-one-dimensional dipolar condensates. In particular, the repulsive LHY terms correcting the mean-field results, scales more steeply with the linear density, n_{1D}, than the mean-field (which scales with n_{1D}^2). This is in stark contrast with binary mixtures, where the LHY correction at low densities is negative and scales with $n_{1D}^{1/2}$. As a result, whereas in quasi-one-dimensional binary mixtures quantum droplets are stabilized against expansion by the LHY for a repulsive mean-field, for the dipolar case, droplets are stabilized against soliton formation for a residually attractive mean-field interaction. As a consequence, the condensate density profile (which acquires eventually a flat-top form) differs radically from the soliton profile expected in mean-field theory. Quasi-one-dimensional dipolar condensates hence provide an intriguing novel scenario for the study of the effects of quantum fluctuations in low-dimensional geometries, including e.g. the

modification of three-body loss rates.

Our results of the first part of the Thesis show that quantum fluctuations may significantly change not only the stability, but also other well-established properties of Bose mixtures, as the buoyancy effect. A similar physics could be observed in immiscible binary mixtures, in which at least one of the components (forming the quantum bubble) is dipolar within the regime of mean-field quasi-cancellation. This could be an interesting topic for future studies. The physics may be however very non-trivial, since the nonlocal anisotropic character of the dipole-dipole interaction may significantly affect how the bath affects the quantum bubble, and the droplet properties in general, and buoyancy in particular, may depend non-trivially on the geometry of the bath. Another interesting scenario for future studies could be that in which the bath is itself a quantum droplet.

Concerning the second part of the Thesis, the application of the Hugenholz-Pines technique may be extended to other geometries, such as e.g. two-to-three dimensional crossover. Moreover, one may study how a modification of the transversal confinement (e.g. a non-harmonic confinement) may affect the condensate properties (since it modifies the transversal states, and with it the LHY energy correction). The physics of low-dimensional dipolar systems, including their dynamics, may be hence a fruitful topic for future studies.

Appendix **A**

Appendix

A.1 The Fourier transformed dipole-dipole potential

In this Appendix we derive, following Ref. [SSC12], the Fourier transform of the dipole-dipole interaction potential, introduced in Eq. (5.1.2):

$$V_{\mathrm{dd}}(\mathbf{r}) = \frac{C_{\mathrm{dd}}}{4\pi} \frac{1 - 3\cos^2\theta_r}{r^3}. \tag{A.1.1}$$

The Fourier transform, in addition to provide physical insights on the properties of dipolar gases, is particularly useful in numerical calculations, due to the fact that the spatial $\frac{1}{r^3}$ dependence diverges at $r = 0$. Such a problem is avoided, as seen below, when working in the Fourier domain.

For the Fourier transform we employ the convention

$$\tilde{V}_{\mathrm{dd}}(\mathbf{k}) = \mathcal{F}\left[V_{\mathrm{dd}}(\mathbf{r})\right](\mathbf{k}) = \int \frac{C_{\mathrm{dd}}}{4\pi} \frac{1}{r^3}(1 - 3\cos^2\theta_r)\mathrm{e}^{-\mathrm{i}\mathbf{k}\cdot\mathbf{r}} \, \mathrm{d}^3 r \tag{A.1.2}$$

We need to perform two replacements before we can continue with the evaluation of the integral above. First we notice that:

$$1 - 3\cos^2\theta_r = -4\sqrt{\frac{\pi}{5}} Y_{20}(\theta_r) \tag{A.1.3}$$

where Y_{lm} are the spherical harmonics. Second, one can employ the expansion of a plane wave in spherical harmonics:

$$e^{-i\mathbf{k}\cdot\mathbf{r}} = 4\pi \sum_{l=0}^{\infty} i^l j_l(kr) \sum_{m=-l}^{l} \overline{Y_{lm}(\theta_r, \varphi_r)} Y_{lm}(\theta_k, \varphi_k) \tag{A.1.4}$$

where j_l is the l-th spherical Bessel function of first kind.

Plugging (A.1.3) and (A.1.4) into (A.1.2)

$$\tilde{V}_{\mathrm{dd}} = -4\sqrt{\frac{\pi}{5}}C_{\mathrm{dd}} \int \mathrm{d}r\, \frac{1}{r} \int \mathrm{d}\theta_r \sin\theta_r \int \mathrm{d}\varphi_r\, Y_{20}(\theta_r)$$

$$\times \sum_{l=0}^{\infty} i^l j_l(kr) \sum_{m=-l}^{l} \overline{Y_{lm}(\theta_r, \varphi_r)} Y_{lm}(\theta_k, \varphi_k) \tag{A.1.5}$$

We can make use of the orthonormality of the spherical harmonics:

$$\int \mathrm{d}\theta_r \sin\theta_r \int \mathrm{d}\varphi_r\, Y_{20}(\theta_r)\overline{Y_{lm}(\theta_r, \varphi_r)} = \delta_{l2}\delta_{m0}, \tag{A.1.6}$$

obtaining

$$\tilde{V}_{\mathrm{dd}} = 4\sqrt{\frac{\pi}{5}}C_{\mathrm{dd}} \int \mathrm{d}r\, \frac{1}{r} j_2(\mathbf{k}\cdot\mathbf{r})Y_{20}(\mathbf{k}) \tag{A.1.7}$$

Using that $\int \mathrm{d}r\, \frac{1}{r}j_2(kr) = \frac{1}{3}$ we can simplify the expression:

$$\tilde{V}_{\mathrm{dd}} = \frac{4}{3}C_{\mathrm{dd}}\sqrt{\frac{\pi}{5}}Y_{20}(\mathbf{k}) \stackrel{(A.1.3)}{=} \frac{C_{\mathrm{dd}}}{3}(3\cos^2\theta_k - 1) \tag{A.1.8}$$

A.2 Evaluation of Eq. (7.2.12)

In this Appendix we provide a detailed derivation of Eq. (7.2.12), which we employed in the analysis of quantum fluctuations in quasi-one dimensional dipolar condensates.

By inserting the radial wave-functions $R_{n_r,m}(\rho)$ and $R_{0,0}(\rho)$ into the Hankel transform, we obtain

$$\lambda_{n_r,m}(k_\rho) = \int_0^{\infty} \mathrm{d}\rho\, \rho R_{n_r,m}(\rho)R_{0,0}(\rho)J_m(k_\rho\rho)$$

$$= \int_0^{\infty} \mathrm{d}\rho\, \rho \frac{(-1)^n}{l_\perp\sqrt{\pi}}\sqrt{\frac{n!}{(n+m)!}}\left(\frac{\rho}{l_\perp}\right)^m L_n^m\left(\frac{\rho^2}{l_\perp^2}\right)e^{-\rho^2/2l_\perp}\frac{1}{l_\perp\sqrt{\pi}}e^{-\rho^2/2l_\perp}J_m(k_\rho\rho)$$

$$= \frac{(-1)^n}{l_\perp^2\pi}\sqrt{\frac{n!}{(n+m)!}}\int_0^{\infty} \mathrm{d}\rho\, \rho\left(\frac{\rho}{l_\perp}\right)^m L_n^m\left(\frac{\rho^2}{l_\perp^2}\right)e^{-\rho^2/l_\perp}J_m(k_\rho\rho) \tag{A.2.9}$$

Introducing the dimensionless variables $\tilde{\rho} := \frac{\rho}{l_\perp}$ and $\tilde{k}_\rho := k_\rho l_\perp$, we may re-write:

$$\lambda_{n_r,m}(k_\rho) = \frac{(-1)^n}{\pi}\sqrt{\frac{n!}{(n+m)!}}\int_0^\infty \mathrm{d}\tilde{\rho}\,\tilde{\rho}^{m+1}L_n^m(\tilde{\rho}^2)e^{\tilde{\rho}^2}. \qquad (A.2.10)$$

Using Eq. (7.421.4) of Ref. [GR94] we find

$$\lambda_{n_r,m}(k_\rho) = \frac{(-1)^n}{\pi}\sqrt{\frac{n!}{(n+m)!}}2^{-m-1}\tilde{k}_\rho^m e^{-\tilde{k}_\rho^2/4}\Lambda(\tilde{k}_\rho^2) \qquad (A.2.11)$$

where with the help of Eq. (8.970.1) in [GR94], we can re-write $\Lambda(\tilde{k}_\rho^2) = \lim_{\delta\to 0}(-\delta)^n$ $L_n^m\left(\frac{\tilde{k}_\rho^2}{4\delta}\right)$ in the form:

$$\Lambda(\tilde{k}_\rho^2) = \lim_{\delta\to 0}(-\delta)^n\sum_{j=0}^n (-1)^j\binom{n+m}{n-j}\frac{1}{j!}\left(\frac{\tilde{k}_\rho^2}{4\delta}\right)^j. \qquad (A.2.12)$$

Note that the terms do not vanish, only in the case of $j = n$, which leads us to Eq. (7.2.12).

Bibliography

[01]   *The Nobel Prize in Physics 2001.* NobelPrize.org. 2001. URL: `https://www.nobelprize.org/prizes/physics/2001/press-release/` (visited on 03/08/2022) (cit. on p. 4).

[Aik+12]   K. Aikawa et al. "Bose-Einstein Condensation of Erbium." In: *Phys. Rev. Lett.* 108.21 (2012), p. 210401. DOI: `10.1103/PhysRevLett.108.210401` (cit. on p. 62).

[And+21]   L. Anderegg et al. "Observation of Microwave Shielding of Ultracold Molecules." In: *Science* 373.6556 (2021), pp. 779–782. DOI: `10.1126/science.abg9502` (cit. on p. 63).

[And+95]   M. H. Anderson et al. "Observation of Bose-Einstein Condensation in a Dilute Atomic Vapor." In: *Science* 269.5221 (1995), pp. 198–201. DOI: `10.1126/science.269.5221.198` (cit. on p. 4).

[Bai+16]   D. Baillie, R. M. Wilson, R. N. Bisset, and P. B. Blakie. "Self-Bound Dipolar Droplet: A Localized Matter Wave in Free Space." In: *Phys. Rev. A* 94.2 (2016), p. 021602. DOI: `10.1103/PhysRevA.94.021602` (cit. on p. 83).

[BB15]   R. N. Bisset and P. B. Blakie. "Crystallization of a Dilute Atomic Dipolar Condensate." In: *Phys. Rev. A* 92.6 (2015), p. 061603. DOI: `10.1103/PhysRevA.92.061603` (cit. on p. 79).

[BDZ08]   I. Bloch, J. Dalibard, and W. Zwerger. "Many-Body Physics with Ultracold Gases." In: *Rev. Mod. Phys.* 80.3 (2008), pp. 885–964. DOI: `10.1103/RevModPhys.80.885` (cit. on p. 8).

[Bel58]   S. T. Beliaev. "Application of the Methods of Quantum Field Theory to a System of Bosons." In: 34(7) (1958), p. 289 (cit. on p. 31).

[Bis+10]   G. Bismut et al. "Collective Excitations of a Dipolar Bose-Einstein Condensate." In: *Phys. Rev. Lett.* 105.4 (2010), p. 040404. DOI: 10.1103/PhysRevLett.105.040404 (cit. on p. 61).

[Bla+21]   T. Bland et al. "Two-Dimensional Supersolidity in a Circular Trap." 2021. arXiv: 2107.06680 [cond-mat] (cit. on p. 84).

[Bla+22]   T. Bland et al. "Domain Supersolids in Binary Dipolar Condensates." 2022. arXiv: 2203.11119 [cond-mat] (cit. on p. 58).

[Bog47]   N. Bogoliubov. "On the Theory of Superfluidity." In: *J. Phys* 11.1 (1947), p. 23 (cit. on pp. 10, 14).

[Bos24]   N. Bose. "Plancks Gesetz Und Lichtquantenhypothese." In: *Zeitschrift fur Physik* 26 (1924), pp. 178–181. DOI: 10.1007/BF01327326 (cit. on p. 3).

[Böt+19a]   F. Böttcher et al. "Dilute Dipolar Quantum Droplets beyond the Extended Gross-Pitaevskii Equation." In: *Phys. Rev. Research* 1.3 (2019), p. 033088. DOI: 10.1103/PhysRevResearch.1.033088 (cit. on p. 98).

[Böt+19b]   F. Böttcher et al. "Transient Supersolid Properties in an Array of Dipolar Quantum Droplets." In: *Phys. Rev. X* 9.1 (2019), p. 011051. DOI: 10.1103/PhysRevX.9.011051 (cit. on p. 84).

[Böt+20]   F. Böttcher et al. "New States of Matter with Fine-Tuned Interactions: Quantum Droplets and Dipolar Supersolids." In: *Rep. Prog. Phys.* 84.1 (2020), p. 012403. DOI: 10.1088/1361-6633/abc9ab (cit. on p. 84).

[BP12]   M. Boninsegni and N. V. Prokof'ev. "Colloquium: Supersolids: What and Where Are They?" In: *Rev. Mod. Phys.* 84.2 (2012), pp. 759–776. DOI: 10.1103/RevModPhys.84.759 (cit. on p. 84).

[Bur+20]   A. Burchianti et al. "A Dual-Species Bose-Einstein Condensate with Attractive Interspecies Interactions." In: *Condensed Matter* 5.1 (1 2020), p. 21. DOI: 10.3390/condmat5010021 (cit. on p. 26).

[Cab+18]   C. R. Cabrera et al. "Quantum Liquid Droplets in a Mixture of Bose-Einstein Condensates." In: *Science* 359.6373 (2018), pp. 301–304. DOI: 10.1126/science.aao5686 (cit. on pp. 26, 28, 29, 57).

[Cab18]   C. R. Cabrera. "Quantum Liquid Droplets in a Mixture of Bose-Einstein Condensates." Universitat Politècnica de Catalunya, 2018 (cit. on p. 54).

[Chi+10] C. Chin, R. Grimm, P. Julienne, and E. Tiesinga. "Feshbach Resonances in Ultracold Gases." In: *Rev. Mod. Phys.* 82.2 (2010), pp. 1225–1286. DOI: 10.1103/RevModPhys.82.1225 (cit. on pp. 8, 9, 96).

[Cho+16] L. Chomaz et al. "Quantum-Fluctuation-Driven Crossover from a Dilute Bose-Einstein Condensate to a Macrodroplet in a Dipolar Quantum Fluid." In: *Phys. Rev. X* 6.4 (2016), p. 041039. DOI: 10.1103/PhysRevX.6.041039 (cit. on pp. 73, 78, 95).

[Cho+18] L. Chomaz et al. "Observation of Roton Mode Population in a Dipolar Quantum Gas." In: *Nature Physics* 14.5 (2018), pp. 442–446. DOI: 10.1038/s41567-018-0054-7 (cit. on pp. 74, 75).

[Cho+19] L. Chomaz et al. "Long-Lived and Transient Supersolid Behaviors in Dipolar Quantum Gases." In: *Phys. Rev. X* 9.2 (2019), p. 021012. DOI: 10.1103/PhysRevX.9.021012 (cit. on p. 84).

[Cho+22] L. Chomaz et al. "Dipolar Physics: A Review of Experiments with Magnetic Quantum Gases." 2022. arXiv: 2201.02672 [cond-mat, physics:physics, physics:quant-ph] (cit. on p. 82).

[CHR13] M. H. W. Chan, R. B. Hallock, and L. Reatto. "Overview on Solid 4He and the Issue of Supersolidity." In: *J Low Temp Phys* 172.5 (2013), pp. 317–363. DOI: 10.1007/s10909-013-0882-x (cit. on p. 84).

[Cod] Codata. *CODATA Value: Bohr Magneton.* URL: https://physics.nist.gov/cgi-bin/cuu/Value?mub (visited on 04/08/2022) (cit. on p. 63).

[Cor96] E. Cornell. "Very Cold Indeed: The Nanokelvin Physics of Bose-Einstein Condensation." In: *J Res Natl Inst Stand Technol* 101.4 (1996), pp. 419–434. DOI: 10.6028/jres.101.045 (cit. on p. 4).

[CW02] E. A. Cornell and C. E. Wieman. "Nobel Lecture: Bose-Einstein Condensation in a Dilute Gas, the First 70 Years and Some Recent Experiments." In: *Rev. Mod. Phys.* 74.3 (2002), pp. 875–893. DOI: 10.1103/RevModPhys.74.875 (cit. on p. 3).

[Dav+95] K. B. Davis et al. "Bose-Einstein Condensation in a Gas of Sodium Atoms." In: *Phys. Rev. Lett.* 75.22 (1995), pp. 3969–3973. DOI: 10.1103/PhysRevLett.75.3969 (cit. on p. 4).

[DEr+19] C. D'Errico et al. "Observation of Quantum Droplets in a Heteronuclear Bosonic Mixture." In: *Phys. Rev. Research* 1.3 (2019), p. 033155. DOI: 10.1103/PhysRevResearch.1.033155 (cit. on p. 26).

[Edl+17]   D. Edler et al. "Quantum Fluctuations in Quasi-One-Dimensional Dipolar Bose-Einstein Condensates." In: *Phys. Rev. Lett.* 119.5 (2017), p. 050403. DOI: 10.1103/PhysRevLett.119.050403 (cit. on pp. 86, 87, 96, 97).

[Edl+22]   D. Edler, L. A. P. Ardila, C. R. Cabrera, and L. Santos. "Anomalous Buoyancy of Quantum Bubbles in Immiscible Bose Mixtures." In: *Phys. Rev. Research* 4.3 (2022), p. 033017. DOI: 10.1103/PhysRevResearch.4.033017 (cit. on pp. 40, 48, 49, 55, 56).

[EGO05]   C. Eberlein, S. Giovanazzi, and D. H. J. O'Dell. "Exact Solution of the Thomas-Fermi Equation for a Trapped Bose-Einstein Condensate with Dipole-Dipole Interactions." In: *Phys. Rev. A* 71.3 (2005), p. 033618. DOI: 10.1103/PhysRevA.71.033618 (cit. on pp. 69, 70).

[Ein25]   A. Einstein. "Zur Quantentheorie Des Idealen Gases." In: *Sitzung der physikalisch-mathematischen Klasse* (1925) (cit. on p. 3).

[Fan61]   U. Fano. "Effects of Configuration Interaction on Intensities and Phase Shifts." In: *Phys. Rev.* 124.6 (1961), pp. 1866–1878. DOI: 10.1103/PhysRev.124.1866 (cit. on p. 8).

[Fes58]   H. Feshbach. "Unified Theory of Nuclear Reactions." In: *Annals of Physics* 5.4 (1958), pp. 357–390. DOI: 10.1016/0003-4916(58)90007-1 (cit. on p. 8).

[Fey54]   R. P. Feynman. "Atomic Theory of the Two-Fluid Model of Liquid Helium." In: *Phys. Rev.* 94.2 (1954), pp. 262–277. DOI: 10.1103/PhysRev.94.262 (cit. on p. 73).

[Gal+20]   A. Gallemí, S. M. Roccuzzo, S. Stringari, and A. Recati. "Quantized Vortices in Dipolar Supersolid Bose-Einstein-condensed Gases." In: *Phys. Rev. A* 102.2 (2020), p. 023322. DOI: 10.1103/PhysRevA.102.023322 (cit. on p. 84).

[GGP02]   S. Giovanazzi, A. Görlitz, and T. Pfau. "Tuning the Dipolar Interaction in Quantum Gases." In: *Phys. Rev. Lett.* 89.13 (2002), p. 130401. DOI: 10.1103/PhysRevLett.89.130401 (cit. on p. 63).

[GP08]   T. F. Gallagher and P. Pillet. "Dipole–Dipole Interactions of Rydberg Atoms." In: *Advances In Atomic, Molecular, and Optical Physics*. Vol. 56. Advances in Atomic, Molecular, and Optical Physics. Academic Press, 2008, pp. 161–218. DOI: 10.1016/S1049-250X(08)00013-X (cit. on p. 61).

[GR94]   I. S. Gradštejn and J. M. Ryžik. *Table of Integrals, Series, and Products*. 5. ed. New York [u.a.], 1994 (cit. on pp. 90, 99, 111).

[Gri+05]   A. Griesmaier et al. "Bose-Einstein Condensation of Chromium." In: *Phys. Rev. Lett.* 94.16 (2005), p. 160401. DOI: `10.1103/PhysRevLett.94.160401` (cit. on p. 61).

[Gro61]   E. P. Gross. "Structure of a Quantized Vortex in Boson Systems." In: *Il Nuovo Cimento (1955-1965)* 20.3 (1961), pp. 454–477. DOI: `10.1007/BF02731494` (cit. on p. 11).

[GS03]   D. M. Gangardt and G. V. Shlyapnikov. "Stability and Phase Coherence of Trapped 1D Bose Gases." In: *Phys. Rev. Lett.* 90.1 (2003), p. 010401. DOI: `10.1103/PhysRevLett.90.010401` (cit. on p. 97).

[Guo+19]   M. Guo et al. "The Low-Energy Goldstone Mode in a Trapped Dipolar Supersolid." In: *Nature* 574.7778 (7778 2019), pp. 386–389. DOI: `10.1038/s41586-019-1569-5` (cit. on p. 84).

[Guo+20]   Z. Guo, F. Jia, L. Li, and D. Wang. "Quantum Droplet in a Mixture of Rb and Na Bose-Einstein Condensates." In: 2020 (2020), E01.102 (cit. on p. 26).

[Hal+11]   E. Haller et al. "Three-Body Correlation Functions and Recombination Rates for Bosons in Three Dimensions and One Dimension." In: *Phys. Rev. Lett.* 107.23 (2011), p. 230404. DOI: `10.1103/PhysRevLett.107.230404` (cit. on p. 96).

[Hal+98]   D. S. Hall et al. "Dynamics of Component Separation in a Binary Mixture of Bose-Einstein Condensates." In: *Phys. Rev. Lett.* 81.8 (1998), pp. 1539–1542. DOI: `10.1103/PhysRevLett.81.1539` (cit. on p. 40).

[Hei+08]   R. Heidemann et al. "Rydberg Excitation of Bose-Einstein Condensates." In: *Phys. Rev. Lett.* 100.3 (2008), p. 033601. DOI: `10.1103/PhysRevLett.100.033601` (cit. on p. 61).

[Her+21]   J. Hertkorn et al. "Supersolidity in Two-Dimensional Trapped Dipolar Droplet Arrays." In: *Phys. Rev. Lett.* 127.15 (2021), p. 155301. DOI: `10.1103/PhysRevLett.127.155301` (cit. on p. 84).

[HP59]   N. M. Hugenholtz and D. Pines. "Ground-State Energy and Excitation Spectrum of a System of Interacting Bosons." In: *Phys. Rev.* 116.3 (1959), pp. 489–506. DOI: `10.1103/PhysRev.116.489` (cit. on pp. 31, 36, 37, 80).

[HS96]   T.-L. Ho and V. B. Shenoy. "Binary Mixtures of Bose Condensates of Alkali Atoms." In: *Phys. Rev. Lett.* 77.16 (1996), pp. 3276–3279. DOI: `10.1103/PhysRevLett.77.3276` (cit. on p. 40).

[Ing+99]   M. Inguscio, S. Stringari, C. E. Wieman, and S. italiana di fisica, eds. *Bose-Einstein Condensation in Atomic Gases: Varenna on Lake Como, Villa Monastero, 7-17 July 1998.* Proceedings of the International School of Physics "Enrico Fermi" course 140. Amsterdam ; Washington, DC: IOS Press, 1999. 637 pp. (cit. on pp. 7, 8).

[Kad+16]   H. Kadau et al. "Observing the Rosensweig Instability of a Quantum Ferrofluid." In: *Nature* 530.7589 (2016), pp. 194–197. DOI: `10.1038/nature16485` (cit. on pp. 78, 81).

[Koc+08]   T. Koch et al. "Stabilization of a Purely Dipolar Quantum Gas against Collapse." In: *Nat Phys* 4.3 (2008), pp. 218–222. DOI: `10.1038/nphys887` (cit. on pp. 61, 66).

[KSS85]   Y. Kagan, B. V. Svistunov, and G. V. Shlyapnikov. "Effect of Bose Condensation on Inelastic Processes in Gases." In: *Soviet Journal of Experimental and Theoretical Physics Letters* 42 (1985), p. 209 (cit. on pp. 86, 96).

[Lah+07]   T. Lahaye et al. "Strong Dipolar Effects in a Quantum Ferrofluid." In: *Nature* 448.7154 (2007), pp. 672–675. DOI: `10.1038/nature06036` (cit. on pp. 61, 66).

[Lah+08]   T. Lahaye et al. "d-Wave Collapse and Explosion of a Dipolar Bose-Einstein Condensate." In: *Phys. Rev. Lett.* 101.8 (2008), p. 080401. DOI: `10.1103/PhysRevLett.101.080401` (cit. on pp. 61, 66, 68, 78).

[Lah+09]   T. Lahaye et al. "The Physics of Dipolar Bosonic Quantum Gases." In: *Rep. Prog. Phys.* 72.12 (2009), p. 126401. DOI: `10.1088/0034-4885/72/12/126401` (cit. on pp. 63, 64, 66, 67, 69).

[Lan47]   L. D. Landau. "On the Theory of Superfluidity of Helium II." In: 11 (1947), p. 91 (cit. on p. 73).

[Lar63]   D. M. Larsen. "Binary Mixtures of Dilute Bose Gases with Repulsive Interactions at Low Temperature." In: *Annals of Physics* 24 (1963), pp. 89–101. DOI: `10.1016/0003-4916(63)90066-6` (cit. on pp. 21, 23).

[LB21]   L. Lavoine and T. Bourdel. "Beyond-Mean-Field Crossover from One Dimension to Three Dimensions in Quantum Droplets of Binary Mixtures." In: *Phys. Rev. A* 103.3 (2021), p. 033312. DOI: `10.1103/PhysRevA.103.033312` (cit. on p. 47).

[Léo+17]   J. Léonard et al. "Supersolid Formation in a Quantum Gas Breaking a Continuous Translational Symmetry." In: *Nature* 543.7643 (7643 2017), pp. 87–90. DOI: `10.1038/nature21067` (cit. on p. 84).

[LHY57]   T. D. Lee, K. Huang, and C. N. Yang. "Eigenvalues and Eigenfunctions of a Bose System of Hard Spheres and Its Low-Temperature Properties." In: *Phys. Rev.* 106.6 (1957), pp. 1135–1145. DOI: `10.1103/PhysRev.106.1135` (cit. on p. 15).

[Li+17]   J.-R. Li et al. "A Stripe Phase with Supersolid Properties in Spin–Orbit-Coupled Bose–Einstein Condensates." In: *Nature* 543.7643 (7643 2017), pp. 91–94. DOI: `10.1038/nature21431` (cit. on p. 84).

[Li+21]   J.-R. Li et al. "Tuning of Dipolar Interactions and Evaporative Cooling in a Three-Dimensional Molecular Quantum Gas." In: *Nat. Phys.* 17.10 (10 2021), pp. 1144–1148. DOI: `10.1038/s41567-021-01329-6` (cit. on p. 63).

[LP11]   A. R. P. Lima and A. Pelster. "Quantum Fluctuations in Dipolar Bose Gases." In: *Phys. Rev. A* 84.4 (2011), p. 041604. DOI: `10.1103/PhysRevA.84.041604` (cit. on pp. 16, 80, 81, 85).

[LP12]   A. R. P. Lima and A. Pelster. "Beyond Mean-Field Low-Lying Excitations of Dipolar Bose Gases." In: *Phys. Rev. A* 86.6 (2012), p. 063609. DOI: `10.1103/PhysRevA.86.063609` (cit. on pp. 16, 80).

[Lu+11]   M. Lu, N. Q. Burdick, S. H. Youn, and B. L. Lev. "Strongly Dipolar Bose-Einstein Condensate of Dysprosium." In: *Phys. Rev. Lett.* 107.19 (2011), p. 190401. DOI: `10.1103/PhysRevLett.107.190401` (cit. on p. 62).

[Min+19]   F. Minardi et al. "Effective Expression of the Lee-Huang-Yang Energy Functional for Heteronuclear Mixtures." In: *Phys. Rev. A* 100.6 (2019), p. 063636. DOI: `10.1103/PhysRevA.100.063636`. arXiv: `1908.00804` (cit. on p. 23).

[MRB12]   M. Mayle, B. P. Ruzic, and J. L. Bohn. "Statistical Aspects of Ultracold Resonant Scattering." In: *Phys. Rev. A* 85.6 (2012), p. 062712. DOI: `10.1103/PhysRevA.85.062712` (cit. on p. 63).

[Mya+97]   C. J. Myatt et al. "Production of Two Overlapping Bose-Einstein Condensates by Sympathetic Cooling." In: *Phys. Rev. Lett.* 78.4 (1997), pp. 586–589. DOI: `10.1103/PhysRevLett.78.586` (cit. on p. 19).

[Nat+19]   G. Natale et al. "Excitation Spectrum of a Trapped Dipolar Supersolid and Its Experimental Evidence." In: *Phys. Rev. Lett.* 123.5 (2019), p. 050402. DOI: `10.1103/PhysRevLett.123.050402` (cit. on p. 84).

[Ni+08]   K.-K. Ni et al. "A High Phase-Space-Density Gas of Polar Molecules." In: *Science* 322.5899 (2008), pp. 231–235. DOI: `10.1126/science.1163861` (cit. on p. 61).

[Ni+10]   K.-K. Ni et al. "Dipolar Collisions of Polar Molecules in the Quantum Regime." In: *Nature* 464.7293 (7293 2010), pp. 1324–1328. DOI: 10.1038/nature08953 (cit. on p. 61).

[Nol15]   W. Nolting. *Grundkurs Theoretische Physik / Wolfgang Nolting ; 5,2: Quantenmechanik - Methoden Und Anwendungen.* 8. Auflage. Springer-Lehrbuch. Berlin, 2015 (cit. on p. 8).

[Nor+21]   M. A. Norcia et al. "Two-Dimensional Supersolidity in a Dipolar Quantum Gas." In: *Nature* 596.7872 (7872 2021), pp. 357–361. DOI: 10.1038/s41586-021-03725-7 (cit. on p. 84).

[Öhb99]   P. Öhberg. "Stability Properties of the Two-Component Bose-Einstein Condensate." In: *Phys. Rev. A* 59.1 (1999), pp. 634–638. DOI: 10.1103/PhysRevA.59.634 (cit. on p. 40).

[Osp+10a]   S. Ospelkaus et al. "Controlling the Hyperfine State of Rovibronic Ground-State Polar Molecules." In: *Phys. Rev. Lett.* 104.3 (2010), p. 030402. DOI: 10.1103/PhysRevLett.104.030402 (cit. on p. 61).

[Osp+10b]   S. Ospelkaus et al. "Quantum-State Controlled Chemical Reactions of Ultracold Potassium-Rubidium Molecules." In: *Science* 327.5967 (2010), pp. 853–857. DOI: 10.1126/science.1184121 (cit. on p. 63).

[PA16]   D. S. Petrov and G. E. Astrakharchik. "Ultradilute Low-Dimensional Liquids." In: *Phys. Rev. Lett.* 117.10 (2016), p. 100401. DOI: 10.1103/PhysRevLett.117.100401 (cit. on pp. 85, 93).

[PB98]   H. Pu and N. P. Bigelow. "Properties of Two-Species Bose Condensates." In: *Phys. Rev. Lett.* 80.6 (1998), pp. 1130–1133. DOI: 10.1103/PhysRevLett.80.1130 (cit. on p. 40).

[Pet+19]   D. Petter et al. "Probing the Roton Excitation Spectrum of a Stable Dipolar Bose Gas." In: *Phys. Rev. Lett.* 122.18 (2019), p. 183401. DOI: 10.1103/PhysRevLett.122.183401 (cit. on pp. 73, 74).

[Pet15]   D. S. Petrov. "Quantum Mechanical Stabilization of a Collapsing Bose-Bose Mixture." In: *Phys. Rev. Lett.* 115.15 (2015), p. 155302. DOI: 10.1103/PhysRevLett.115.155302 (cit. on pp. 22, 24, 27, 43, 85).

[Pit61]   L. P. Pitaevskii. "Vortex Lines in an Imperfect Bose Gas." In: *Sov. Phys. JETP* 13.2 (1961), pp. 451–454 (cit. on p. 11).

[PO08]   N. G. Parker and D. H. J. O'Dell. "Thomas-Fermi versus One- and Two-Dimensional Regimes of a Trapped Dipolar Bose-Einstein Condensate." In: *Phys. Rev. A* 78.4 (2008), p. 041601. DOI: 10.1103/PhysRevA.78.041601 (cit. on p. 69).

[Pol+21]   E. Poli et al. "Maintaining Supersolidity in One and Two Dimensions." In: *Phys. Rev. A* 104.6 (2021), p. 063307. DOI: 10.1103/PhysRevA.104.063307 (cit. on pp. 80, 84).

[PP21]   A. Pricoupenko and D. S. Petrov. "Higher-Order Effective Interactions for Bosons near a Two-Body Zero Crossing." In: *Phys. Rev. A* 103.3 (2021), p. 033326. DOI: 10.1103/PhysRevA.103.033326 (cit. on p. 92).

[PS04]   L. P. Pitaevskij and S. Stringari. *Bose-Einstein Condensation*. Reprinted (twice). International Series of Monographs on Physics. Oxford: Clarendon Press, 2004 (cit. on pp. 14, 71).

[PS97]   M. E. Peskin and D. V. Schroeder. *An Introduction to Quantum Field Theory*. 4. printing. Reading, Mass. [u.a.], 1997 (cit. on p. 36).

[Roc+20]   S. M. Roccuzzo, A. Gallemí, A. Recati, and S. Stringari. "Rotating a Supersolid Dipolar Gas." In: *Phys. Rev. Lett.* 124.4 (2020), p. 045702. DOI: 10.1103/PhysRevLett.124.045702 (cit. on p. 84).

[Sai16]   H. Saito. "Path-Integral Monte Carlo Study on a Droplet of a Dipolar Bose–Einstein Condensate Stabilized by Quantum Fluctuation." In: *J. Phys. Soc. Jpn.* 85.5 (2016), p. 053001. DOI: 10.7566/JPSJ.85.053001 (cit. on p. 83).

[San+00]   L. Santos, G. V. Shlyapnikov, P. Zoller, and M. Lewenstein. "Bose-Einstein Condensation in Trapped Dipolar Gases." In: *Phys. Rev. Lett.* 85.9 (2000), pp. 1791–1794. DOI: 10.1103/PhysRevLett.85.1791 (cit. on p. 65).

[Sch+16]   M. Schmitt et al. "Self-Bound Droplets of a Dilute Magnetic Quantum Liquid." In: *Nature* 539 (2016). DOI: 10.1038/nature20126. arXiv: 1607.07355 (cit. on p. 83).

[Sch+22]   A. Schindewolf et al. "Evaporation of Microwave-Shielded Polar Molecules to Quantum Degeneracy." 2022. arXiv: 2201.05143 [cond-mat, physics:physics, physics:quant-ph] (cit. on p. 63).

[Sem+18]   G. Semeghini et al. "Self-Bound Quantum Droplets of Atomic Mixtures in Free Space." In: *Phys. Rev. Lett.* 120.23 (2018), p. 235301. DOI: 10.1103/PhysRevLett.120.235301 (cit. on pp. 26, 27, 57).

[Soh+21]   M. Sohmen et al. "Birth, Life, and Death of a Dipolar Supersolid." In: *Phys. Rev. Lett.* 126.23 (2021), p. 233401. DOI: 10.1103/PhysRevLett.126.233401 (cit. on p. 84).

[SS07]   S. Sinha and L. Santos. "Cold Dipolar Gases in Quasi-One-Dimensional Geometries." In: *Phys. Rev. Lett.* 99.14 (2007), p. 140406. DOI: 10.1103/PhysRevLett.99.140406 (cit. on pp. 85, 87).

[SSC12]   C. Salomon, G. V. Shlyapnikov, and L. F. Cugliandolo, eds. *Many-Body Physics with Ultracold Gases: Lecture Notes of the Les Houches Summer School: Volume 94, July 2010*. Lecture Notes of the Les Houches Summer School. Oxford, New York: Oxford University Press, 2012. 374 pp. (cit. on pp. 65, 70, 109).

[SSL03]   L. Santos, G. V. Shlyapnikov, and M. Lewenstein. "Roton-Maxon Spectrum and Stability of Trapped Dipolar Bose-Einstein Condensates." In: *Phys. Rev. Lett.* 90.25 (2003), p. 250403. DOI: 10.1103/PhysRevLett.90.250403 (cit. on pp. 72, 73).

[Stu+05] J. Stuhler et al. "Observation of Dipole-Dipole Interaction in a Degenerate Quantum Gas." In: *Phys. Rev. Lett.* 95.15 (2005), p. 150406. DOI: 10.1103/PhysRevLett.95.150406 (cit. on p. 61).

[SWM10]   M. Saffman, T. G. Walker, and K. Mølmer. "Quantum Information with Rydberg Atoms." In: *Rev. Mod. Phys.* 82.3 (2010), pp. 2313–2363. DOI: 10.1103/RevModPhys.82.2313 (cit. on p. 61).

[Tan+18a] Y. Tang, W. Kao, K.-Y. Li, and B. L. Lev. "Tuning the Dipole-Dipole Interaction in a Quantum Gas with a Rotating Magnetic Field." In: *Phys. Rev. Lett.* 120.23 (2018), p. 230401. DOI: 10.1103/PhysRevLett.120.230401 (cit. on p. 64).

[Tan+18b] L. Tanzi et al. "Feshbach Resonances in Potassium Bose-Bose Mixtures." In: *Phys. Rev. A* 98.6 (2018), p. 062712. DOI: 10.1103/PhysRevA.98.062712 (cit. on p. 57).

[Tan+19a] L. Tanzi et al. "Observation of a Dipolar Quantum Gas with Metastable Supersolid Properties." In: *Phys. Rev. Lett.* 122.13 (2019), p. 130405. DOI: 10.1103/PhysRevLett.122.130405 (cit. on p. 84).

[Tan+19b] L. Tanzi et al. "Supersolid Symmetry Breaking from Compressional Oscillations in a Dipolar Quantum Gas." In: *Nature* 574.7778 (7778 2019), pp. 382–385. DOI: 10.1038/s41586-019-1568-6 (cit. on p. 84).

[Tim+99] E. Timmermans, P. Tommasini, M. Hussein, and A. Kerman. "Feshbach Resonances in Atomic Bose–Einstein Condensates." In: *Physics Reports* 315.1 (1999), pp. 199–230. DOI: 10.1016/S0370-1573(99)00025-3 (cit. on p. 8).

[Tim98]   E. Timmermans. "Phase Separation of Bose-Einstein Condensates."
            In: *Phys. Rev. Lett.* 81.26 (1998), pp. 5718–5721. DOI: 10.1103/
            PhysRevLett.81.5718 (cit. on pp. 20, 40, 45, 50, 52).

[Ton+04]   D. Tong et al. "Local Blockade of Rydberg Excitation in an Ultracold
            Gas." In: *Phys. Rev. Lett.* 93.6 (2004), p. 063001. DOI: 10.1103/
            PhysRevLett.93.063001 (cit. on p. 61).

[TTH97]   E. Timmermans, P. Tommasini, and K. Huang. "Variational Thomas-
            Fermi Theory of a Nonuniform Bose Condensate at Zero Tempera-
            ture." In: *Phys. Rev. A* 55.5 (1997), pp. 3645–3657. DOI: 10.1103/
            PhysRevA.55.3645 (cit. on p. 15).

[Ued10]   M. Ueda. *Fundamentals and New Frontiers of Bose-Einstein Conden-
            sation.* 2010. DOI: 10.1142/7216 (cit. on p. 6).

[Wen+17]   M. Wenzel et al. "Striped States in a Many-Body System of Tilted
            Dipoles." In: *Phys. Rev. A* 96.5 (2017), p. 053630. DOI: 10.1103/
            PhysRevA.96.053630 (cit. on p. 83).

[Wig32]   E. Wigner. "On the Quantum Correction For Thermodynamic Equi-
            librium." In: *Phys. Rev.* 40.5 (1932), pp. 749–759. DOI: 10.1103/
            PhysRev.40.749 (cit. on p. 15).

[WS16a]   F. Wächtler and L. Santos. "Ground-State Properties and Elementary
            Excitations of Quantum Droplets in Dipolar Bose-Einstein Conden-
            sates." 2016. DOI: 10.1103/PhysRevA.94.043618. arXiv: 1605.
            08676 [cond-mat] (cit. on p. 83).

[WS16b]   F. Wächtler and L. Santos. "Quantum Filaments in Dipolar Bose-
            Einstein Condensates." In: *Phys. Rev. A* 93.6 (2016). DOI: 10.1103/
            PhysRevA.93.061603. arXiv: 1601.04501 (cit. on p. 81).

[YY00]   S. Yi and L. You. "Trapped Atomic Condensates with Anisotropic
            Interactions." In: *Phys. Rev. A* 61.4 (2000), p. 041604. DOI: 10.1103/
            PhysRevA.61.041604 (cit. on p. 64).

[YY01]   S. Yi and L. You. "Trapped Condensates of Atoms with Dipole In-
            teractions." In: *Phys. Rev. A* 63.5 (2001), p. 053607. DOI: 10.1103/
            PhysRevA.63.053607 (cit. on p. 64).

[ZMP19]   Y.-C. Zhang, F. Maucher, and T. Pohl. "Supersolidity around a Criti-
            cal Point in Dipolar Bose-Einstein Condensates." In: *Phys. Rev. Lett.*
            123.1 (2019), p. 015301. DOI: 10.1103/PhysRevLett.123.015301
            (cit. on p. 84).

[ZPM21]   Y.-C. Zhang, T. Pohl, and F. Maucher. "Phases of Supersolids in Confined Dipolar Bose-Einstein Condensates." In: *Phys. Rev. A* 104.1 (2021), p. 013310. DOI: 10.1103/PhysRevA.104.013310 (cit. on p. 84).

Appendix **B**

Curriculum Vitae

Personal Information

Name	Daniel Edler
Date of Birth	1991-01-08 in Hannover

Education

1997 – 2001	Grundschule Bockenem
2001 – 2003	Ambergauschule Bockenem
2003 – 2010	Jacobson-Gymnasium Seesen
2010 – 2011	Bachelor of Science, Meteorologie, Leibniz Universität Hannover
2011 – 2014	Bachelor of Science, Physik, Leibniz Universität Hannover
2014 – 2016	Master of Science, Physics, Leibniz Universität Hannover
2016 – 2022	PhD, Leibniz Universität Hannover

Appendix C

Publications

- D. Edler et al. "Quantum Fluctuations in Quasi-One-Dimensional Dipolar Bose-Einstein Condensates." In: *Physical Review Letters* 119.5 (2017), p. 050403. DOI: 10.1103/PhysRevLett.119.050403.

- D. Edler, L. A. P. Ardila, C. R. Cabrera, and L. Santos. "Anomalous Buoyancy of Quantum Bubbles in Immiscible Bose Mixtures." In *Physikcal Review Research* 4.3 (2022), p. 033017. DOI: 10.1103/PhysRevResearch.4.033017

- This document. DOI: 10.15488/12547

Appendix D

Acknowledgements